



**AFRL-RB-WP-TR-2009-3045**

**VERIFICATION OF COLD WORKING AND  
INTERFERENCE LEVELS AT FASTENER HOLES**

**Thomas B. Mills, Kyle T. Honeycutt, Scott A. Prost-Domasky, and Craig L. Brooks  
APES, Inc.**

**FEBRUARY 2009  
Final Report**

**THIS IS A SMALL BUSINESS INNOVATION RESEARCH (SBIR) PHASE I REPORT.**

**Approved for public release; distribution unlimited.**

*See additional restrictions described on inside pages*

**STINFO COPY**

**AIR FORCE RESEARCH LABORATORY  
AIR VEHICLES DIRECTORATE  
WRIGHT-PATTERSON AIR FORCE BASE, OH 45433-7542  
AIR FORCE MATERIEL COMMAND  
UNITED STATES AIR FORCE**

## NOTICE AND SIGNATURE PAGE

Using Government drawings, specifications, or other data included in this document for any purpose other than Government procurement does not in any way obligate the U.S. Government. The fact that the Government formulated or supplied the drawings, specifications, or other data does not license the holder or any other person or corporation; or convey any rights or permission to manufacture, use, or sell any patented invention that may relate to them.

This report was cleared for public release by the USAF 88<sup>th</sup> Air Base Wing (88 ABW) Public Affairs Office (PAO) and is available to the general public, including foreign nationals. Copies may be obtained from the Defense Technical Information Center (DTIC) (<http://www.dtic.mil>).

AFRL-RB-WP-TR-2009-3045 HAS BEEN REVIEWED AND IS APPROVED FOR PUBLICATION IN ACCORDANCE WITH ASSIGNED DISTRIBUTION STATEMENT.

*\*//Signature//*

---

ROBERT REUTER  
Contract Monitor  
Structural Mechanics Branch

*//Signature//*

---

ANDREW SPARKS  
Structural Mechanics Branch  
Structures Division

This report is published in the interest of scientific and technical information exchange, and its publication does not constitute the Government's approval or disapproval of its ideas or findings.

\*Disseminated copies will show "*//Signature//*" stamped or typed above the signature blocks.

| <b>REPORT DOCUMENTATION PAGE</b>   |                                    |                                     |   | <i>Form Approved</i><br>OMB No. 0704-0188   |  |
|--|------------------------------------|-------------------------------------|---|---|--|
| <p>The public reporting burden for this collection of information is estimated to average 1 hour per response, including the time for reviewing instructions, searching existing data sources, gathering and maintaining the data needed, and completing and reviewing the collection of information. Send comments regarding this burden estimate or any other aspect of this collection of information, including suggestions for reducing this burden, to Department of Defense, Washington Headquarters Services, Directorate for Information Operations and Reports (0704-0188), 1215 Jefferson Davis Highway, Suite 1204, Arlington, VA 22202-4302. Respondents should be aware that notwithstanding any other provision of law, no person shall be subject to any penalty for failing to comply with a collection of information if it does not display a currently valid OMB control number. <b>PLEASE DO NOT RETURN YOUR FORM TO THE ABOVE ADDRESS.</b></p> |                                    |                                     |   |   |  |
| <b>1. REPORT DATE (DD-MM-YY)</b><br>February 2009  |                                    | <b>2. REPORT TYPE</b><br>Final      |   | <b>3. DATES COVERED (From - To)</b><br>26 Mar 2008 – 31 October 2008                |  |
| <b>4. TITLE AND SUBTITLE</b><br>VERIFICATION OF COLD WORKING AND INTERFERENCE LEVELS AT FASTENER HOLES   |                                    |                                     |   | <b>5a. CONTRACT NUMBER</b><br>FA8650-08-M-3842                                      |  |
|  |                                    |                                     |   | <b>5b. GRANT NUMBER</b>   |  |
|  |                                    |                                     |   | <b>5c. PROGRAM ELEMENT NUMBER</b><br>N/A  |  |
| <b>6. AUTHOR(S)</b><br>Thomas B. Mills, Kyle T. Honeycutt, Scott A. Prost-Domasky, and Craig L. Brooks   |                                    |                                     |   | <b>5d. PROJECT NUMBER</b><br>A0FS   |  |
|  |                                    |                                     |   | <b>5e. TASK NUMBER</b>  |  |
|  |                                    |                                     |   | <b>5f. WORK UNIT NUMBER</b><br>0B   |  |
| <b>7. PERFORMING ORGANIZATION NAME(S) AND ADDRESS(ES)</b><br>APES, Inc.<br>6669 Fyler Avenue<br>St. Louis, MO 63139  |                                    |                                     |   | <b>8. PERFORMING ORGANIZATION REPORT NUMBER</b>                                     |  |
| <b>9. SPONSORING/MONITORING AGENCY NAME(S) AND ADDRESS(ES)</b><br><br>Air Force Research Laboratory<br>Air Vehicles Directorate<br>Wright-Patterson Air Force Base, OH 45433-7542<br>Air Force Materiel Command<br>United States Air Force   |                                    |                                     |   | <b>10. SPONSORING/MONITORING AGENCY ACRONYM(S)</b><br>AFRL/RBSM                     |  |
|  |                                    |                                     |   | <b>11. SPONSORING/MONITORING AGENCY REPORT NUMBER(S)</b><br>AFRL-RB-WP-TR-2009-3045 |  |
| <b>12. DISTRIBUTION/AVAILABILITY STATEMENT</b><br>Approved for public release; distribution unlimited.   |                                    |                                     |   |   |  |
| <b>13. SUPPLEMENTARY NOTES</b><br>This is a Small Business Innovation Research (SBIR) Phase I report.<br>PAO Case Number: 88ABW 2009-1095, 20 Mar 2009. Report contains color.<br>APES, Inc. waives its SBIR data rights to the material in this report (see reverse side of this page for waiver letter).   |                                    |                                     |   |   |  |
| <b>14. ABSTRACT</b><br>This report was developed under a SBIR contract for Topic AF081-088.<br>The overall objective of Phase I was to perform the initial research to understand the residual stress behavior around cold-worked holes that are subsequently subjected to operation load cycles. The desired end state is to define the path for developing a comprehensive analytical simulation of the service life capability in multiple applications that complement USAF fleet infrastructures. The research knowledge gained in Phase I formulated a sound approach for Phase II technology development and concurrent demonstration. The program that evolved factors in substantial USAF buy-in, which should expedite the products into benefits for the air vehicles.  |                                    |                                     |   |   |  |
| <b>15. SUBJECT TERMS</b><br>SBIR Report, Cold-working, fatigue, life prediction  |                                    |                                     |   |   |  |
| <b>16. SECURITY CLASSIFICATION OF:</b>   |                                    |                                     | <b>17. LIMITATION OF ABSTRACT:</b><br>SAR | <b>18. NUMBER OF PAGES</b><br>94  | <b>19a. NAME OF RESPONSIBLE PERSON (Monitor)</b><br>Robert Reuter<br><b>19b. TELEPHONE NUMBER (Include Area Code)</b><br>N/A |
| <b>a. REPORT</b><br>Unclassified   | <b>b. ABSTRACT</b><br>Unclassified | <b>c. THIS PAGE</b><br>Unclassified |   |   |  |



**analytical processes / engineered solutions**

**6669 FYLER AVE. • ST. LOUIS, MO • 63139**

**PHONE: 314.644.6040 • FAX: 314.644.1309**

April 10, 2009

Reuter, Robert A Civ  
USAF AFMC AFRL/RBSM  
Wright-Patterson AFB, OH 45324-4444

Subject: Contract Number FA8650-08-M-3842, Phase I SBIR

Dear Mr. Reuter:

APES, Inc. hereby waives its SBIR Data Rights to all contents of the final report for subject contract. The Government is granted an unlimited nonexclusive license to use, modify, reproduce, release, perform, and display or disclose this report and the data contained herein.

Sincerely,

A handwritten signature in black ink, appearing to read "Craig L Brooks". The signature is fluid and cursive, with the first name "Craig" being particularly prominent.

Craig L Brooks  
Chief Engineer

# TABLE of CONTENTS

|   |             |
|---|-------------|
| <b>LIST OF FIGURES</b> .....  | <b>V</b>    |
| <b>LIST OF TABLES</b> .....   | <b>VIII</b> |
| <b>EXECUTIVE SUMMARY</b> .....  | <b>1</b>    |
| <b>1 PROGRAM OVERVIEW</b> .....   | <b>4</b>    |
| 1.1 Introduction.....   | 4           |
| 1.2 Program Vision and Goal .....   | 5           |
| 1.3 Phase I Technical Objectives .....  | 6           |
| 1.4 Phase I Work Plan.....  | 6           |
| <b>2 TECHNICAL BACKGROUND AND LITERATURE REVIEW</b> .....                         | <b>8</b>    |
| 2.1 Holistic Structural Life Prediction (HOLSIP) .....                            | 8           |
| 2.1.1 <i>Reliable residual stress measurements</i> .....                          | 10          |
| 2.1.2 <i>Analytical methodology development</i> .....                             | 10          |
| 2.2 Literature Review.....  | 10          |
| <b>3 TECHNICAL APPROACH &amp; ACCOMPLISHMENTS IN PHASE I</b> .....                | <b>12</b>   |
| 3.1 Cold working of Holes in Aluminum Alloy .....                                 | 12          |
| 3.2 Measurement of Residual Stresses near Cold worked Holes.....                  | 13          |
| 3.2.1 <i>X-Ray Diffraction (XRD)</i> .....  | 14          |
| 3.2.2 <i>Digital Image Correlation (DIC)</i> .....                                | 19          |
| 3.2.3 <i>Direct Measurements, Inc. (DMI) Optical Strain Gages</i> .....           | 26          |
| 3.2.4 <i>Bolt Hole and Surface Eddy Current</i> .....                             | 27          |
| 3.3 Fatigue Testing.....  | 28          |
| 3.3.1 <i>Fatigue Experiments on Baseline and Cold-Worked Coupons</i> .....        | 28          |
| 3.3.2 <i>Monitoring of the Residual Stress Field on the Fatigue Coupons</i> ..... | 32          |
| 3.3.3 <i>Fractography of Fatigue Test Coupons</i> .....                           | 36          |
| 3.4 Analytical Assessment of Residual Stresses.....                               | 46          |
| 3.4.1 <i>Evaluation of StressCheck® Incremental Plasticity Algorithm</i> .....    | 46          |
| 3.4.2 <i>Verification of StressCheck® Against NRC Analysis</i> .....              | 49          |
| 3.4.3 <i>AP/ES Modeling of NRC Aging Aircraft 2007 Paper Results</i> .....        | 51          |
| 3.4.4 <i>Phase I Test Coupon Residual Stresses</i> .....                          | 54          |
| 3.5 Holistic Life Predictions of Cold Worked Specimens .....                      | 55          |
| 3.5.1 <i>Analysis Method and Baseline Specimens</i> .....                         | 55          |
| 3.5.2 <i>Results for Cold Worked Coupons</i> .....                                | 58          |
| 3.5.3 <i>Sensitivity of Predictions to Model Components</i> .....                 | 63          |
| 3.6 Coordinate Phase II Demo Articles with A-10 and F-16 ASIP .....               | 67          |
| <b>4 COMMERCIALIZATION POTENTIAL</b> .....  | <b>68</b>   |
| <b>5 SUMMARY</b> .....  | <b>70</b>   |
| <b>6 UNRESOLVED ISSUES AND RECOMMENDATIONS</b> .....                              | <b>73</b>   |
| 6.1 Residual Stress Measurements.....   | 73          |

|          |  |           |
|----------|--|-----------|
| 6.1.1    | <i>X-ray diffraction (XRD)</i> .....                   | 73        |
| 6.1.2    | <i>DMI</i> .....                                       | 73        |
| 6.1.3    | <i>DIC</i> .....                                       | 73        |
| 6.1.4    | <i>Eddy current (ET or EC)</i> .....                   | 74        |
| 6.2      | <i>Modeling</i> .....                                  | 74        |
| 6.2.1    | <i>Crack Retardation</i> .....                         | 74        |
| 6.2.2    | <i>Three-dimensional Effects of Cold working</i> ..... | 74        |
| 6.2.3    | <i>Residual Stress Relaxation</i> .....                | 74        |
| 6.2.4    | <i>Material Behavior</i> .....                         | 74        |
| <b>7</b> | <b>REFERENCES</b> .....                                | <b>76</b> |
|          | <b>APPENDIX</b> .....                                  | <b>78</b> |

## LIST of FIGURES

|   |    |
|---|----|
| Figure 1. Elements of Holistic Analysis Will Be Needed to Demonstrate Robustness of Cold Working Solutions. ....  | 8  |
| Figure 2. Fatigue Test Specimen Design. Dimensions in Inches. ....  | 12 |
| Figure 3. X-Ray Diffraction (XRD) Specimen Nomenclature. ....   | 15 |
| Figure 4. X-Ray Diffraction (XRD) Measurement Variability for 5 Specimens. Entrance Side. ....  | 16 |
| Figure 5. X-Ray Diffraction (XRD) Measurement Variability for 5 Specimens. Exit Side.....   | 17 |
| Figure 6. X-Ray Diffraction (XRD) Measurement Variability for 3 Line Profiles. Coupon 3D 16, Entrance Side. ....  | 18 |
| Figure 7. Comparison of StressCheck <sup>®</sup> Computations with XRD Measurements. ....   | 18 |
| Figure 8. Typical Image of Speckled Paint on Test Specimen. ....  | 20 |
| Figure 9. Measurement of Maximum (e1) and Minimum (e2) Principal Strains With Digital Image Correlation. Shown is Top Line Profile. Entrance Side.....                          | 21 |
| Figure 10. Measurement of Maximum (e1) and Minimum (e2) Principal Strains With Digital Image Correlation. Shown is Left Line Profile. Entrance Side. ....                       | 21 |
| Figure 11. Measurement of Maximum (e1) and Minimum (e2) Principal Strains With Digital Image Correlation. Shown is Bottom Line Profile. Entrance Side. ....                     | 22 |
| Figure 12. Scatter in Maximum (e1) and Minimum (e2) Principal Strain Measurements with Digital Image Correlation. Shown is Top Line Profile.....                                | 22 |
| Figure 13. Color Contour of the Measurement of Maximum (e1) Principal Strain With Digital Image Correlation; Entrance Face. ....  | 23 |
| Figure 14. Digital Image Correlation (DIC) Measurement Averaged over 5 Specimens are Compared to Finite Element Analysis (FEA) Results. Entrance Line Profiles. ....            | 24 |
| Figure 15. Digital Image Correlation (DIC) Measurement Averaged over 5 Specimens are Compared to Finite Element Analysis (FEA) Results. Exit Line Profiles.....                 | 24 |
| Figure 16. Entrance and Exit Line Profiles (Averaged over 5 Specimens) Using Digital Image Correlation (DIC) Measurement Compared to Finite Element Analysis (FEA) Results..... | 25 |
| Figure 17. Round DMI Gage Should Be More Suitable for Cold working Measurements than Linear Gages. ....   | 27 |
| Figure 18. V5 spectrum used for the first baseline test (too mild). ....  | 29 |
| Figure 19. V1 spectrum used for second baseline tests (still too mild). ....  | 29 |
| Figure 20. V9 spectrum used for baseline tests 3 - 5 (used for subsequent cold worked coupons). ....  | 30 |
| Figure 21. Fatigue Test Specimen Design. ....   | 30 |

|   |    |
|---|----|
| Figure 22. DMI Gage Strain Descriptions. “x” direction is perpendicular to load direction. ....   | 33 |
| Figure 23. Evolution of the Strain $E_{xx}$ During the Life of Cold Worked Coupon 5B39. Gage 49.<br>.....   | 34 |
| Figure 24. Coupon 5B39 with DMI Gage Mounted. Gage appears to be misaligned and at least 2<br>inside edges of the gage are distorted or damaged. ....                             | 34 |
| Figure 25. Marker band data and AFGROW computation for baseline coupon 5B19 (#1).....   | 38 |
| Figure 26. Marker band data and AFGROW computation for baseline coupon 5B40 (#2).....   | 38 |
| Figure 27. Marker band data and AFGROW computation for baseline coupon 5B25 (#3).....   | 39 |
| Figure 28. Marker band data and AFGROW computation for baseline coupon 5B26 (#4).....   | 39 |
| Figure 29. Marker band data and AFGROW computation for baseline coupon 3D12 (#5).....   | 40 |
| Figure 30. Example of the appearance of the V9 loading sequence on a fracture face. ....  | 40 |
| Figure 31. Crack growth data plotted for one non-cold worked coupon and seven cold worked<br>coupons. ....  | 41 |
| Figure 32. Schematic of general fracture behavior for cold worked coupons. ....   | 42 |
| Figure 33. Crack growth data for coupon 3D16 with crack growth behavior "regions" labeled. ....   | 43 |
| Figure 34. da/dN vs. a plots for 4 intermediate life coupons. ....  | 44 |
| Figure 35. da/dN vs a plots for 2 long life coupons and 1 short life coupon. ....   | 45 |
| Figure 36. Eyeball curve fits of da/dN vs. a data for three types of coupon behavior.....   | 45 |
| Figure 37. Comparison with Burlat Cold Working Simulations, Isotropic Hardening. ....   | 48 |
| Figure 38. Comparison with Burlat Cold Working Simulations, Kinematic Hardening.....  | 48 |
| Figure 39. Effect of Edge Margin on Residual Stress on Entrance Plane. ....   | 50 |
| Figure 40. Effect of Edge Margin on Residual Stress on Middle Plane. ....   | 50 |
| Figure 41. Effect of Edge Margin on Residual Stress on Exit Plane. ....   | 51 |
| Figure 42. StressCheck® Simulations Demonstrate Effect of Varying Material Constitutive<br>Relations (All Materials are Ramberg-Osgood Curve Fits). ....                          | 53 |
| Figure 43. StressCheck® Simulation Compares Favorably to NRC’s FEA Results. ....  | 53 |
| Figure 44. StressCheck® Computations of Cold Worked and Non Cold Worked Coupons. ....   | 55 |
| Figure 45. R=0.1 Crack growth rate assumptions for baseline analyses. ....  | 57 |
| Figure 46. Uncracked average stress distribution curve $\sigma_{Kt-FF}$ used for Excel macro predictions.<br>.....  | 57 |
| Figure 47. Comparison of variable amplitude prediction, constant amplitude prediction, Excel<br>macro method, and crack length measured from one baseline non-CW experiment. .... | 58 |
| Figure 48. Comparison of industry predictive methods with cold worked test result. ....   | 59 |
| Figure 49. Radial residual stress profile assumed for all analyses. ....  | 60 |

Figure 50. Crack growth rate curve used for cold work analyses. Residual hoop stresses cause a shift from positive to negative R-ratios. .... 61

Figure 51. Back-calculated  $\sigma_{R/S-Hoop}$  compared to stress profiles from FEA and XRD. .... 62

Figure 52. Life predictions for several  $\sigma_{R/S-Hoop}$  scenarios. .... 63

Figure 53. Bounding scenarios for XRD Residual Hoop Stress  $\sigma_{R/S-Hoop}$ . Maxima and minima are taken across all CW coupons, all three locations (top, left, bottom), and both the entrance and exit side of the specimen. .... 64

Figure 54. Life predictions using bounding scenarios XRD-min and XRD-max..... 65

Figure 55. Progressive sensitivities with initial crack = 0.0007 inch. .... 65

Figure 56. Progressive sensitivities with initial crack = 0.0004 inch. .... 66

## LIST of TABLES

|  |    |
|--|----|
| Table 1 Summary of Possible Compatibility Issues between Various RSQ Methods. .... | 14 |
| Table 2. Residual Stress Measurement Test Matrix. ....                             | 17 |
| Table 3. Fatigue Test Results.....   | 31 |
| Table 4. Summary of DMI Gage Readings. ....  | 35 |
| Table 5. Marker band reconstruction data. ....                                     | 37 |
| Table 6. Commercialization results schedule .....                                  | 69 |

## EXECUTIVE SUMMARY

This report is the final deliverable for the Phase I Small Business Innovation Research (SBIR) Topic, AF081-088, Verification of Cold Working and Interference Levels at Fastener Holes executed by Analytical Processes and Engineered Solutions (APES), Inc., the Texas Research Institute-Austin (TRI-Austin), National Research Council of Canada (NRC), Edison Welding Institute (EWI) and Direct Measurements, Incorporated (DMI).

The overall objective of Phase I was to perform the initial research to understand the residual stress behavior around cold-worked holes that are subsequently subjected to operation load cycles. The desired end state is to define the path for developing a comprehensive analytical simulation of the service life capability in multiple applications that compliment USAF fleet infrastructures. The research knowledge gained in Phase I formulated a sound approach for Phase II technology development and concurrent demonstration. The program that evolved factors in substantial USAF ‘buy-in,’ which should expedite the products into benefits for the air vehicles.

Specific goals accomplished in Phase I program were to:

1. Use multiple NDI methods (X-ray diffraction, Digital Image Correlation, Direct Measurement gauges, and Eddy Current techniques) to collect viable engineering data that provides data as to the “states of stress,” including residual stresses, in and around cold-worked holes. These data also included provisions for potential relaxation and/or redistribution of stresses. Each of the NDI methods used had particular merits, but none emerged as the “silver bullets,” the perfect NDI tool.
2. Regression of data collected and advanced fractographic examination of the failure process identified unique behaviors that post test analytical studies were able to replicate. Corroboration of the failure scenarios and analytical processes provides the framework for developing robust application models and methods.
3. Establish the process for expediting potential solutions for inclusion of the benefits of the subject SBIR into USAF aircraft by utilizing and tailoring ASIP formats and concepts.

All goals were successfully met.

The literature review focused on previous attempts to develop models and correlate coupon life predictions to fatigue experiment results (none of the literature we reviewed described fractography of cracks propagating through residual stress fields). Attempts in the literature to successfully predict the fatigue lives of cold worked structures have so far been inconsistent—methods such as weight functions which essentially use Green’s functions to ‘convert’ stresses to Mode I Stress Intensity Factors (SIFs) work well for one author but not for another. Weight functions have been shown to often be excellent predictors of SIFs, but it is apparent that 1) weight functions for the crack opening stress fields is not enough 2) analysts has so far missed key damage drivers (besides the crack opening stresses, that is) or 3) both. Direct application of residual stress, either as computed with a numerical method such as finite elements or “measured” by NDI tools, and classical LEFM are not adequate. The crack propagation predictions made by applying “conventional” damage tolerance methods does not reliably approximate the time or path of failure and is thus unacceptable to the long range objectives.

This Phase I effort included evaluation of the capabilities of several NDI techniques to measure and characterize residual stresses from the cold working process and after subsequent fatigue loading. Measurement techniques applied before, during, and after the fatigue experiments were used to capture crack propagation trends that were used to validate life prediction models. Residual stress measurements were made with four (4) techniques: x-ray diffraction (XRD), digital image correlation (DIC), eddy current and DMI optical strain gages. The four methods each have restricted applicability and limitations, but each provides a distinct opportunity. XRD was one of the most expensive of the 4 and thus number of data points is restricted by budget. The XRD data appeared reliable but the scope or depth of field of the measurement needs to be tempered with modeling parameters and the specific scope of measurement. XRD methods are suitable for pre-experimental applications, and some post laboratory measurement, but not feasible in the present state for in-service aircraft applications. The DIC, a considerably less expensive method than XRD, produced high-resolution residual strain values. The DIC was considered the most promising method for further laboratory experiments, and also as having great potential for in-service applications. The DMI gages offer valuable unique identity bar coding of each location, and could have an important tracking benefit as well as long term shifting of stress criticality. While the technology has considerable technical merits, the available products are not substantiated and have significant restrictions for our solutions. The Eddy Current methods appear to have the best potential as a cost effective solution in the field, but further development is needed.

Fifteen (15) coupons were tested in Phase I—five (5) non-cold worked and ten (10) cold worked. Each coupon was fatigue tested with a variable amplitude spectrum designed to produce excellent crack propagation marks on aluminum 7075-T651, the alloy tested in this program. Each of the ten (10) cold worked coupons had the same nominal offset,  $e/D \sim 1.5$  and the same nominal cold working level,  $CX \sim 4\%$  (residual stress measurements by XRD and DIC revealed substantial differences in stress fields presumably the same CX level). Cold working improved the lives of the specimens on average 1500% over non-cold worked specimen lives.

Analytical model development was challenging; there seem to be little guidance from the literature review, as techniques that appeared to work for one set of experiments did not work for others. Previous methods used only the residual stresses that were perpendicular to the crack plane; these stresses would tend to open or close a crack. However, most methods tended to over-predict the experimental lives by 2 to 10 times, indicating key damage drivers were probably being ignored in their analyses. Examination of the fracture surfaces from our experimental program revealed that the crack propagation featured three (3) distinct regions—a short but steep region of crack growth, followed by a long but shallow region of crack growth (which consisted of majority of the entire crack propagation life), and finally, a short and steep region of rapid crack growth until the coupon failed. This behavior was in stark contrast to the ‘predicted’ behavior using only the residual stresses—typically, there were only two distinct regions—a long shallow region followed by the short, steep region to coupon failure. Clearly, a key mechanism of crack growth was being missed. Our analyses points to a few possible candidates: 1) plasticity is affecting the crack growth more than just by residual stress, and/or 2) other mechanisms such as biaxiality of the stress field are significantly affecting crack propagation., and/or 3) relaxation or redistribution of residual stresses states. Excellent post-diction were achieved through a combination of modeling methods establishing confidence in our selected path forward. Phase I provided a series of controlled experiments using advanced experimental methods and interesting results from innovative post-diction techniques. The end

result is a well-defined Phase II approach for research activities that is designed to address unresolved issues that will enable engineering solutions to be formulated for the problem.

This report is divided into five major sections:

- I. Program Overview
- II. Technical Background and Literature Review
- III. Phase I Technical Accomplishments
- IV. Commercialization Potential
- V. Unresolved Issues and Recommendations

# 1 PROGRAM OVERVIEW

## 1.1 Introduction

The USAF statement of need for this technology focuses on the fact that the potential benefits of cold working a hole, or of using interference fasteners, include significantly increased life of a structure subjected to fatigue loading. However, full realization of this potential from a maintenance and engineering standpoint is hindered by the fact that there is currently no adequate field technique for determining how well the material structure immediately surrounding the hole has responded to the cold working process. Thus, there is a distinct need be able to:

1. Determine the success of a cold working treatment at a fastener hole,
2. Quantify the results of the treatment in a robust crack growth and residual life analysis,
3. Monitor the evolution or relaxation of the residual stress state as usage on the component accumulates,
4. Understand the effectiveness of the residual stress field in the presence of a crack, and
5. Evaluate and integrate field-sustainable tools needed to determine and provide inputs to the above items.

An ideal framework for the development, application, and integration of such technologies has been emerging in the literature over the last 12 years (Brooks, et al 1998, Brooks, et al 2002, and Brooks, et al 2003), and over the last seven years, interest has spawned an international working group, with private and defense participants from the US, Canada, Australia, and the UK (Wanhill, 2009). The philosophy is known as the holistic structural integrity process (HOLSIP).

In this effort, Analytical Processes / Engineered Solutions, Inc. (APES), and its team comprised of:

- Texas Research Institute-Austin (TRI),
- National Research Council of Canada (NRC)
- Edison Welding Institute (EWI)
- Stress Engineering Services (SES)
- Fatigue Technology Incorporated (FTI)

proposed a multi-faceted research effort with goal of technology integration at the end of Phase II. APES has secured the support of the A-10 ASIP and F-16 ASIP offices, both of which have serious interest in the advancement of fatigue life estimation of cold worked structure and in seeing technologies emerge that address the five needs listed above. Both of these programs have “Aging Aircraft Systems” and will use the product offered by this program, as they each share the ultimate goal of sustainable, integrated technology for the depot for this application.

The success of holistic structural integrity processes (or any process refinement for that matter) relies on proper design, execution and demonstration of three primary tasks or “cases”, namely:

1. The Technical Case
2. The Business Case
3. The Integration/Commercialization Case

We believe the program we have proposed for Phase II will solidly address these three “cases” by the end of that Phase. We have the support and interaction of two ASIP offices as well as that of a recognized world leader in cold work technology (FTI). This close involvement will ensure that we follow a path that will maximize technology potential and ensure that cold work benefits are more fully realized.

## **1.2 Program Vision and Goal**

The team assembled by APES has developed a plan for Phase II that will meet specific needs of the USAF war fighters that have expressed support for our technical and integration approaches. Furthermore, our team’s vision has produced a program plan that builds on the science of quantifying residual stress in the laboratory and moves towards a more sustainable approach for quantifying and monitoring residual stresses on aircraft structure. The following additional goals received some attention in Phase I and all will be pursued in earnest in Phase II in order to best meet the needs of the end-users:

- A. Refine algorithms that capture holistic material behavior and effectively model the key parameters important to feeding life predictions of crack growth at cold worked fastener holes.
- B. Develop algorithms that allow for the evolution (relaxation) of the residual stress state over time as either caused by physical cracking and/or by deformation of the material around the hole caused by mechanical loading and code these algorithms in COM to allow them to work with the crack growth code, AFGROW.
- C. Support cold worked life prediction algorithm validation using extensive test program.
- D. Examine low-cost, field-sustainable technologies to measure residual stresses at cold-worked fastener holes. These methods include optical deformation gauges developed by Direct Measurements Incorporated (DMI) and more traditional non-destructive inspection (NDT) method, eddy current
- E. Correlate the measurements obtained by these alternate technologies (point D) with readings obtained from the X-ray diffraction (XRD) and digital image correlation (DIC).
- F. Use alternate technologies (described in point D above) to evaluate stress state evolution (relaxation) as part of the Air Force required fatigue test demonstrations.
- G. Correlate all cold work experiments from Task C using tools integrated from Tasks A, B, E, and F.
- H. Work with the F-16 and A-10 ASIP managers to identify opportunities to directly address structural problems they are experiencing in their fleets for the purposes of technology demonstration (Phase II) and potential transition (Phase III). Both System Program Offices for these weapon systems supplied our team with letters of support during Phase I (see Appendix) and will continue to follow this program with interest during Phase II.

- I. Work with Fatigue Technology Incorporated to commercialize life prediction technologies for cold worked materials. This partnership provides a substantial technology transition potential.
- J. Work with AFRL/RBSM to conduct blind predictions of cold worked hole fatigue experiments as a demonstration and validation case (in addition to the demonstration and validation cases in G above).

### **1.3 Phase I Technical Objectives**

The Goals of the Phase I, as defined by the AFRL SBIR solicitation, are to:

1. Use X-ray diffraction (or other suitable method) to quantify residual stresses in cold-worked holes. **Status:** *Objective Achieved. See Section 3.2.1*
2. Develop analytical methods that work with AFGROW to produce life predictions for cold-worked holes. **Status:** *Objective Achieved. See Section 3.4.*
3. Verify models with coupon-level testing. **Status:** *Objective Achieved. See Section 3.5.*

The following additional goals received some attention in Phase I and all will be pursued in earnest in Phase II in order to best meet the needs of the end-users:

- A. Examine low-cost, field-sustainable technologies to measure residual stresses at cold-worked fastener holes. These methods include optical deformation gauges developed by Direct Measurements Incorporated (DMI) and more traditional non-destructive inspection (NDI) methods such as ultrasonic and eddy current.
- B. Correlate the measurements obtained by these alternate technologies with readings obtained from the X-ray diffraction (XRD).
- C. Develop algorithms that allow for the evolution (relaxation) of the residual stress state over time as either caused by physical cracking and/or by deformation of the material around the hole caused mechanical or thermal loading and code these algorithms in COM to allow them to work with the crack growth code, AFGROW.
- D. Use alternate technologies to evaluate stress state evolution (relaxation) as part of the Air Force required fatigue test demonstrations. The standard fighter wing spectrum, FALSTAFF, Van Dijk, et al (1975), will be used on some of the coupon tests to impart a substantial compressive component to the externally applied stress at the hole and to provide some continuity with the needs of the fighter/attack customers supporting our effort (F-16 and A-10).
- E. Work with the F-16 and A-10 ASIP offices to identify opportunities for technology demonstrations during Phase II that would directly address structural problems they are experiencing in their fleets.

### **1.4 Phase I Work Plan**

Nine (9) tasks were identified in Phase I. The Phase I work plan included the collaboration of experts in the fields of cold working, non destructive inspection (NDI) techniques, NDI data synthesis, and aircraft structural analysis.

The Phase I Work Plan included the following tasks:

*Task 1: Cold-working of plate-with-hole coupons*

*Task 2: Use of XRD to Quantify Residual Stress in Cold-Worked Holes*

*Task 3: Use Alternate Technologies to Quantify Residual Stress in Cold-Worked Holes*

*Task 4: Conduct Fatigue Experiments on Baseline and Cold-Worked Coupons*

*Task 5: Periodic Monitoring of the Residual Stress Field on the Fatigue Coupons*

*Task 6: Development of Residual Stress Relaxation Algorithms for use with AFGROW*

*Task 7: Simulation of Crack Growth in Residual Stress Fields.*

*Task 8: Coordinate Phase II Demo Articles with A-10 and F-16 ASIP*

*Task 9: Produce Phase I Final Report*

## 2 Technical Background and Literature Review

### 2.1 Holistic Structural Life Prediction (HOLSIP)

Holistic Life Assessment Methods (HLAMs) are used for assessment of the life of structural components; implementing those assessments into a Holistic Structural Integrity Process (HOLSIP) ensures continued safety, readiness, and controlled maintenance costs. These methods augment and enhance traditional safe-life and damage tolerance analysis paradigms in many ways, the most important of which are understanding and modeling the cradle-to-grave physical degradation and failure processes. With this “understanding” comes the attempt to account for realistic damage propagation mechanisms and failure modes, which are then incorporated into design, analysis, and sustainment activities, Figure 1.

The fundamental issue that drives the need for HOLSIP is a deficient understanding (to varied degrees) of the physical degradation process. This has given rise to the current design and analysis philosophies, which cover deficient understandings via many “safety factors.” However, these safety factors are nearly always empirical, are sometimes not safe enough, and because they are typically based on a constrained set of conditions, contribute strongly to disconnection of the analytical models from the physical state of the structure. This disconnection makes it difficult for the current design and analysis philosophies to account for new, non-traditional, or unanticipated effects (either detrimental or beneficial) on the degradation process; effects such as corrosion, time-dependent mechanisms, residual stress fields, material improvements, cold-working, surface finish, fastener fit, surface improvements, etc. The HOLSIP process facilitates a more substantive link between the analytical and the physical states by modeling the actual physical states and degradation of those physical states.

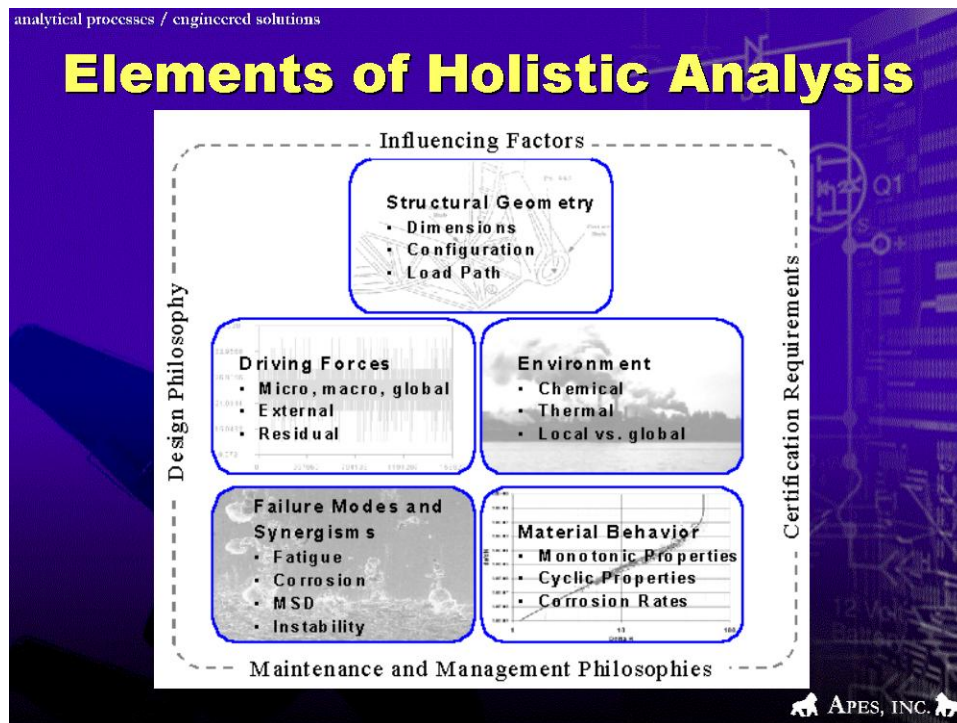


Figure 1. Elements of Holistic Analysis Will Be Needed to Demonstrate Robustness of Cold Working Solutions.

History has shown us that attempts to make traditionally-designed structure “safe enough” can come with considerable financial and operational burden caused in part, by premature component retirement, overzealous inspection, and unnecessary or ill-timed maintenance. Empirical safety factors are often applied in conditions completely unlike those under which the safety factor was developed, because “no better technique exists.” The holistic approach evolves existing technologies in assessment capability and is able to quantify and simulate the probabilistic nature of durability, crack growth, and other detrimental (or beneficial) mechanisms as they combine to age structure and eventually cause failure. Realistic modeling of stress states and damage progression mechanisms allow the holistic approach to be portable to new locations, platforms, or industries.

The analytical methods in HOLSIP have the capability to model environmental degradation that evolves in time, complex stress fields, and material improvement techniques, among others. They can assess the criticality of structures subject, for example, to corrosion pitting, sustained stresses, or other effects, either with or without cyclic loading. These methods can be applied during design or at any stage during the service life when damage is detected, or when operations vary from original expectations. Application of these methods and technologies has been successful in explaining several previously unsolved field failures from C-130s, C-141s, F/A-18s, and others.

Several recent laboratory and finite element studies have focused on developing and demonstrating some of the capabilities of the analytical methods present in HOLSIP. These include development of a fatigue model based on discontinuities such as inclusions and porosity inherent to a material (Brooks, 1998), exfoliation/fatigue models (Brooks, 2003), models for corrosion pitting effects on crack tip stress intensities based on 2D and 3D *p*-version finite element techniques (Prost-Domasky, 2003), and even a program that used blind predictions to accurately demonstrate the effects of corrosion pitting in 7050-T7451 aluminum (Mills, 2004). HLAM has been used to account for the complex stress states and degradation mechanisms resulting from fretting fatigue in coupons and lap joints, with the end result being a predictive structural lifing model (Brooks, 2006).

By using the actual degradation state as a benchmark for the holistic degradation, we allow investigative experimental and laboratory techniques to verify the analytical methods, even in the early stages of degradation when localized stresses are critical and the measurable degradation is small. By capturing the probabilistic state of a base material’s intrinsic discontinuities, we are able to predict both lower and upper bound fatigue behavior, assess risk, and also impose varied stress states, time dependencies, stress concentrations, or other mechanisms affecting structural degradation. Extreme damage sizes such as FOD damage or those specified by traditional damage tolerance design guidelines can be easily introduced into the method and are a subset of the probabilistic HLAM analysis.

Overall, HLAM will help new designs avoid shortcomings of existing “unknown” and “over-generalized” design rules and practices. Obviously, one desires to predict the upper and lower bounds of laboratory coupon tests, leading to a confidence that the structural degradation mechanisms are known and accounted. This increased confidence in quantifying structural effects and the probabilistic nature of the degradation mechanisms then allows appropriate levels of risk to be utilized on each piece of structure and tailored to each system. For example, acceptable levels of risk could differ between unmanned combat air vehicles (UCAVs), manned fighters, commercial transports, and space operations vehicles.

The HOLSIP process provides a powerful design and analysis tool to ascertain the basic fatigue response of a structure from the as-manufactured state, including the early stages of damage formation. HLAM makes for smart design wherein particular system susceptibilities, such as surface integrity issues or material improvement techniques can be included in Failure Modes Effects and Criticality Analyses (FMECA). These lessons learned can guide material selection, structural design, manufacturing procedures, and also inspection and maintenance requirements. In this way, methods to protect the structure can be put in place to guard against a specific and quantified structural degradation, the magnitudes of which would be known with confidence and illustrated quickly through the use of analysis databases.

This program will tailor the Holistic Life Assessment Methods to structural integrity of structures with engineered residual stresses. There are three primary considerations—1) obtaining reliable residual stress measurements 2) developing robust analytical methods that properly account for residual stress effects on crack propagation and 3) shifts in failure modes that can be caused by engineering residual stresses.

### **2.1.1 Reliable residual stress measurements**

They are a number of techniques used to measure residual stresses in metal structure. Structural life predictions typically are very sensitive to the quality of the data inputs, of which residual stress distributions are a significant part of the overall data needs. Because of this sensitivity, reliable residual stress measurements through the entire thickness (at a minimum up to and including the peak of the tensile stress that results from equilibrium with the compressive residual stress fields) will be needed for a robust life prediction methodology. Residual stress measurement techniques and their respective reliabilities were explored in Phase I, were proposed for Phase II of this program, and are discussed in Section 3.2 of this report.

### **2.1.2 Analytical methodology development**

To take full advantage of the benefits of engineered residual stresses in structural integrity, robust analytical methods that properly account for residual stress effects on crack propagation are needed. The analytical methods must be validated by application to post- and prediction of structural lives in coupons that have engineered residual stresses; considerable effort was expended in this Phase I toward the validation goal.

## **2.2 Literature Review**

A review of research papers in the open literature for analytical models which are able to accurately account for the residual stress effects on cold worked holes reveals a number of promising yet not fully validated approaches, ranging from finite element based to weight functions. A few representative works are discussed here. An important early paper by Grandt, (1975) in the 1970s identified a weight function based method that used the crack opening displacement functions to feed weight function integrals proposed by Rice (1972). Cathey and Grandt (1980) followed that up with a combined analytical-experimental investigation using the same methods proposed by Grandt (1975) earlier. Saunder and Grandt (2000) presented a paper at the Aging Aircraft conference that described the results of an extensive experimental investigation of cold worked coupons with variations in hole-edge distances; faster crack growth occurred on the entrance side of the cold working process, suggesting that the entrance side is either more damaged or has less induced residual stresses (which are compressive, and therefore

will tend to inhibit crack growth) than the exit side. More recently, Moreira et al (2004) also used the Rice weight functions and crack opening displacement functions that Petroski and Achenbach (1978) proposed to compute the weight function integrals. They also computed the J-integral with the finite element method, and got excellent agreement with the weight function computed Stress Intensity Factors.

An extensive finite element simulation of the entire cold working process was documented by Pavier, et al (1999). They used both 2D and 3D finite element models, and computed substantial differences in residual stresses depending on the location through the thickness—residual stresses on the entrance side were substantially different than the residual stresses on the exit side. Their approach for computing SIFs was complex, and probably would require access to source code of a fairly powerful finite element tool capable of computing full three-dimensional residual stress states (which we do not currently possess, for instance, ABAQUS and MARC Analysis). Kang, et al (2002) also published the results of an extensive finite element simulation, and added calculations with both isotropic and kinematic hardening. Burlat et al (2008) combined an in-depth finite element study of residual stresses with experimental tests and correlated the finite element results and fractography (with pinpointed crack nucleation points) with failures by fatigue loading. One interesting observation in Burlat was that if fatigue loading was ‘low,’ cracks tended to nucleate at the corner of the hole with the exit face; if fatigue loading was ‘high,’ cracks tended to nucleate at the bore of the hole, away from either the exit or entrance sides. The Burlat analytical results will also be compared to StressCheck® results below.

### 3 Technical Approach & Accomplishments in Phase I

The technical approach and accomplishments for this Phase I effort can essentially be subdivided into five (5) major categories:

1. Cold working of Holes in Aluminum Alloy
2. Measurement of Residual Stresses near Cold worked Holes
3. Fatigue Testing
4. Analytical Assessment of Residual Stresses
5. Holistic Life Predictions of Cold Worked Specimens

The activities in each are now described:

#### 3.1 Cold working of Holes in Aluminum Alloy

The National Research Council (NRC) of Canada manufactured all test specimens, both with and without cold working. NRC used a split mandrel cold working set produced by Fatigue Technology Incorporated (FTI) to introduce the cold working in the coupons. NRC manufactured fifteen (15) fatigue coupons (plate-with-hole geometry) from aluminum alloy 7075-T651 plate. Ten (10) of the coupons were cold worked using identical set of parameters (defined by the degree of cold work, nominally 4% of the initial diameter), and five (5) coupons did not receive any cold work treatment. Each coupon had the same nominal dimensions; the NRC drawing for these specimens is shown in Figure 2 below.

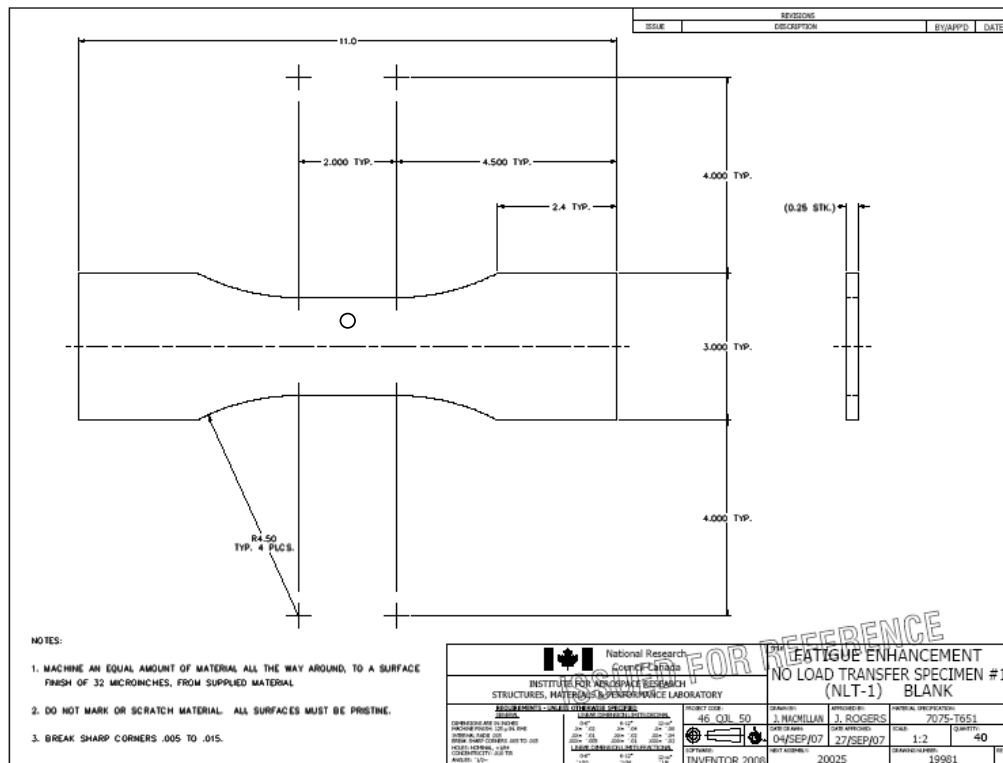


Figure 2. Fatigue Test Specimen Design. Dimensions in Inches.

Testing ten coupons that have been cold-worked using identical parameters allowed us to characterize the repeatability of the process, the variability of the residual stresses across the thickness, and the scatter in the residual stress measurements as provided by XRD and the alternative technologies discussed below. Numerical simulations of cold-working process showed that it does not produce a uniform stress distribution through the thickness; Shi, et al (2007) for instance conducted parametric studies using elastic-plastic FEA and found considerably differences in residual stress on the entrance side of the hole compared to residual stresses on the mid-plane and exit side of the hole, especially in greater thicknesses such as the 0.25 inch material being considered here. The five untreated coupons will provide the baseline fatigue data necessary for calibrating the crack growth models and for demonstrating the relative impact of the cold-work process.

### **3.2 Measurement of Residual Stresses near Cold worked Holes**

Four different technologies were used to quantify residual stress on the 10 cold-worked coupons described in the previous section and in the next sections:

1. X-ray diffraction
2. Digital image correlation, DIC
3. DMI optical strain gauges
4. Bolt hole and surface eddy current

Many of these techniques for residual stress quantification (RSQ) are not compatible. (compatibility issues between RSQ methods are highlighted in Table 1), thus a larger number of specimens were tested even though there is only one particular test condition. APES considered it important to capture:

- The variability in the stress/strain measurements for one particular cold-work process with replicates. (The differences due to cold-work levels, edge margins, test stresses, and load spectra were determined and developed as models progress successfully)
- Determine the capabilities of the NDI to quantify the stress/strain relationships, correlate the results of NDI methods, and gain insight into their state-or-readiness for cold work hole applications.

The team originally desired using Neutron Diffraction (ND) as well, but budget limitations would not allow for it in Phase I, as each specimen analysis costs up to \$10,000. In fact, residual stress analysis using XRD would not have been possible in the Phase I if not for a significant cost share between team member NRC and PROTO (who does the actual XRD measurements).

Table 1 Summary of Possible Compatibility Issues between Various RSQ Methods.

|                        | X-Ray Diffraction | DIC  | DMI Strain   | Surface Eddy Current  | Bolt hole Eddy Current |
|------------------------|-------------------|--|--|---|------------------------|
| X-Ray Diffraction      | Expensive \$\$    | X-ray cannot be performed with DIC in place. Paint would have to be removed prior to X-ray, so strain relaxation cannot be measured during fatigue by DIC. | DMI gauges cannot be installed on X-ray coupons prior to cold-work and X-ray measurements. DMI strain would only measure relaxation. | No issues   | No issues              |
| DIC                    |                   |  | DIC and DMI cannot be on the same specimen at the same time. DIC paint would have to be removed prior to putting down DMI gauges     | DIC paint could interfere with eddy current signal (Dave??).  | No issues              |
| DMI Strain             |                   |  |  | If DMI gauges are metallic, surface eddy current could still work, but there may be probe liftoff issues. | No issues              |
| Surface Eddy Current   |                   |  |  |   | No issues              |
| Bolt hole Eddy Current |                   |  |  |   |                        |

In Table 1, it is clear that X-ray diffraction (besides being expensive) has compatibility issues with any RSQ method that requires a surface coating or bonded instrumentation. There are no compatibility issues between XRD and the eddy current techniques.

Likewise, the surface eddy current techniques might have difficulties working with the DIC paint. The DMI gauges, if they are not conducting, will definitely interfere with the surface eddy current measurements. Even if they are metallic, there could be some probe liftoff issues.

Bolt hole eddy current does not have compatibility issues with any of the other techniques, since the others are not applied down the bore of the hole.

With these various issues in mind, the following test matrix was been designed to produce the maximum amount of information with the minimum amount of compatibility issues:

- Group A, 5 coupons: No cold work. Baseline fatigue only. DMI gauges may be of value here to observe peak spectrum effects; however, they were not used to monitor Group A coupons.
- Group B, 5 coupons. DIC paint, cold work, DIC image capture, strip paint, X-ray, fatigue test and conduct surface and bolt hole eddy current during fatigue. (option: install small DMI gauges on opposite side of hole, so on front of specimen EC left side and DMI right side, and with EC right side and DMI left on back of specimen.)
- Group C, 5 coupons: DMI gauge install front and back, cold work, initial DMI strain read, fatigue test and take subsequent DMI readings and bolt hole eddy current readings (+ surface if possible).

### 3.2.1 X-Ray Diffraction (XRD)

This task was completed with the assistance of the National Research Council of Canada (NRC). NRC has the necessary equipment to conduct XRD; however, they elected to contract with PROTO's X-ray diffraction capability to make the residual stress measurements. XRD was used to quantify residual stress in five (5) cold worked coupons. Residual stress profiles of the five coupons were compared with each other to quantify variability in the cold work process and to provide a baseline for comparing to the alternate technologies. Due to the excessive cost of this

technique (\$500 for each data point), residual stresses were measured at only 24 points on each coupon—this may sound like a lot, until you consider that this number represented 12 widely spaced points on each side (entrance and exit), on rays originating at the hole and going in 3 directions (from the hole to near side of the gage section, from the hole to the far side of the gage section, and from the hole ‘left’ as you are looking down on the flat face of the coupon).

PROTO made stress measurements due to cold working in 3 different directions on the coupon design in Figure 3: 1) from the hole edge to the short side—called the Top Profile, 2) from the hole edge to the far side in Figure 1 (from the hole leftward)—called the Bottom Profile, and 3) from the hole edge towards the load application point, called the Left Profile (up on Figure 3). In addition, the XRD measurements were made on the two faces, which are labeled “Entrance Side” and “Exit Side,” which correspond to the Entrance and Exit sides of the cold working process. The variation in measurements using the XRD technique is shown in Figure 4.

**Locations for taking XRD measurements  
(both entrance and exit sides)**

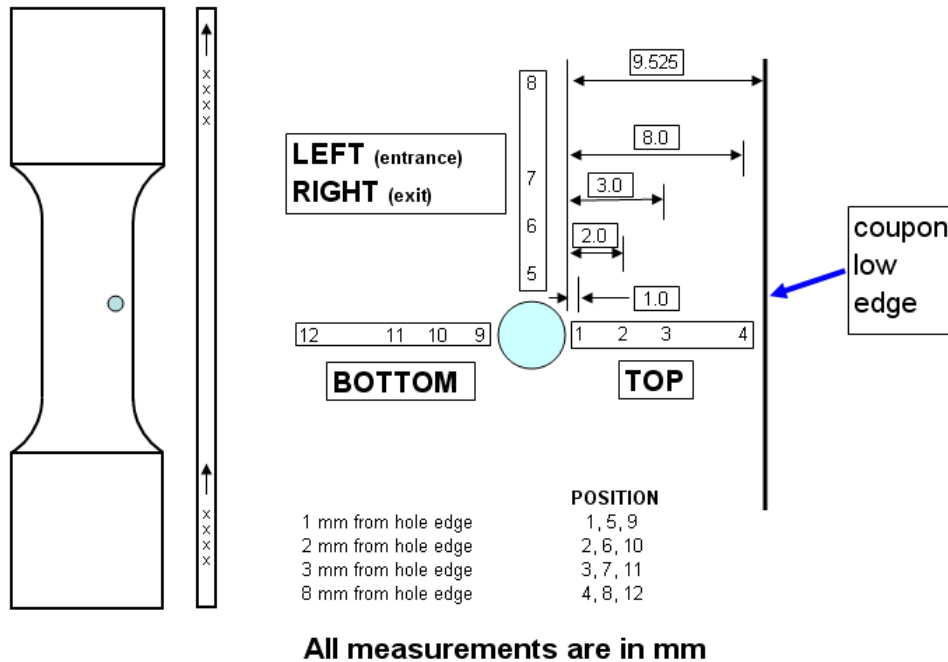


Figure 3. X-Ray Diffraction (XRD) Specimen Nomenclature.

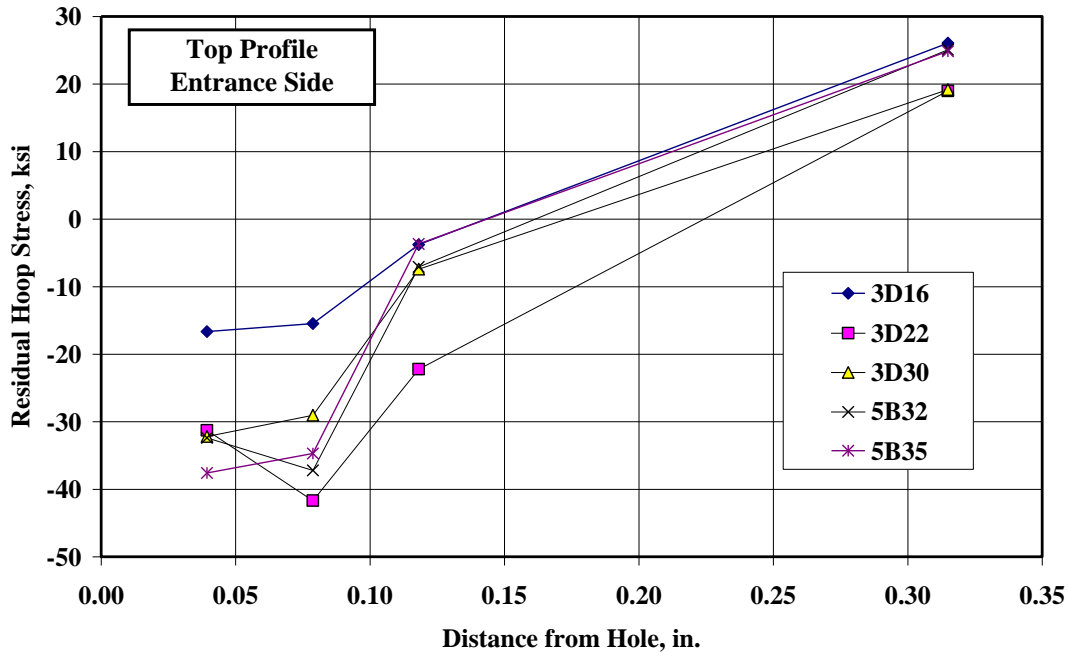


Figure 4. X-Ray Diffraction (XRD) Measurement Variability for 5 Specimens. Entrance Side.

There appears to be a remarkable consistency in the measurements, EXCEPT for coupon 3D16, which has a residual stress at the initial point ( $x=0.04$  in.) about half (-15 ksi) of the other 4 coupons (about -30 ksi). The results of Figure 4 are typical of the variations seen in the other measurements: exit side, left profiles, and bottom profiles. These measurements suggested another use for the DMI gages or calibrated eddy current techniques; namely, DMI gages might be useful for measuring the variability of the cold working process, and might suggest either reworking of the hole might be necessary to improve the quality of the cold working on a particular hole. This turned out to be more challenging task than anticipated—though DMI gages were used on 5 coupons in the fatigue test program, problems with placement of the gages prior to cold working resulted in gages being damaged and, in two cases, gages did not remain adhered to the surface, so had to be replaced before starting the fatigue test program, resulting in complete loss of information about the residual strains due to cold working on those coupons.

As mentioned above, six (6) profiles of residual stresses were given for each coupon—3 profiles (Top Line (marked TLP), Left Line (marked LLP), and Bottom Line (marked BLP)) each on the Exit and Entrance sides of each coupon. This allowed us to judge variability from Exit to Entrance side, variability between coupons that have been cold worked to the same level, and variability due to location on the coupon sides as a function of azimuth relative to the hole. A comparison of Figure 4 (TLP Entrance side) above with (TLP Exit side) below reveal representative levels of differences between the Exit and Entrance side hoop stresses—there is large variability even in the relative ratio of the (magnitude of the) Entrance to the (magnitude of the) Exit side across all 5 coupons, with a mean Entrance to Exit side measurement of 0.72 and a Coefficient of Variation (COV) of 84% in that ratio. The maximum ratio was 447%, the minimum ratio was 1.5%.

Because the coupons were not symmetric (the cold worked holes were offset a small amount so that the holes were closer to one free edge in the gage section than they were to the other free

edge), we expected and subsequently observed some variability in the residual stress measurements due to the azimuth used for the line profile, Figure 6 below, which shows the variability on the Entrance side for coupon 3D16. Across all 5 coupons, the mean ratio of the TLP to the BLP was 1.84, with COV of 136%; the mean ratio of the TLP to the LLP was 2.07, with COV of 177%.

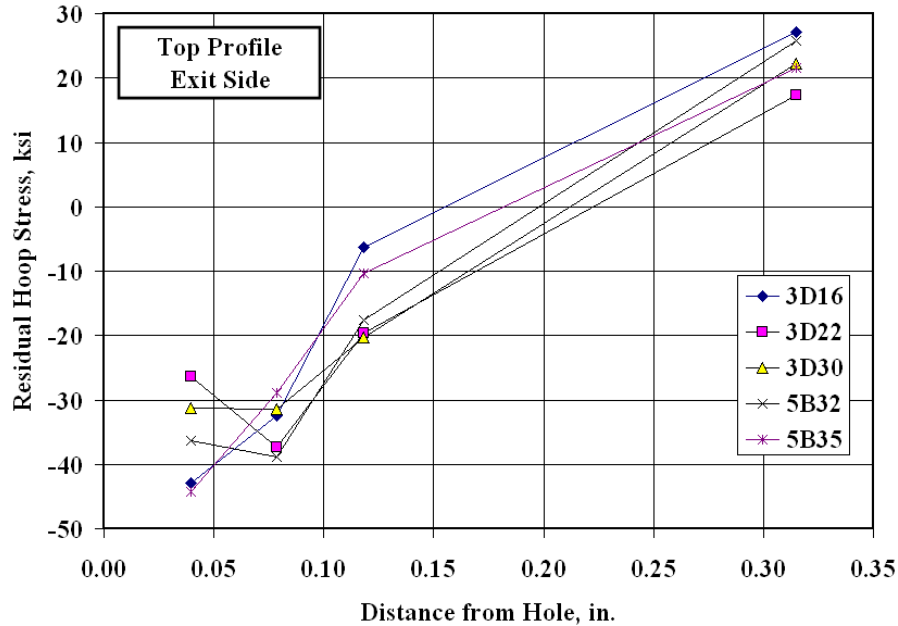


Figure 5. X-Ray Diffraction (XRD) Measurement Variability for 5 Specimens. Exit Side.

The computed radial and hoop stresses are compared to the XRD measurements in Figure 7. There are many significant differences between the computations and the XRD measurements. In particular, concentrating on the hoop stress alone, since hoop stress is the stress that would drive crack propagation, the minimum (or maximum compressive) computed hoop stress is about -20 ksi, while the XRD measured minimum hoop stress is -32 ksi. The location of the minimum hoop stress is about the same, in the range of 0.06 in. to 0.09 in. from the hole edge.

While it would have been ideal to be able to take subsequent XRD readings at intervals during fatigue loading, it was not practical to do this during Phase I, as the XRD is expensive, and the XRD laboratory is far removed from the fatigue testing laboratory; taking intermediate XRD reading would cause considerable delays in the testing program. A summary of the Residual Stress Measurement test matrix, executed by TRI-Austin is found in Table 2 below.

Table 2. Residual Stress Measurement Test Matrix.

| Group | Coldworking Level | NDI Method   | Replicates |
|-------|-------------------|--------------|------------|
| 1     | None              | None         | 5          |
| 2     | Nominal           | DIC, XRD, EC | 5          |
| 3     | Nominal           | DMI, EC      | 5          |

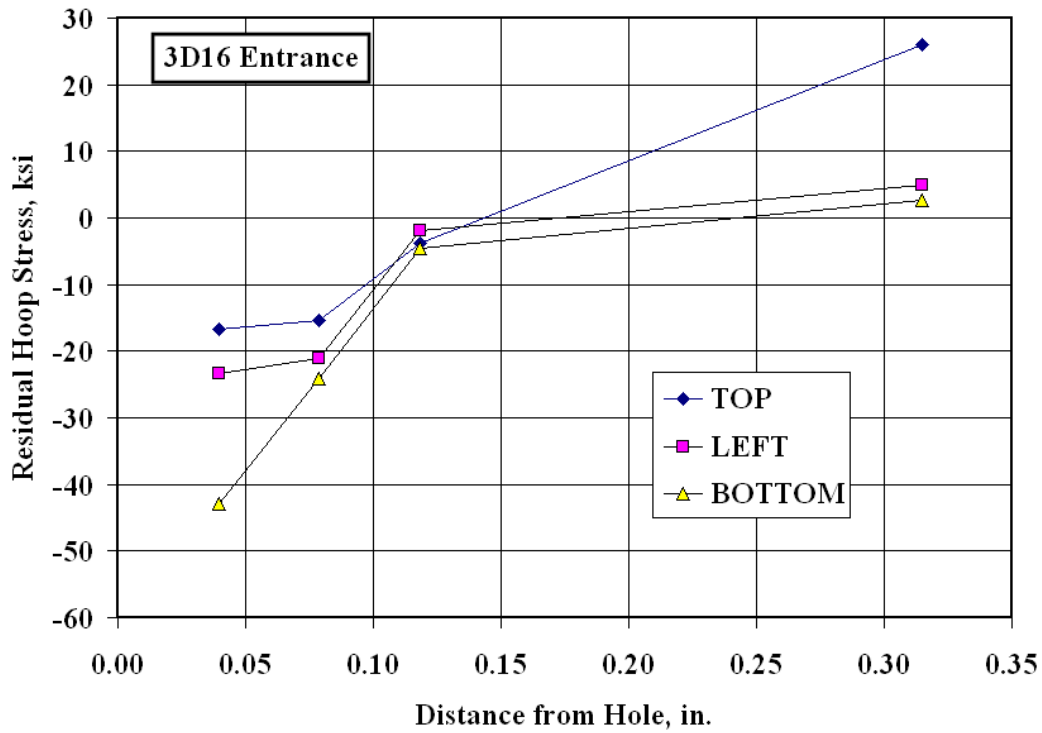


Figure 6. X-Ray Diffraction (XRD) Measurement Variability for 3 Line Profiles. Coupon 3D 16, Entrance Side.

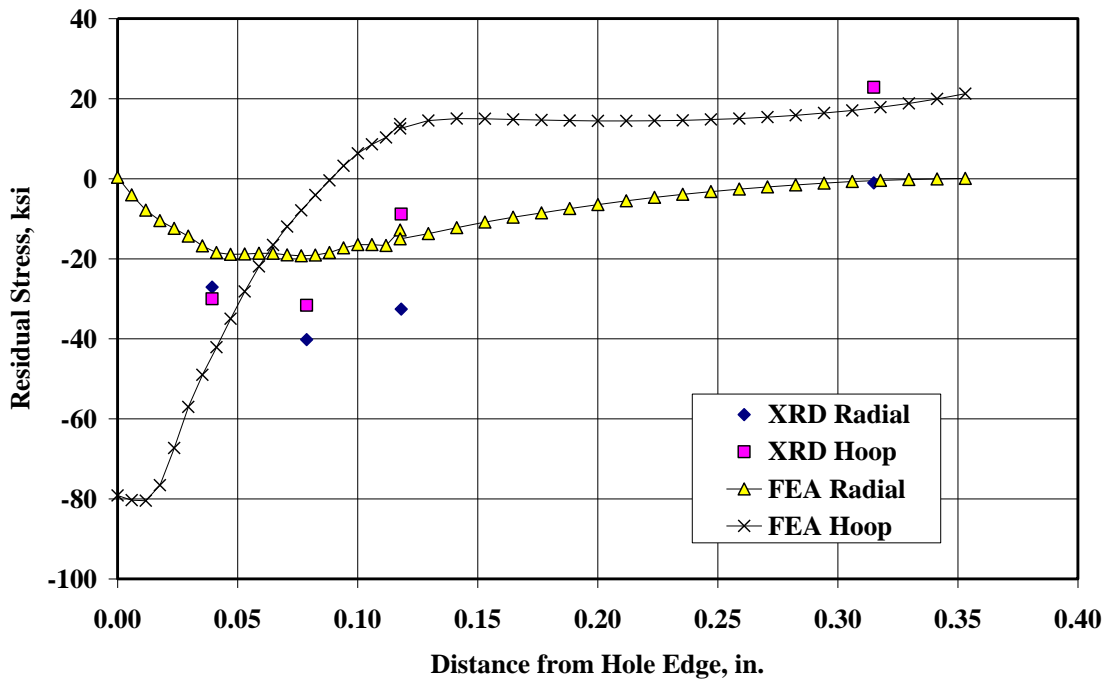


Figure 7. Comparison of StressCheck® Computations with XRD Measurements.

The complete set of XRD data taken for this project is found in the Appendix.

A summary of our findings is found below.

#### FINDINGS:

- Results indicate X-ray diffraction (XRD) provides reasonably well-behaved profiles of “computed stress”.
- There is large variability even in the relative ratio of the (magnitude of the) Entrance to the (magnitude of the) Exit side across all 5 coupons, with a mean Entrance to Exit side measurement of 0.72 and a Coefficient of Variation (COV) of 84% in that ratio. The maximum ratio was 447%; the minimum ratio was 1.5%.
- Residual stress results could be improved by selecting specimen and measurements more closely spaced to provide more accurate distribution definition.
- The biggest advantage of the XRD technique is the perceived accuracy of the stress measurements; however, APES is not an expert in the XRD technique, so is not in a position to judge the merits of that statement. It is notable that of all the XRD papers in the open literature that were reviewed, not a single author questioned the accuracy of the XRD measurements. Another advantage of the XRD technique is that stresses are the result of the measurements; stresses are needed in particular for the crack growth analysis tools.
- A significant disadvantage of the XRD technique is the perceived cost—PROTO measured residual stresses on the two sides of 5 coupons, and provided 3 line profiles on each side (for a total of  $5 \times 2 \times 3 = 30$  profiles). However, there were only 4 points on each line profiles (that is, 120 total XRD measurements across 5 coupons), which is probably inadequate spatial resolution for the purposes of a detailed crack growth analysis.

#### 3.2.2 Digital Image Correlation (DIC)

In the DIC technique, strain measurements due to cold working were made by: 1) speckling paint on the surfaces of the coupons, Figure 8, 2) taking an image of the surfaces near the hole, 3) performing the cold working operation, 4) taking another image of the surfaces near the hole, and 5) then comparing the two images. The difference between the two images is the residual strain caused by the cold working process. Subsequently, NRC-Canada provided color contours of principal strains on both exit and entrance sides, and spreadsheets with line profiles of the strains from the hole edge in 3 different directions: 1) from the hole edge to the short side in Figure 3 (from the hole leftward)—called the Top Line Profile, 2) from the hole edge to the far side in Figure 3 (from the hole leftward)—called the Bottom Line Profile, and 3) from the hole edge towards the load -application point in Figure 3 (from the hole downward)—called the Left Line Profile. Note that “Right Line Profiles” (RLP)—which go in the direction opposite of that of the LLP, were also given to us by NRC-Canada for this project. All DIC data is plotted in figures of the Appendix to this report.

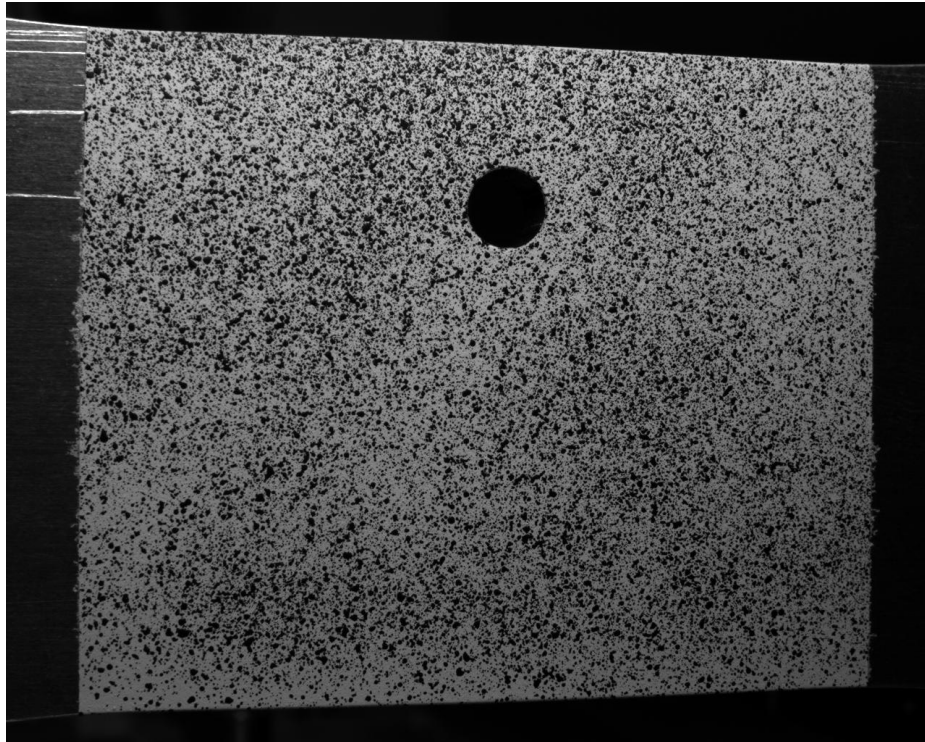


*Figure 8. Typical Image of Speckled Paint on Test Specimen.*

The residual strains averaged across all 5 coupons are shown in Figure 9 (Top Line Profile), Figure 10 (Left Line Profile), and Figure 11 (Bottom Line Profile). The variation in measurements using this technique is shown in Figure 12. NRC, which performed the DIC measurements, thinks variation seen in Figure 12 are due to variability in the cold working process itself (same cold working levels on different coupons result in variability in stresses/strains that are measured with the DIC technique).

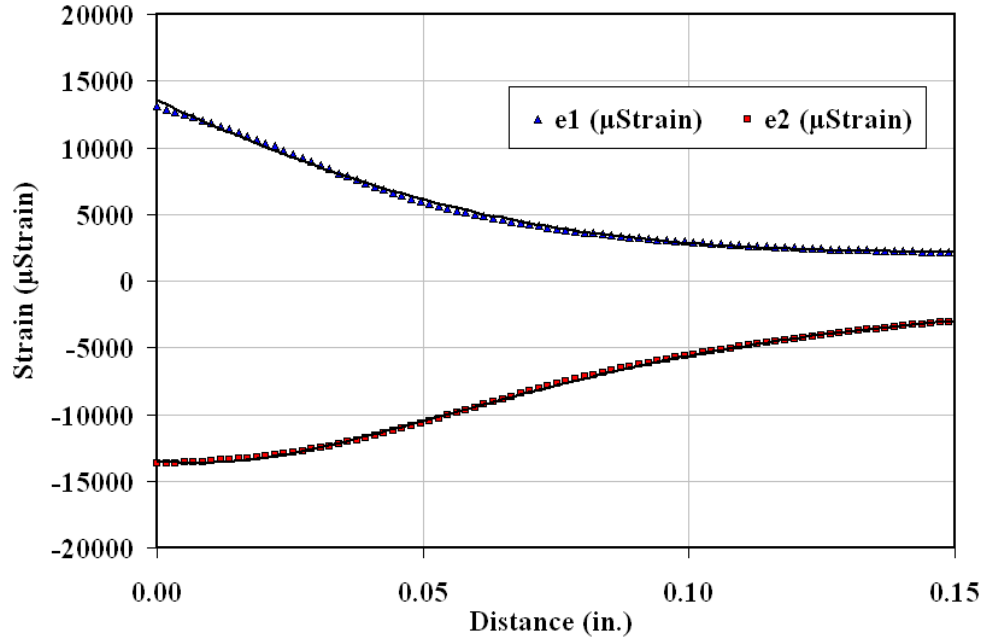


Figure 9. Measurement of Maximum ( $e1$ ) and Minimum ( $e2$ ) Principal Strains With Digital Image Correlation. Shown is Top Line Profile. Entrance Side.

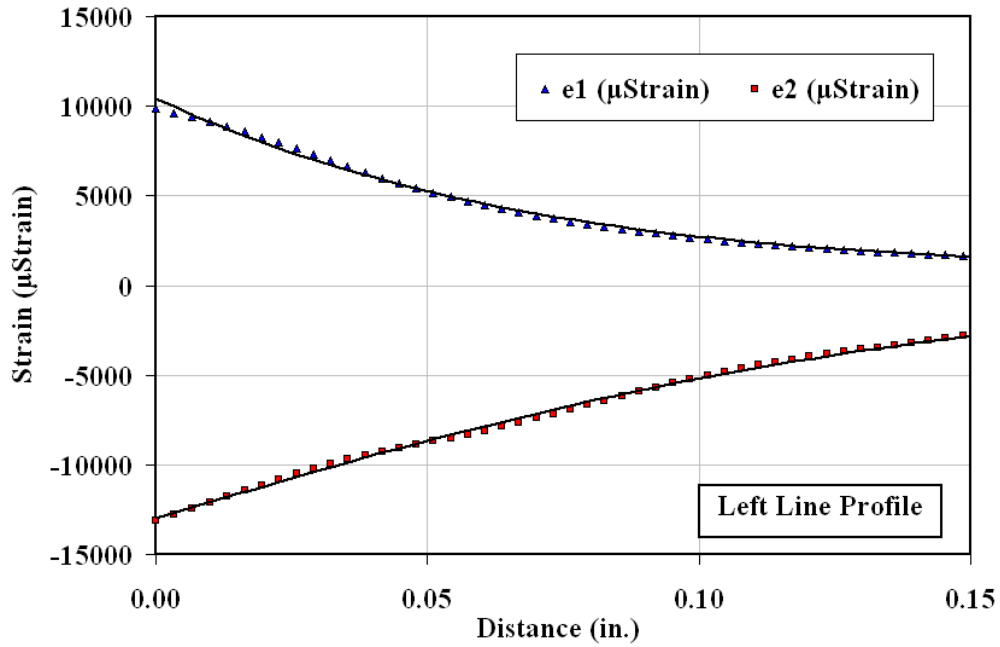


Figure 10. Measurement of Maximum ( $e1$ ) and Minimum ( $e2$ ) Principal Strains With Digital Image Correlation. Shown is Left Line Profile. Entrance Side.

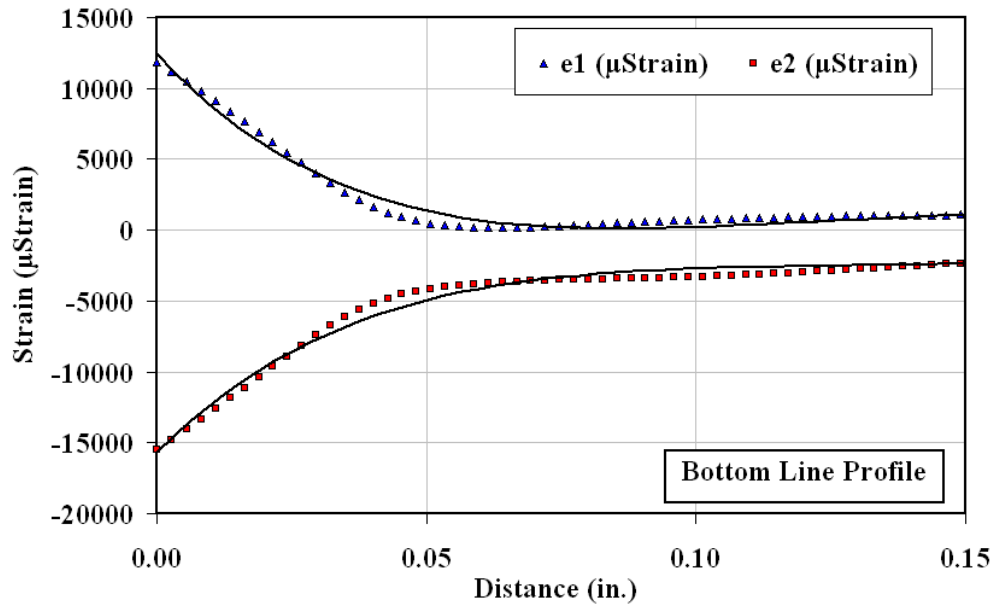


Figure 11. Measurement of Maximum ( $e1$ ) and Minimum ( $e2$ ) Principal Strains With Digital Image Correlation. Shown is Bottom Line Profile. Entrance Side.

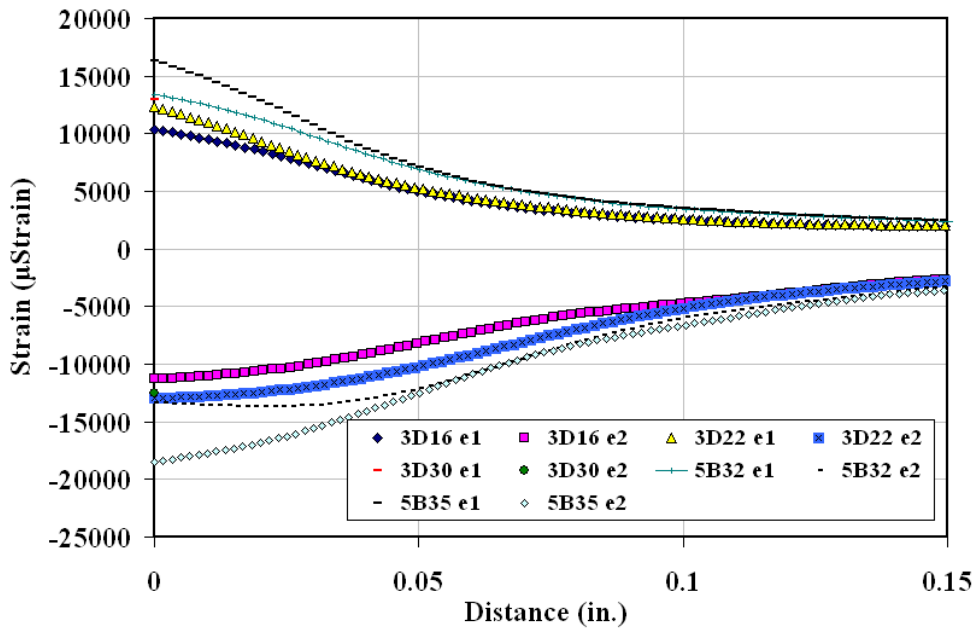


Figure 12. Scatter in Maximum ( $e1$ ) and Minimum ( $e2$ ) Principal Strain Measurements with Digital Image Correlation. Shown is Top Line Profile.

A representative color contour of the maximum principal strain on Coupon 3D16 is shown in Figure 13 below.

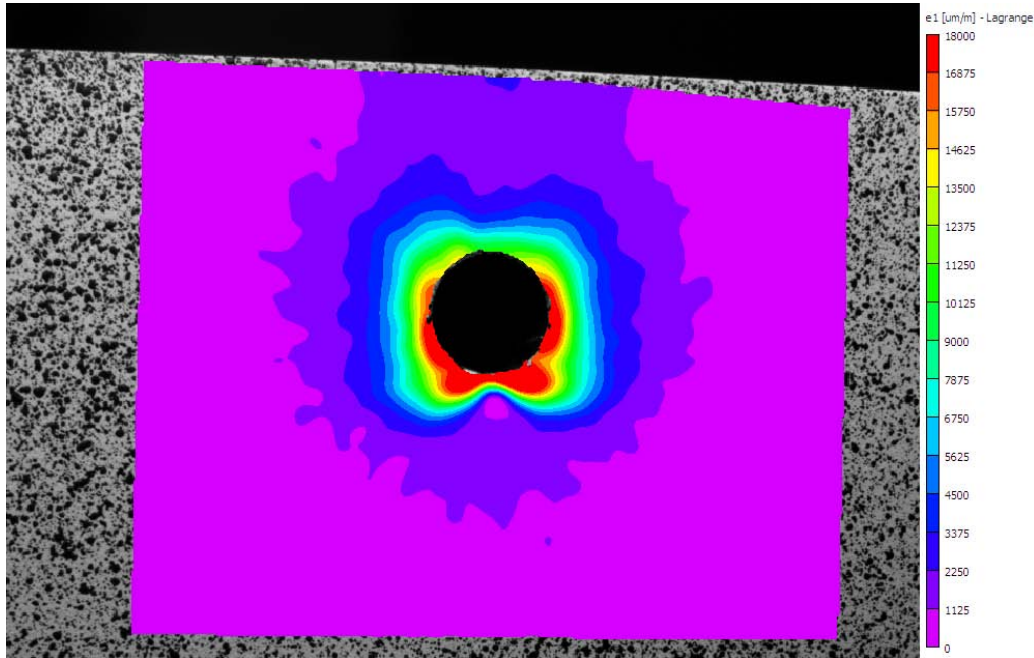


Figure 13. Color Contour of the Measurement of Maximum ( $e_1$ ) Principal Strain With Digital Image Correlation; Entrance Face.

For comparison to measured results, the nominal 4% cold working of the offset hole coupons was simulated with the StressCheck<sup>®</sup>, ESRD, Inc. (2008) incremental plasticity capability, with the material constants Young’s modulus  $E = 10,000 \text{ ksi}$ , Poisson ratio  $\nu = 0.3$ ,  $n = 32$ , and  $\sigma_{yield} = 70 \text{ ksi}$ , was used (since a Ramberg Osgood material curve was used to fit the monotonic stress-strain behavior, only isotropic hardening was available; if kinematic hardening is desired, one must use a bilinear stress-strain relation—this constraint is typical of many commercial FEA codes). All finite element simulations were in two dimensions (2D). Principal Strains  $e_1$  and  $e_2$  were computed and plotted against the averaged (over 5 coupons) exit and entrance line profiles for the top, left and bottom line profiles as measured with the DIC method. Figure 14 and Figure 15 show the results (note the strains are “microstrains” or “ $\mu\text{strains}$ ”, that is,  $1.0\text{E}6$  times the actual strain) for maximum Principal Strain  $e_1$ . When comparing DIC results with 2D FEA results, it might be worthwhile to keep in mind that the DIC measures strains on the two surfaces, the entrance and exit planes, while the 2D FEA results are generally similar to the middle plane results (which cannot be measured by the DIC technique). The residual strains computed with the 2D FEA appear to be not far away from the strains on either the exit or entrance planes, with some notable differences--near the hole edge, for instance, the FEA computed strain  $e_1$  is up to twice as large as the measured strain. The Exit plane results are significantly better; however, the FEA computed  $e_1$  for the “Left Line Profile” (LLP) are about half the measured LLP. The averaged Top Line Profiles from the Entrance and Exit sides are compared to the FE computed residual strains in Figure 16.

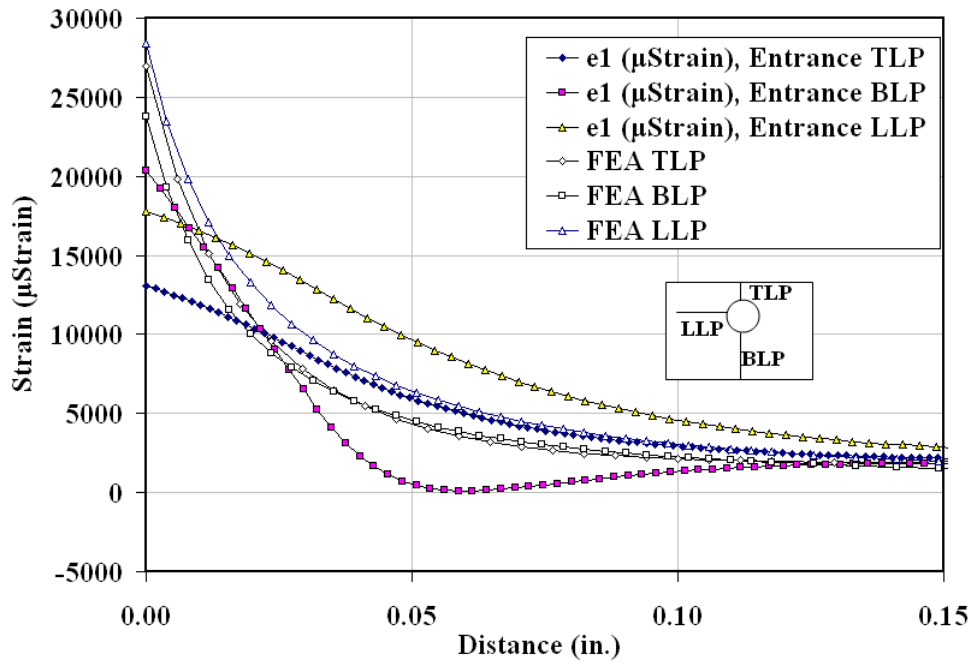


Figure 14. Digital Image Correlation (DIC) Measurement Averaged over 5 Specimens are Compared to Finite Element Analysis (FEA) Results. Entrance Line Profiles.

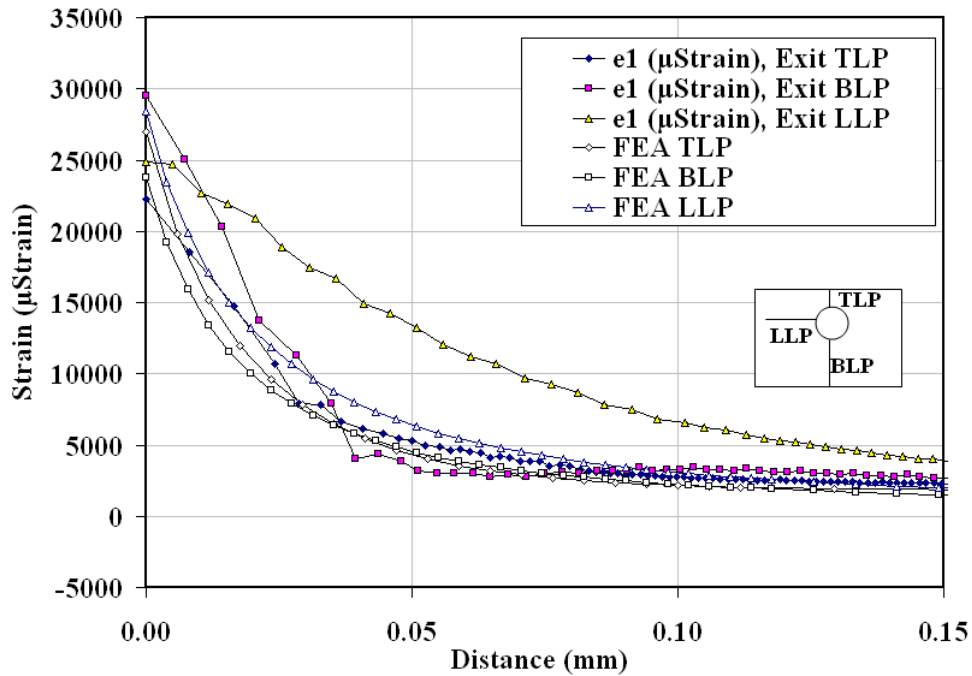


Figure 15. Digital Image Correlation (DIC) Measurement Averaged over 5 Specimens are Compared to Finite Element Analysis (FEA) Results. Exit Line Profiles.

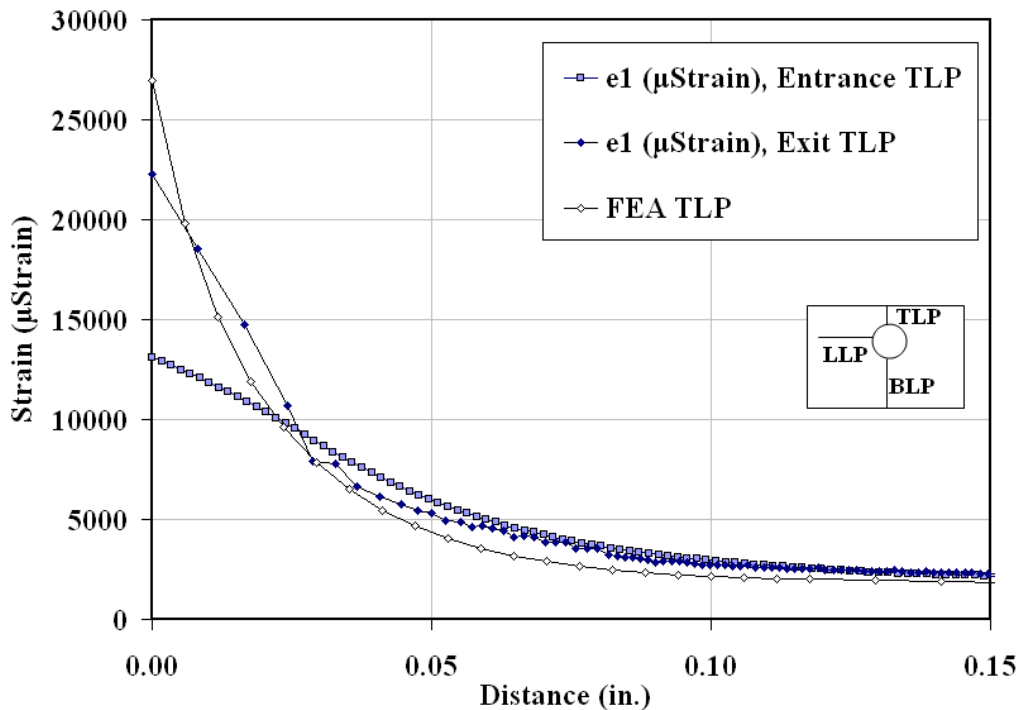


Figure 16. Entrance and Exit Line Profiles (Averaged over 5 Specimens) Using Digital Image Correlation (DIC) Measurement Compared to Finite Element Analysis (FEA) Results.

A summary of our findings is found below.

#### FINDINGS:

- Results indicate DIC provides resolution of approximately 0.0016 to 0.0040 in. (0.04 to 0.10 millimeters).
- It was difficult to characterize the statistical variation in the measurements other than by using visual inspection—measurement points (relative to the hole edges) were not consistent between specimens.
- The Entrance and Exit side averaged strains (over 5 coupons) were reasonably close to each other. Finite element analyses (FEA) compared reasonably well to the measured DIC profiles for distances greater than 0.0276 inches (0.7 mm) from the hole edges, but compared poorly inside of 0.0276 in. (near the hole edge, that is, where much of the crack growth occurs).
- The advantage of the DIC method is the small cost relative to other residual stress or strain measurement techniques (such as XRD). The disadvantage is that the DIC method yields nonlinear strains, while stresses are the quantity needed for the crack growth analyses.
- The strains as computed with finite element analyses of the Cold worked hole compared reasonably well with the DIC strain measurements.

### **3.2.3 Direct Measurements, Inc. (DMI) Optical Strain Gages**

The DMI Strain Measurement System was used for residual stress measurements made during fatigue testing in this program (actually, the DMI gages measure residual strain, not residual stress, an important distinction, as it is difficult to transform nonlinear, plastic strains to nonlinear stresses without an analytical tool such as finite element analysis software, which may or may not be able to simulate reality well for highly nonlinear mechanical systems such as cold worked structures). The DMI system is essentially an optical strain gage, using an optical reader to measure deformations of dot patterns, Direct Measurements, Inc. (2008). A cellophane tape-thin square gage (with the dot patterns located in the frame of the square) is glued to a flat part of the test specimen, with the hole in the middle (the hole can be drilled either before or after the square has been attached to the surface of the specimen).

This strain measurement system, using well established concepts, is a relatively new development in the Non destructive inspection (NDI) industry and is being exploited more fully each day. Though new and relatively untested, it is quite promising, offering significant advantages over currently accepted NDI techniques in the aviation industry: low cost, low impact to current maintenance procedures being the two most significant advantages. The gage for this system can be considered an optical strain measurement technique, as an optical reader is used to measure the deformations of the gage—an area (or length) averaged strain can then be calculated. However, the gage is much less intrusive than a typical strain gage, which uses changes in electrical resistance of a thin wire to measure deformation and then calculate a length averaged strain. Typical strain gages have wires attached to them which go to the data acquisition system; wires can and do disconnect from their moorings, thereby making the strain measurements invalid.

DMI results thus far appear to have shown that the DMI strain gage is capable of measuring the residual strains due to cold working. Further, the results when compared to the photoelastic fringe pattern illustrate that the cold working process is not always symmetrical and the maximum compressive strains occur at the inner boundary of the hole and decay rapidly as the distance from the hole boundary. These variations in strains around the circumference of the hole prompted DMI to develop a circular gage capable of measuring this variation around the hole boundary, Figure 17 below. The gage is segmented in twelve equal segments around the inner and outer boundary. This will allow for twelve values of circumferential and radial strain components to be measured. However, as of the end of Phase I, the software to interpret the strain measurements in the circular gages was not available as promised.

DMI gage measurements and summarized FINDINGS are discussed in the Section 3.3.2 Monitoring of the Residual Stress Field on the Fatigue Coupons.

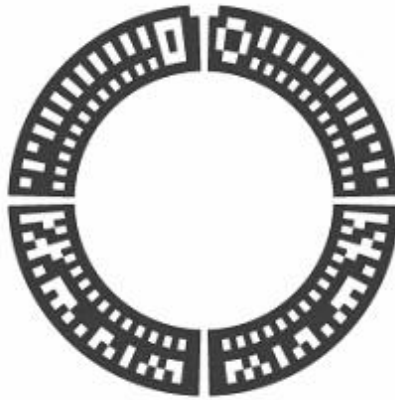


Figure 17. Round DMI Gage Should Be More Suitable for Cold working Measurements than Linear Gages.

### 3.2.4 Bolt Hole and Surface Eddy Current

Eddy current (ET) methods for conductivity measurement were investigated for their potential to be used for quality control of the cold working process and time and stress induced relaxation of residual stresses introduced by the cold working process. Both experiments and modeling were performed during Phase I.

The purpose of the ET modeling work was to determine the volume of material that would be "inspected" by the ET conductivity probes. Standard commercial-off-the-shelf (COTS) probes and instruments were used in the Phase I effort for two reasons: the limited time and scope of a Phase I program, and the deployment of ET technology would be easiest if it could provide information about the cold working of the holes using COTS equipment.

The COTS equipment, a Nortec 500D instrument and Nortec conductivity probe, was used to perform spot checks of conductivity on the surface of test specimens up to the edge of the hole. *With this system, there was no measurable change in conductivity between cold worked and non-cold worked holes.* Modeling was used to evaluate the sensitivity of the probe design to the geometry and lift off. Liftoff did not appear to be an issue. It is difficult to determine if the electromagnetic (EM) field from the probe was optimal for the measurement, since the change in conductivity for this case is not known accurately.

More sophisticated ET probes were used with a robotic manipulator to determine if a more sensitive ET system could at least differentiate between cold worked and non-cold worked holes. These inspections showed some sensitivity to the cold work process, but difficulties with geometry were also encountered. Out of this investigation, a potential simple test for cold working was identified: the deformation caused by the process is detectable via the "lift off" eddy current signal. It is not known if this deformation relaxes along with the relaxation of residual stresses, however.

The attractiveness of ET methods for this problem is mostly due to the much lower cost relative to X-ray diffraction (XRD). Potential follow-on tasks for Phase II work include but are not limited to: better, 3D modeling of the ET probes, use of bolt hole ET probes to characterize stresses inside the hole; and new probe designs to reduce undesirable geometrical effects.

### **3.3 Fatigue Testing**

#### **3.3.1 Fatigue Experiments on Baseline and Cold-Worked Coupons**

TRI Austin conducted fatigue experiments to establish both the baseline fatigue behavior (non cold-worked coupons) and the cold worked fatigue behavior. The original idea was to use mini-FALSTAFF as the load sequence for the tests, but analytical studies of baseline (non cold-worked) coupons showed that even at a maximum gauge section stress (just upwind of the hole) of 37 ksi, life could be expected to be over 500,000 cycles. This would of course push the cold-worked test lives out to greater than 5,000,000 cycles, which was deemed much too long for a Phase I test program. Instead, APES developed a self-marking load spectrum that used some of the primary stress levels (positive and negative) found in the mini-FALSTAFF spectrum. Use of a self-marking spectrum allowed APES to recreate the failure modes and crack growth history from the fracture surface with excellent results (discussed later). The use of this aggressive spectrum (particularly the number of peak load cycles and compressive load cycles) was designed to aggressively work the material in hopes that the mechanical loading could have detrimental effects to the cold work and cause the stress state to evolve.

APES has used the marker load technique on many programs to understand the evolution of fatigue damage and to demonstrate the importance of successfully modeling damage progression, rather than modeling just the end point (cycles to failure). Figure 18 through Figure 20 show the three substitute load spectra trailed on the baseline coupons, with the final spectrum (called V9) being the one used for all of the cold worked coupons.

The use of ten coupons cold-worked using identical parameters allowed us to begin to characterize the repeatability of the process and the scatter in the residual stress measurement as provided by XRD and the alternative technologies discussed earlier. One of the alternative technologies, the optical gauges produced by DMI, required that the gauge be bonded to the coupon prior to cold working, which would mask XRD technique on the surface around the hole where the gauge is applied. Thus, it was necessary to take the XRD readings on coupons that did NOT have DMI gages mounted on them.

Five untreated coupons provided the baseline fatigue data necessary for calibrating the crack growth models and for demonstrating the relative impact of the cold-work process.

All test specimens have the same geometry and load, . The fatigue test results are summarized in Table 3. This test program was executed by TRI-Austin, with specimen preparation performed at NRC in Ottawa.

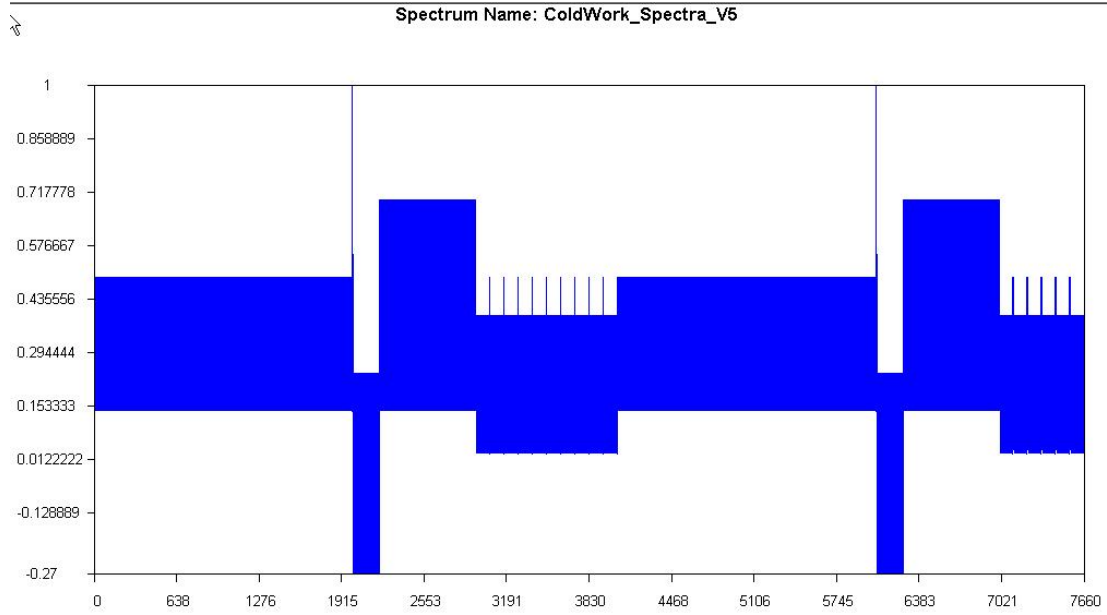


Figure 18. V5 spectrum used for the first baseline test (too mild).

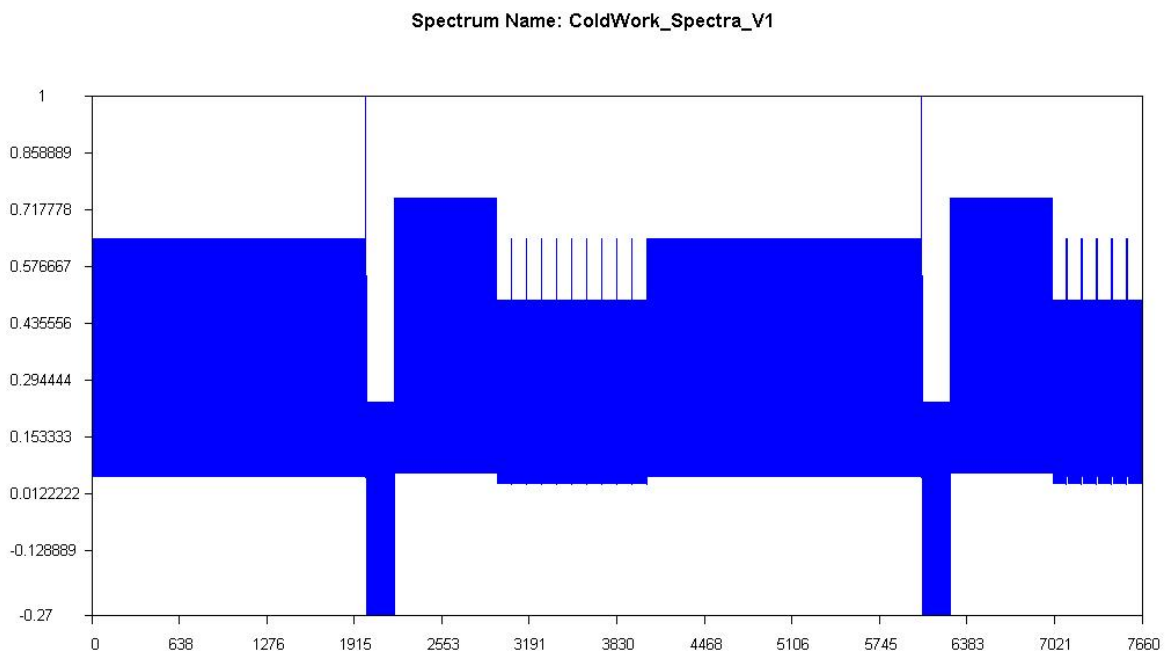


Figure 19. V1 spectrum used for second baseline tests (still too mild).

Spectrum Name: ColdWork\_Spectra\_V9

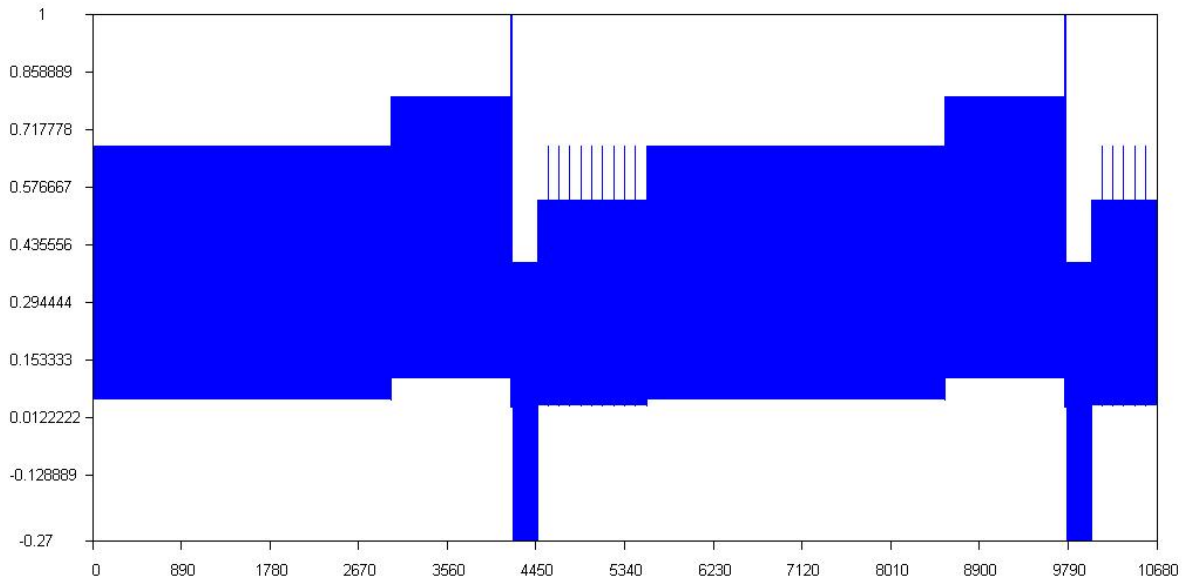


Figure 20. V9 spectrum used for baseline tests 3 - 5 (used for subsequent cold worked coupons).

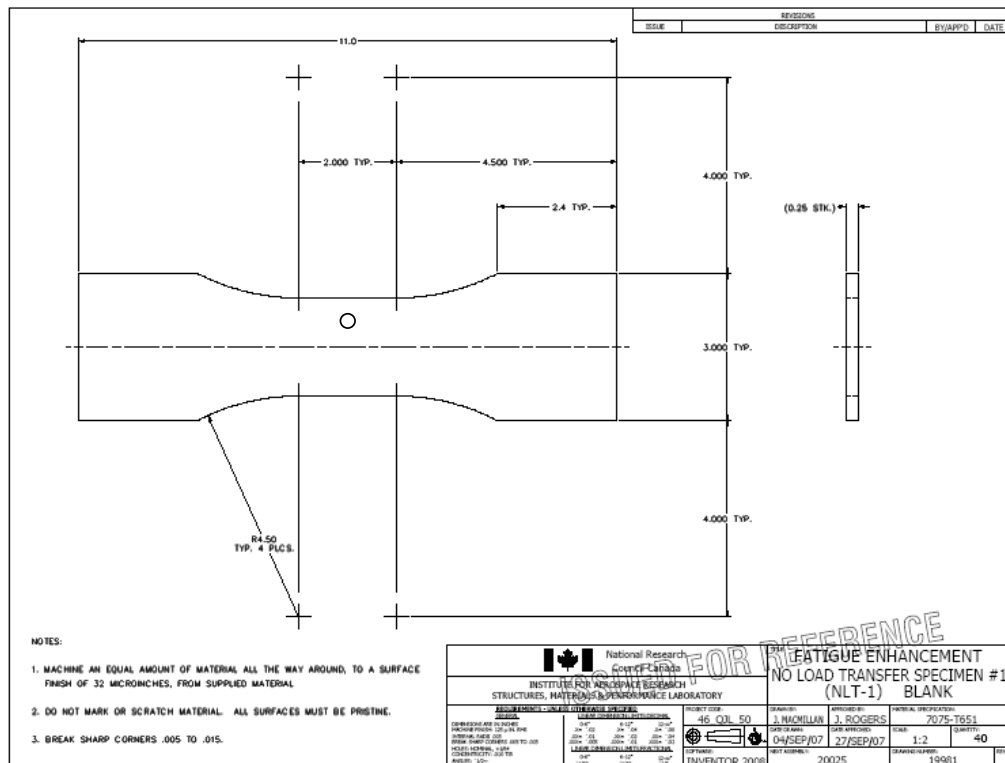


Figure 21. Fatigue Test Specimen Design.

Table 3. Fatigue Test Results.

| Coupon ID | Coldworking | Cycles to Failure | Max. Stress | Spectrum | Notes          |
|-----------|-------------|-------------------|-------------|----------|----------------|
| 5B19      | None        | 568,840           | 36          | V5       |                |
| 5B40      | None        | 201,151           | 36          | V1       |                |
| 5B25      | None        | 23,231            | 38          | V9       |                |
| 5B26      | None        | 25,219            | 37          | V9       |                |
| 3D12      | None        | 40,600            | 36          | V9       |                |
| 3D16      | 4% Nominal  | 399,360           | 37          | V9       |                |
| 3D22      | 4% Nominal  | 761,548           | 37          | V9       |                |
| 3D30      | 4% Nominal  | 484,493           | 37          | V9       |                |
| 5B32      | 4% Nominal  | 489,803           | 37          | V9       |                |
| 5B35      | 4% Nominal  | 164,036           | 37          | V9       |                |
| 5B16      | 4% Nominal  | 328,073           | 37          | V9       |                |
| 5B31      | 4% Nominal  | 606,796           | 37          | V9       |                |
| 5B33      | 4% Nominal  | <i>Not Tested</i> |             |          | Not Tested     |
| 5B39      | 4% Nominal  | 652,830           | 37          | V9       | Failed in grip |
| 5B41      | 4% Nominal  | <i>Not Tested</i> |             |          | Not Tested     |

For the 8 cold worked specimens, the average life was 485,867 cycles, with a standard deviation in life that was 39% of the average. For the 3 non-cold worked specimens tested with the V9 spectrum, the average life was 29,683 cycles, with a standard deviation in life that was 32% of the average (note however, they were all tested at slightly different maximum stresses).

A summary of our findings is found below.

**FINDINGS:**

- For the 8 cold worked specimens, the average life was 485,867 cycles, with a standard deviation in life that was 39% of the average. For the 3 non-cold worked specimens tested with the variable amplitude spectrum, the average life was 29,683 cycles; the standard deviation was 32% of the average.
- Though each coupon was designed to have the same conditions (cold working level and fatigue stresses), there was a large scatter in the results in the cold working coupons, perhaps as large or larger than coupons that were not cold worked.

### **3.3.2 Monitoring of the Residual Stress Field on the Fatigue Coupons**

Relaxation of residual stress due to thermal and/or mechanical loads is a phenomenon that requires careful consideration. For Phase II efforts, the focus will be to develop modeling techniques for stress relaxation under mechanical and thermal loads, but for Phase I, the emphasis was on using existing off-the-shelf technology to measure these changes and, if necessary, to develop a framework suitable for including these evolving stress fields into crack growth analyses. The experimental evidence points to little or no evolution of the residual stress field caused by fatigue stresses, though it is important to keep in mind that the experimental investigation was not exhaustive, consisting of only 10 coupons tested with the same cold working levels and fatigue spectrum. If the Phase II test program reveals evolving residual stress fields, then these changing stress fields will ultimately become an important element to model for establishing a holistic assessment framework for damage progression in cold-worked structure.

During the Phase I fatigue tests, the square DMI gages (the software to interpret the round gages were unavailable as stated previously) were monitored periodically, and occasionally EC and UT readings were to be taken to see how the residual stress fields are changing due to the influence of the mechanical loads; however, the EC and UT did not work at all, so were completely abandoned for the test program. To facilitate measurement and interpretation of the DMI gage readings at the TRI/Austin testing facility, Joah Gonzalez, TRI/Austin, and Craig Brooks traveled to the DMI research labs at University of South Carolina for training on the DMI system. APES purchased an optical reader for the Phase I and future programs at no cost to the customer. The system hardware and software appeared to be well tested and verified for the rectangular gauges, but not for the circular gages. As each gauge is uniquely identified by “bar codes” within the gage, the hardware and software recognize, identify, and process the data automatically based upon the unique number of each gauge. The inherent gage design allows inclusion of additional reference positions on the gauges for making strain measurements (although, this does not appear to be available in their present system package). This capability when exploited will allow for more readings and measurements over smaller areas of material and many more combinations of strain to evaluate effects of complex strain fields. The acquisition of data can either be manual; data is selected by the technician at a point at a desired time, or automated; a sequence of measurements for selected intervals can be made without technician triggering. This capability provides an efficient method for capturing strain levels at several points as the load is cycled, useful approach for comparing the time varying strains along with the evolution of the residual stresses introduced by the cold work process and especially when incorporated during incremental load sequence during testing of the specimen.

The general procedure for measuring residual strains in the DMI gages is to fatigue the coupons for a designated number of cycles, stop the fatigue test machine, and then load with a monotonically increasing load the strains at 3 points: 0% maximum load, 68% maximum load, and 100% maximum load. The strain nomenclature as found in the DMI reader is found in Figure 22 below.

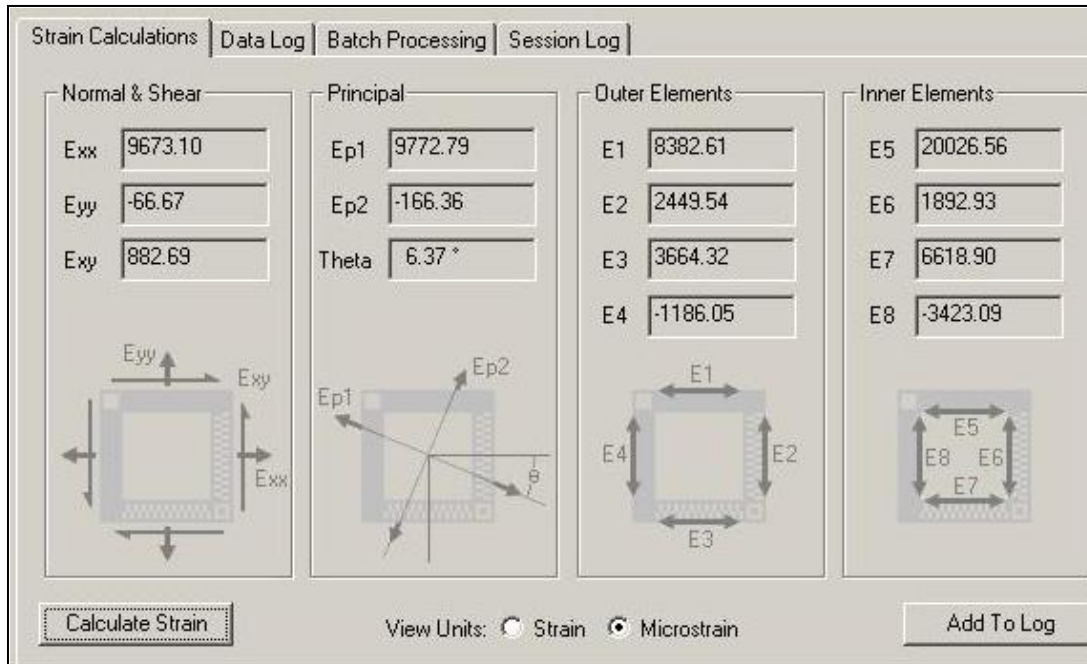


Figure 22. DMI Gage Strain Descriptions. “x” direction is perpendicular to load direction.

A representative result is shown in Figure 23 below, which shows the evolution of the stress  $E_{xx}$  in coupon 5B39 for over 600,000 fatigue cycles—this result, which was repeated over and over again for several coupons that we checked, indicates that there is very little if any residual strain evolution detected by the DMI gages from the initial to the final fatigue cycles. In fact, though DMI has shown these gages can detect crack growth, though there was obviously crack growth in these coupons during the 600,000+ cycles, no crack growth was apparently detected by the DMI gages.

Several difficulties were encountered with the DMI gages. The DMI gages were mounted on the coupons BEFORE the coupon holes were cold worked. Pictures of the gages as received by TRI/Austin indicated that the DMI gages could be misaligned relative to the cold worked holes, the hole edges could actually take a bite out of the DMI gages, and therefore damage the gages, and DMI gages could peel off the coupons if not seated properly—a typical example of the damage that can occur to the gage is shown in Figure 24 below, which shows a DMI gage on the Entrance side of Coupon 5B39 and is a perfect illustration of unforeseen problems that might affect the strain results—note the gage is not aligned properly relative to the hole, and that because of this misalignment, at least two of the inside edges are significantly damaged or possibly distorted.

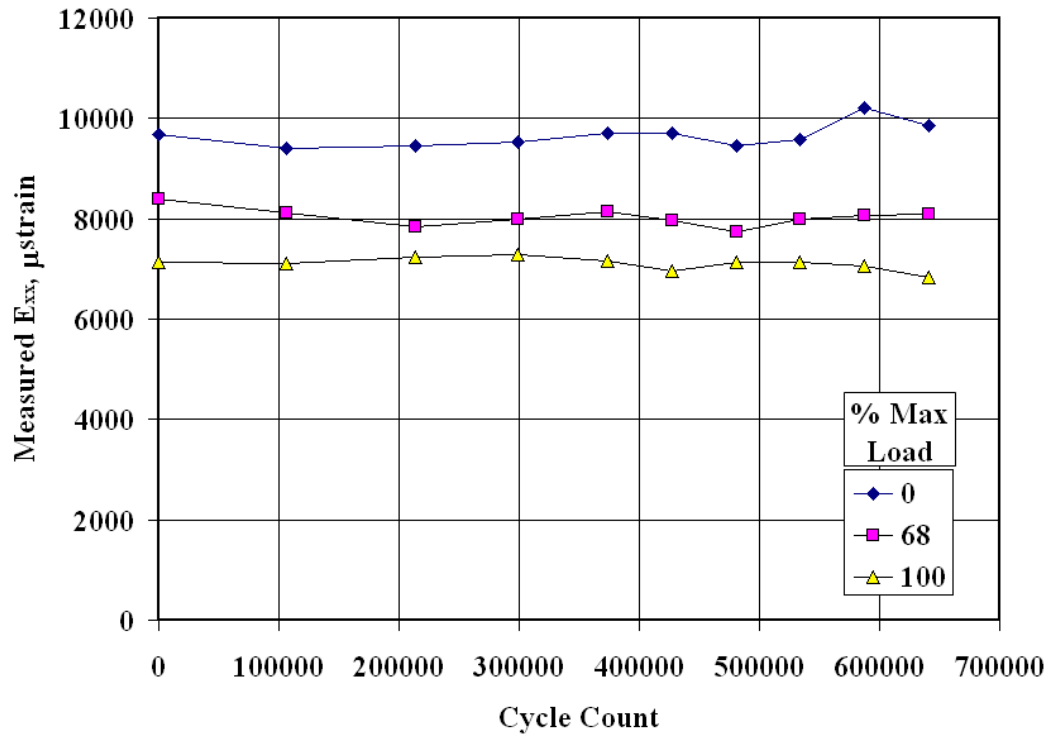


Figure 23. Evolution of the Strain  $E_{xx}$  During the Life of Cold Worked Coupon 5B39. Gage 49.

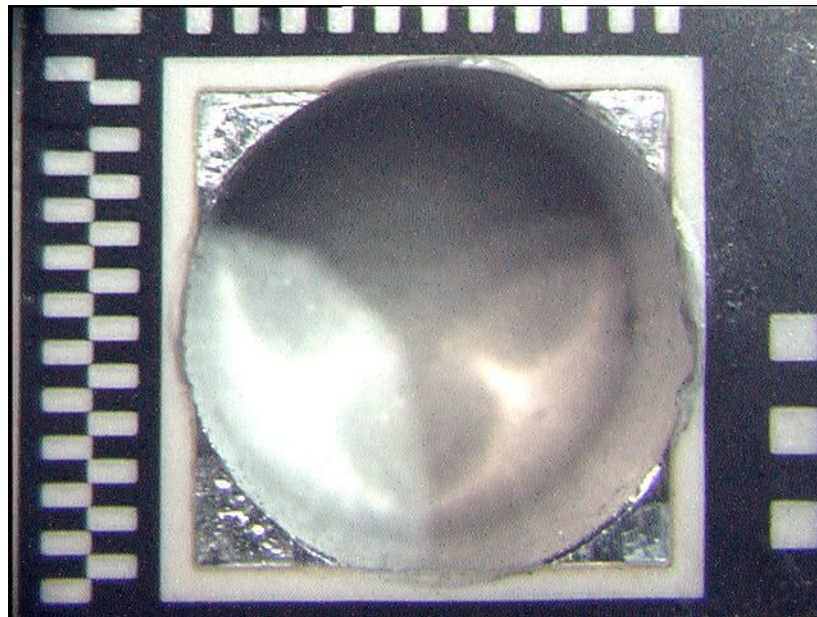


Figure 24. Coupon 5B39 with DMI Gage Mounted. Gage appears to be misaligned and at least 2 inside edges of the gage are distorted or damaged.

During this Phase I program, our experience with these gages show a 30% failure rate (3 of 10 failed or were otherwise unreadable), Table 4.

*Table 4. Summary of DMI Gage Readings.*

| <b>Coupon</b> | <b>Gage</b> | <b>Type</b> | <b>Location</b> | <b>Status as Indicated by DMI Personnel</b> |
|---------------|-------------|-------------|-----------------|---|
| 5B41          | 4           | Circular    | Entrance        | Undamaged                                   |
| 5B41          | 0           | Circular    | Exit            | Damaged; unreadable                         |
| 5B33          | 1           | Circular    | Entrance        | Unreadable                                  |
| 5B33          | 0           | Circular    | Exit            | Undamaged                                   |
| 5B31          | 48          | Square      | Entrance        | Undamaged                                   |
| 5B31          | 47          | Square      | Exit            | Undamaged                                   |
| 5B16          | 46          | Square      | Entrance        | Undamaged                                   |
| 5B16          | 45          | Square      | Exit            | Damaged                                     |
| 5B39          | 41          | Square      | Entrance        | Undamaged                                   |
| 5B39          | 49          | Square      | Exit            | Undamaged                                   |

The hardware and software are functional for the circular gauges in that they contain the different algorithms to analyze the circular gauges, but the software does not present the results in clear defined “circular” graphics and presently uses the rectangular graphics. While DMI has not made the circular gauges available as a product, they have trained us to use the circular gauges as our research tool since the circular appear to be the better application (compared to the rectangular gauges) for the cold work studies.

A summary of our findings is found below.

**FINDINGS:**

- DMI could improve the strain results by developing software that reads and interprets smaller sections of the square gages, which could result in denser distribution of strains near the hole. DMI also could improve the strain results by developing software that reads and interprets the measurements of circular gages.
- It was difficult if not impossible to compare the DMI measured strains to the DIC measured strains (or to the finite element analyses) because of the gage alignment and subsequent damage issues. In addition, the resolution of the DMI gages limits the applicability to a detailed strain analysis—the strain state around cold worked holes are complex; however, as of the end of this project, only 8 strains can be measured on a particular DMI gage.
- The DMI gage are potentially quite useful for documenting evolving residual strains according to published works of the OEM, Direct Measurements, Inc. However, our limited experience with the DMI gages in a cold working application suggests a great deal of care must be taken to ensure proper alignment of the gages, lest the gages be damaged during the cold working process and hence the measured strains rendered

suspect. The disadvantage of the DMI gages is the same as the DIC: the DMI gages yield nonlinear strains, while stresses are the quantity needed for the crack growth analyses.

- Though there was obviously crack growth in all these coupons, no crack growth was apparently detected by the DMI gages.

### 3.3.3 Fractography of Fatigue Test Coupons

A critical portion of understanding the effects of cold work on fatigue response can be gathered directly from the fracture face if an effective self-marking load spectrum (as was developed under this Phase I) is used. To support this Phase I effort, every specimen that was tested, both cold work and non-cold worked, was studied intensely using optical microscopy at magnifications ranging from 8x to 1000x.

The self-marking spectra made a permanent record of crack progression, both rates and shapes, on the fracture face. Typically, there are limitations to the effectiveness of such spectra. For instance, at long crack lengths (high  $K$  values) the marks can tend to lose their distinct appearance as striations become more and more visible. Also, their effectiveness usually diminishes at very small crack sizes (less than 0.001 to 0.008 inch, depending on alloy and stress level) where influences of stress level, geometry, and grain orientation near the origin all play roles in the appearance of marker bands.

Reading the marker bands was challenging in some of the non-cold worked coupons, particularly under the “V9” spectrum, in which the stresses in the spectrum were quite high (root-mean-square {r.m.s.} stress as well as peak stress) and the lives very short. In the coupons that used the “V5” and “V1” spectra, readability was improved, but as will be shown, it was not possible to find every mark, partly due to detectability issues outlined in the previous paragraph, and partly due to many cycles being applied during crack nucleation. Table 5 shows the number of cycles at which the first marker band was observed, the number of the band in the sequence, the total number of bands in the test, the % life mapped, and the crack depth ( $c$ -direction) at the first detectable mark. Specimens above the bold line (3D12 is the last one above) are non-cold worked. Those below are cold worked. Note that for the cold worked coupons, marker detection was always above 90%, and it was usually 100%.

Table 5. Marker band reconstruction data.

| <b>Coupon</b> | <b>First Observation, Cycles</b> | <b>First Observed Mark &amp; (Total)</b> | <b>% Life Mapped</b> | <b>First Observation Crack, in.</b> |
|---------------|----------------------------------|--|----------------------|-------------------------------------|
| 5B19          | 151,800                          | 40 (148)                                 | 73%                  | 0.000913                            |
| 5B40          | 98,180                           | 26 (52)                                  | 50%                  | 0.001071                            |
| 5B25          | 4,470                            | 1 (5)                                    | 100%                 | 0.002583                            |
| 5B26          | 4,470                            | 1 (5)                                    | 100%                 | 0.007165                            |
| 3D12          | 31,390                           | 6 (7)                                    | 23%                  | 0.06885                             |
| 3D16          | 4,470                            | 1 (83)                                   | 100%                 | 0.000425                            |
| 3D22          | 4,470                            | 1 (142)                                  | 100%                 | 0.000394                            |
| 3D30          | 42,070                           | 8 (90)                                   | 91%                  | 0.001732                            |
| 5B32          | 31,390                           | 6 (91)                                   | 94%                  | 0.000394                            |
| 5B35          | 4,470                            | 1  | 100%                 | 0.000362                            |
| 5B31          | 4,470                            | 1  | 100%                 | 0.002142                            |
| 5B39          | 4,470                            | 1  | 100%                 | 0.000315                            |

### Baseline Test Fractography

Figure 25 through Figure 29 show the reconstruction of the fractographic results for the baseline test coupons. Also shown with these fractographic results is an AFGROW simulation in which the initial crack size in the analysis is iterated to create a computed total life essentially equal to the test life. In most of the cases, the computed crack path simulated by AFGROW was quite different than that actually found from fractography (the significance of this is discussed in more detail in later sections). The fractographic data is extrapolated from first detectable mark back to the crack-forming discontinuity (in all of these cases, second-phase particles). The curve shown between the first detectable mark and zero cycles (y axis) is an estimate.

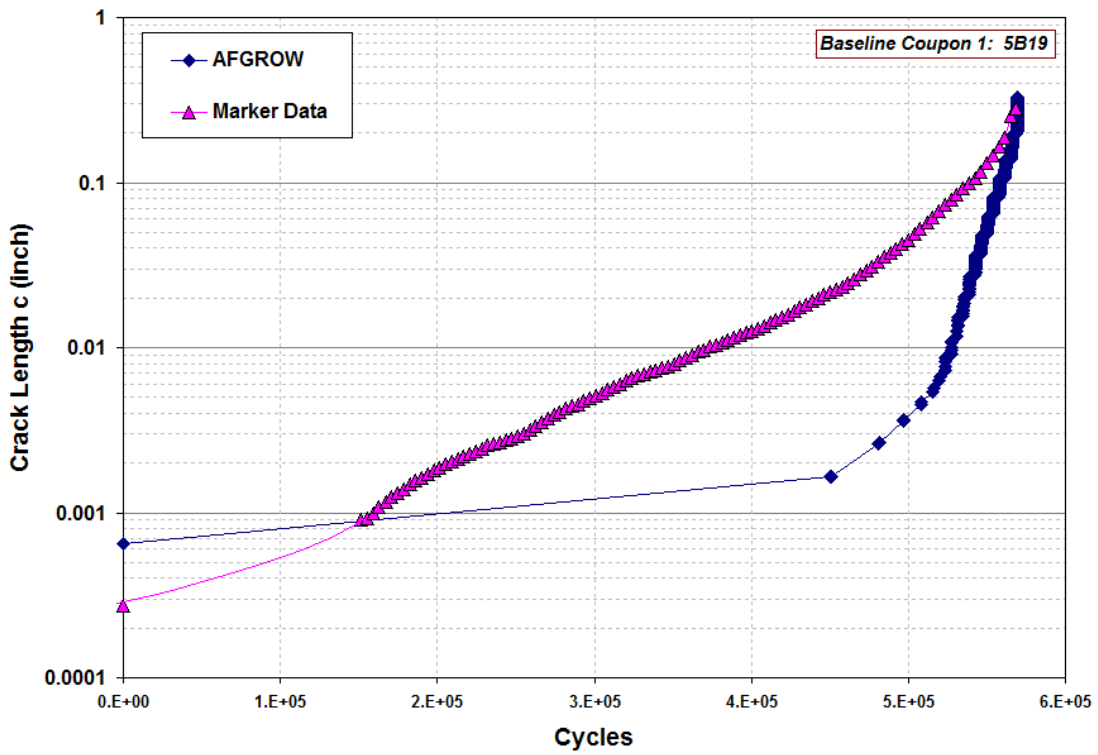


Figure 25. Marker band data and AFGROW computation for baseline coupon 5B19 (#1).

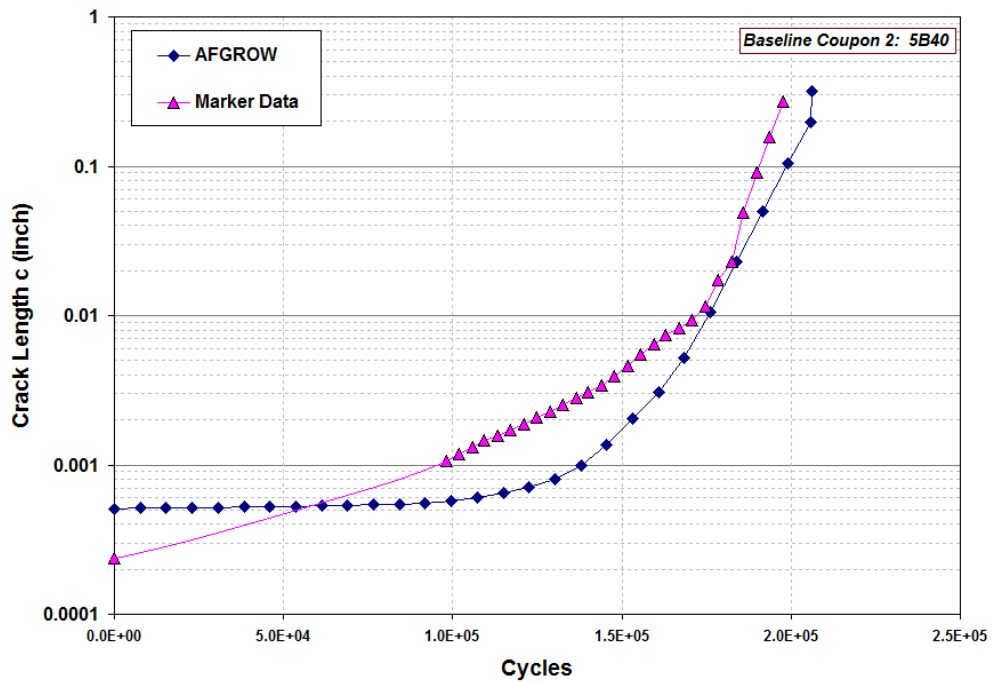


Figure 26. Marker band data and AFGROW computation for baseline coupon 5B40 (#2)

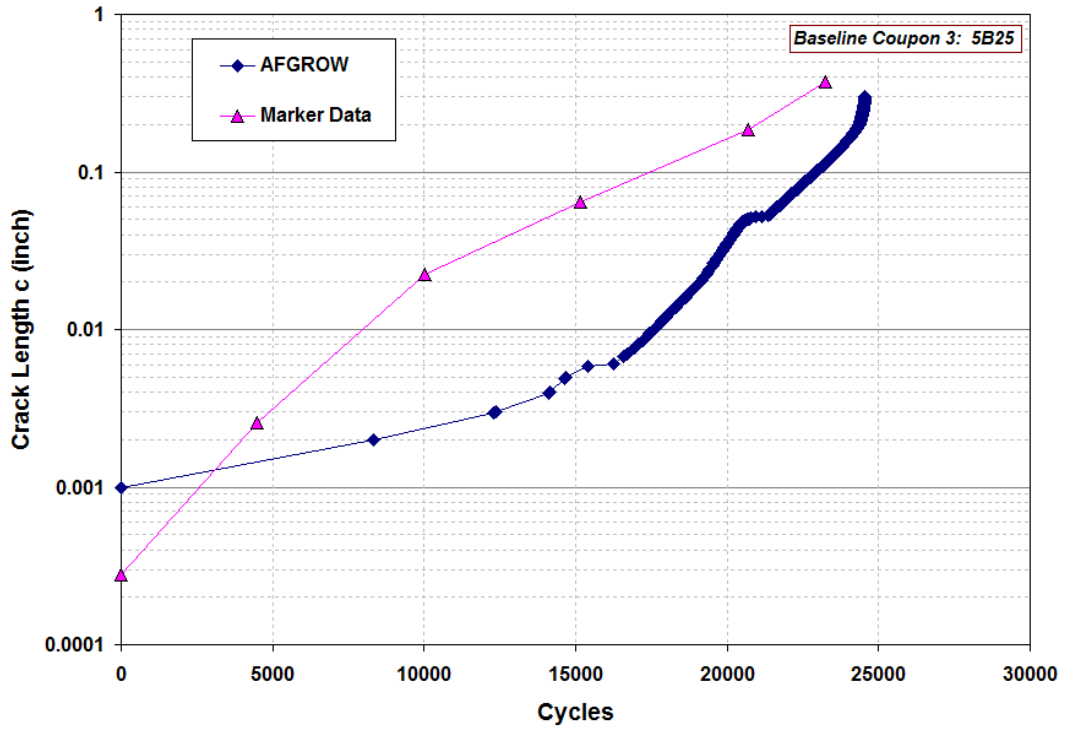


Figure 27. Marker band data and AFGROW computation for baseline coupon 5B25 (#3)

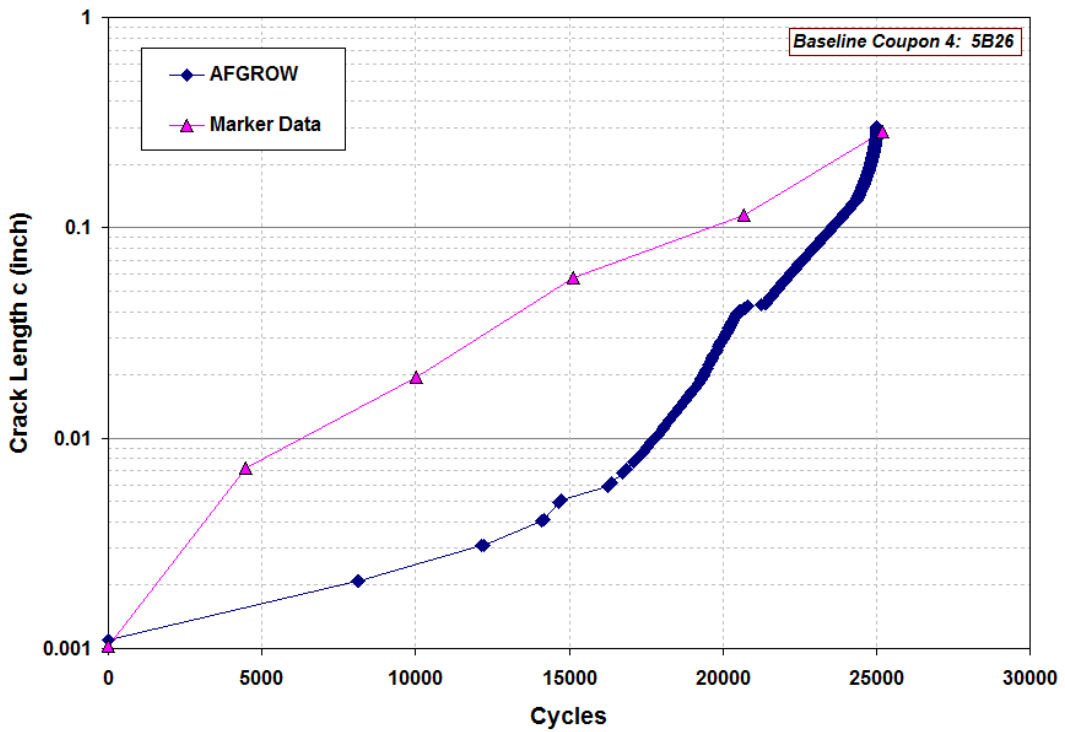


Figure 28. Marker band data and AFGROW computation for baseline coupon 5B26 (#4)

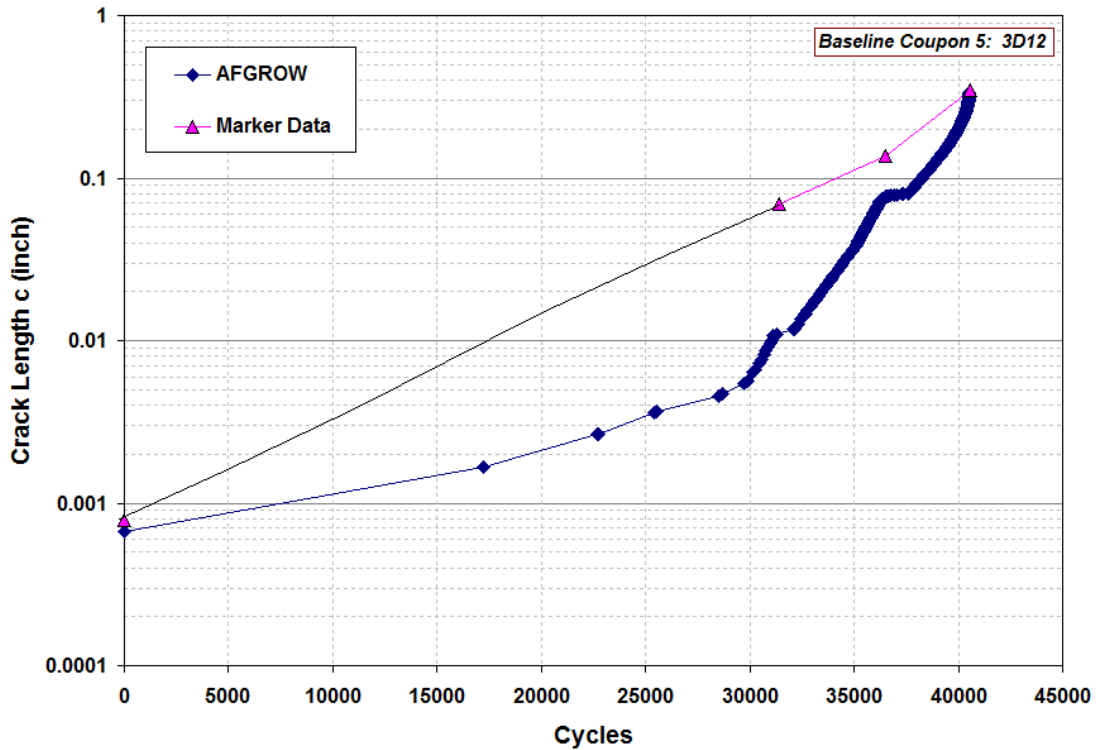


Figure 29. Marker band data and AFGROW computation for baseline coupon 3D12 (#5)

### Cold Worked Coupons

The success of the self-marking spectrum in the cold worked coupons was remarkable; as discussed earlier, the application of the V9 spectrum not only kept test life reasonable, but it also provided complete crack growth histories for most of the coupons (100% crack growth histories were reconstructed for 5 of 7 coupons). An example of what the self-marking spectrum looked like on a fracture face is shown in Figure 30.

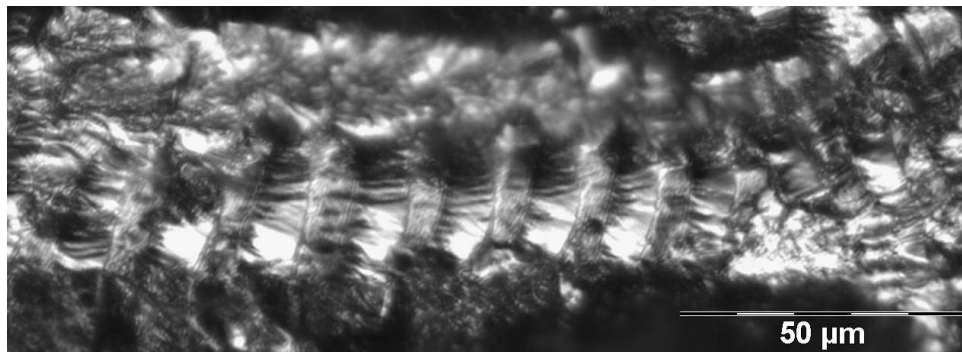


Figure 30. Example of the appearance of the V9 loading sequence on a fracture face.

Figure 31 shows crack growth curves for the seven cold worked coupons, along with the one baseline coupon that was tested using the same spectrum and stress level (V9 spectrum at 37 ksi peak stress). Crack growth data was constructed by traversing the fracture surface perpendicular

to the bore of the hole and parallel to the nearest specimen face; notable conclusions from the figure are:

1. On a log-linear scale, there are three distinct regions of crack growth behavior for the cold worked coupons, namely: (A) rapid initial growth, (B) protracted period of stable crack extension, and (C) rapid acceleration to final fracture after crack depth has exceeded 0.08 inch (2 mm).
2. The improvement in cold worked specimen fatigue lives over the lives of the non-cold worked specimen ranged from a factor of 6.4 to 34.
3. Scatter factor on life of the cold worked coupons was 5.3. Recall that every coupon nominally received the same level of cold work, and also note that most every coupon showed 100% traceable crack growth (e.g., no nucleation period). This would imply that substantial variations exist in the residual stress fields resulting from the cold expansion process.
4. Coupon 5B39 actually fractured in the grip. However, the crack in the grip occurred late in life, which meant that the crack growth data extracted from the hole location (the specimen was broken open at the hole to reveal the fracture face), was still valid. The consistent crack growth behavior of all the specimens (i.e., log-linear growth up to 0.08 inch (2 mm) followed by rapid transition to fracture) made it possible to project the life of that coupon with reasonable confidence. We estimate that 5B39 would have lasted for about 850,000 cycles.

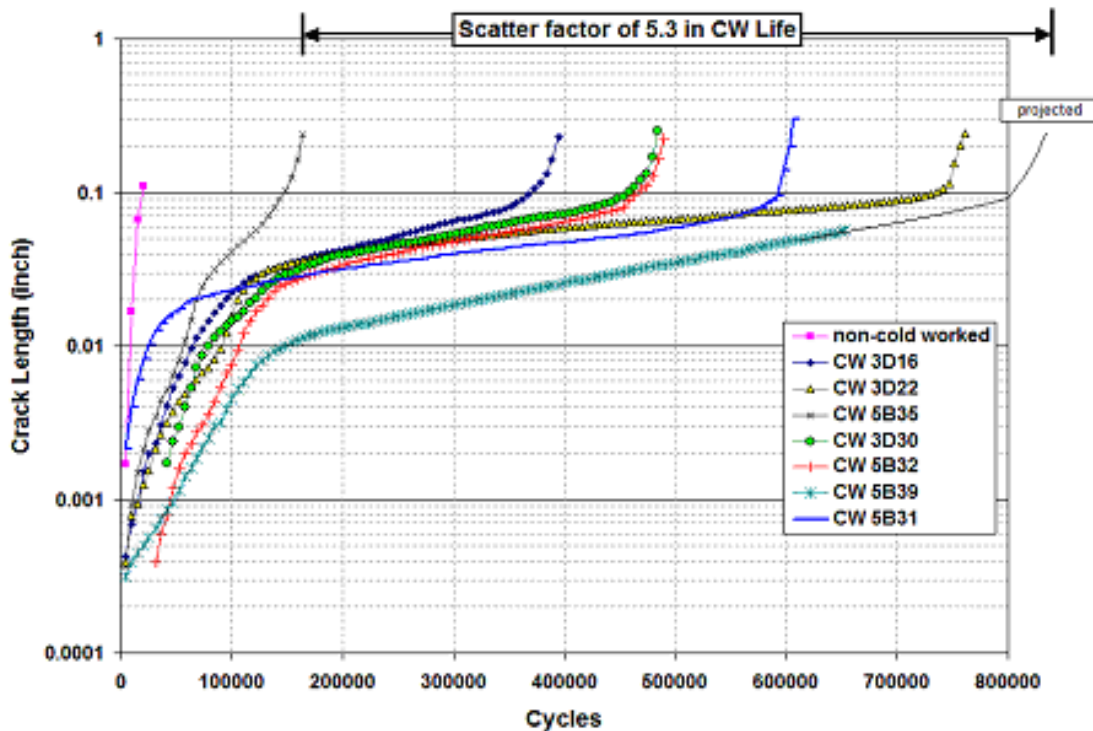


Figure 31. Crack growth data plotted for one non-cold worked coupon and seven cold worked coupons.

Figure 32 schematically shows some of the key observations about the failure modes for the cold worked coupons. Interesting points in this figure are:

1. The failures were dominated by one primary crack from the short side of the fastener hole (short side of the offset fastener hole).
2. Other small secondary cracks existed along the bore of the hole, but these were enveloped by the primary crack as failure progressed.
3. Regions A, B, and C correlate to the three regions identified in the crack growth behavior (discussed earlier). These regions are further identified on a sample crack growth plot from specimen 3D16 (see Figure 33).
  - a. Crack growth in Region A is dominated by the  $K_I$  of the hole
  - b. Crack growth in Region B decelerated as influence of the  $K_I$  lessens and the influence of the cold work residual stresses starts to dominate
  - c. Crack growth in Region C is dominated by rapidly increasing  $K_I$  as the crack moves away from the region of cold work residual stresses.
4. All primary cracks formed along the bore of the hole near to the corner formed with the “entrance side” of the hole. This finding matches those of Carlson (2008) and Pilarczyk (2008) and is supported by the residual stress distributions measured by XRD and by the FEA simulations conducted at NRC (Shi 2007), which show lesser residual stresses at the entrance side. Naturally, this is where cracks would be expected to form.

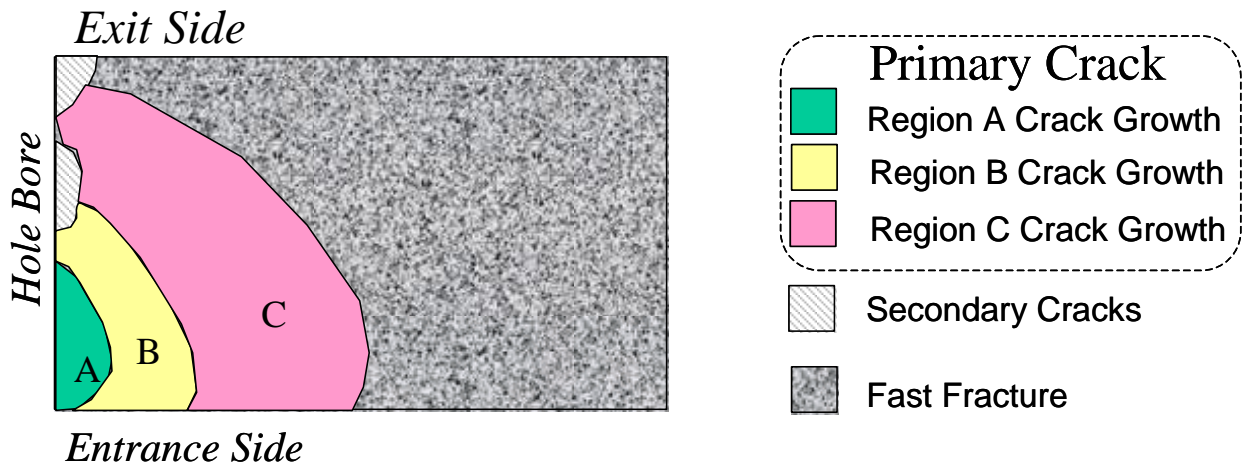


Figure 32. Schematic of general fracture behavior for cold worked coupons.

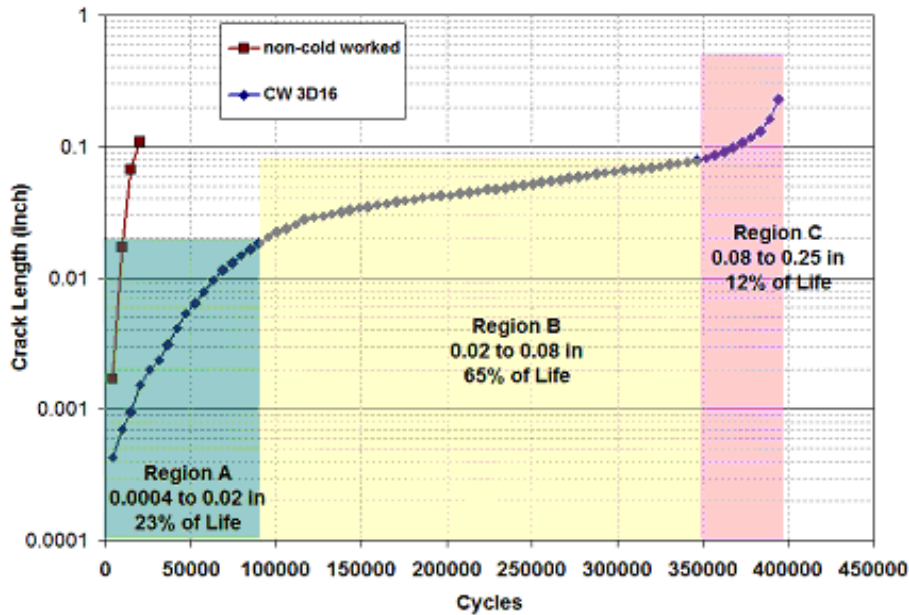


Figure 33. Crack growth data for coupon 3D16 with crack growth behavior "regions" labeled.

Figure 33, above, illustrates how the majority of the life in the cold worked coupons is spent at intermediate crack lengths around 0.02 to 0.08 inch (0.5 mm to 2 mm). The distinct change in slope from Regions A and B, and again between Regions B and C, can clearly be seen when viewing the data as  $da/dN$  (crack extension per cycle) vs.  $a$  (crack length). Figure 34 shows an example of this data using the four cold work coupons with intermediate lives (3D16, 3D30, 5B32, and 5B31). For the sake of data presentation,  $da/dN$  represents an average rate for each marker block, as many different stress levels and amplitudes are represented by the computed crack growth rate during each block. Limited budgets precluded sorting out the contribution and variation of individual components to spacing of the marker bands, although at some crack lengths (particularly longer lengths), this appears to be possible.

In Figure 34, there is an obvious grouping of  $da/dN$  that correlate with Regions A, B, and C as determined from the original, raw crack growth ( $a$  vs.  $N$ ) data. Region B, as expected, is revealed in the  $da/dN$  data through marked deceleration.

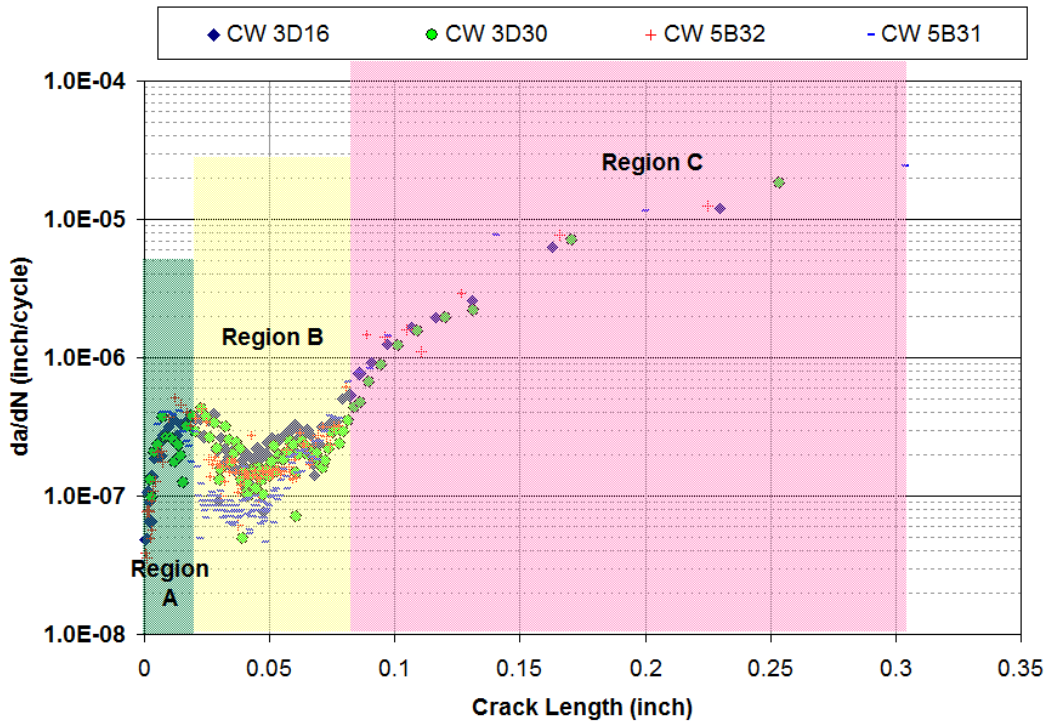


Figure 34.  $da/dN$  vs.  $a$  plots for 4 intermediate life coupons.

Figure 35 shows the same type of information but for coupon 5B35, which had the shortest life of the cold work coupons, and or coupons 5B39 and 3D22, which had the two longest lives of the cold work coupons. This plot helps illustrate the strong difference between crack growth rate data for the shortest life and longest life coupons.

Figure 36 shows curve fits of the  $da/dN$  vs.  $a$  behavior for the shortest life coupon, a long life coupon, and a typical life coupon. This figure is included to more clearly show the differences in crack growth response to what is nominally supposed to be the same level of cold work.

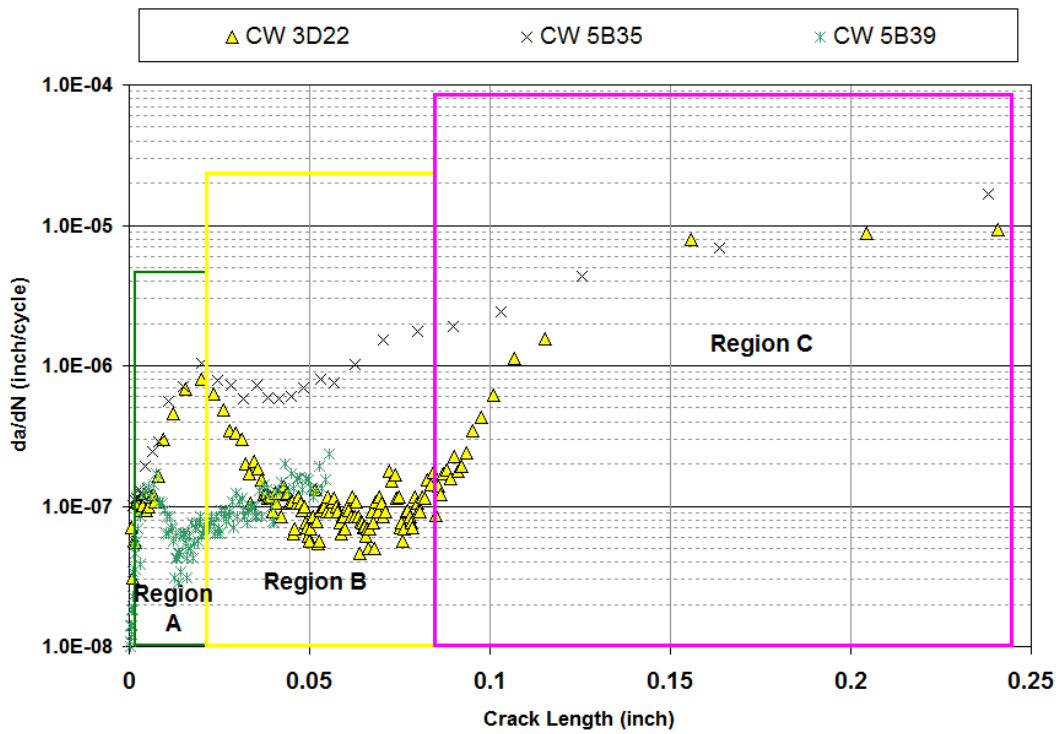


Figure 35.  $da/dN$  vs  $a$  plots for 2 long life coupons and 1 short life coupon.

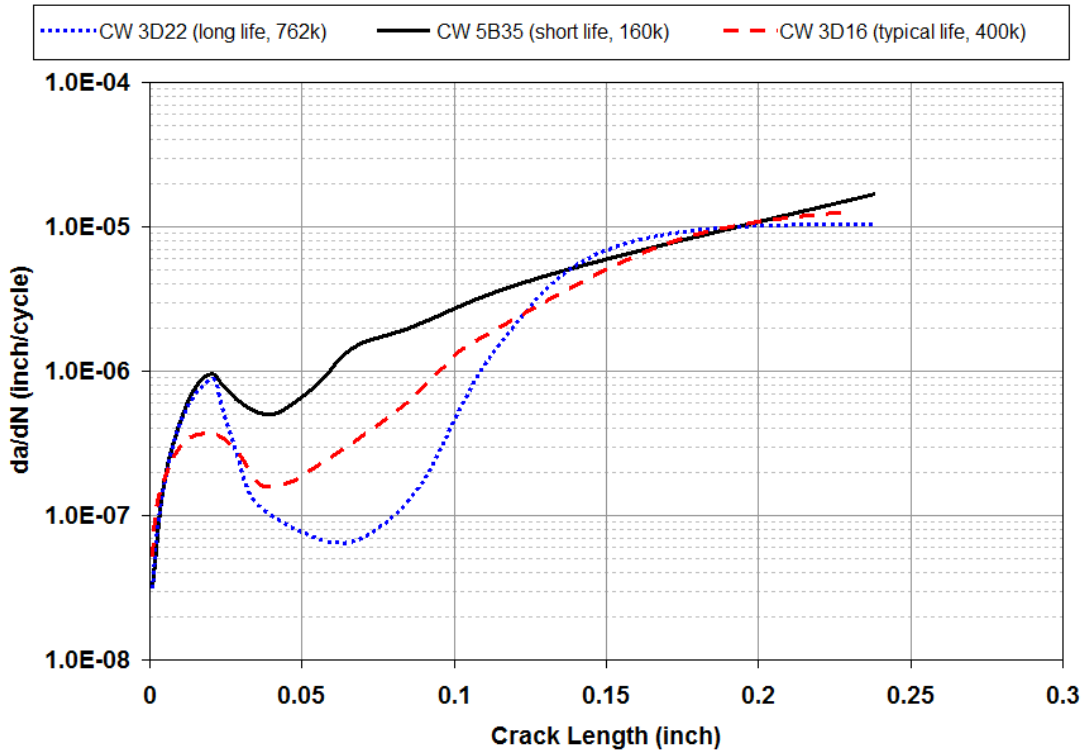


Figure 36. Eyeball curve fits of  $da/dN$  vs.  $a$  data for three types of coupon behavior.

A summary of our findings from the fractography work are found below.

## FINDINGS

- Tests of the baseline (non cold worked) coupons made it possible to optimize a self-marking load sequence for subsequent use with the cold worked coupons.
- Readability of the self-marking spectrum, using optical microscopy, was exceptional.
- For many coupons, particularly the cold worked coupons, marker reading was 100% (all marks detected), which produced a complete record of fatigue life and showed that life was essentially all crack propagation (no nucleation period). The conclusion is that, for the stress levels and degree of cold work considered here, cold working does not retard crack nucleation, rather it greatly decelerates crack propagation.
- Primary fatigue cracks formed from the hole bore near the corner at the “entrance side.” This is the location of least effective compressive residual stress (per XRD data and per FEA simulations of the cold work process performed by NRC).
- Cold working imparted a life improvement ranging from a factor of 6 to a factor of 34.
- Three distinct regions of crack growth behavior were noted for the cold work coupons, namely: (A) initial accelerated growth likely influenced by  $K_t$  of the hole), (B) rapid deceleration and stable crack extension (majority of life), (C) dissipation of cold work effectiveness and rapid crack extension to fracture (length greater than 2mm).
- Total life of the coupons is primarily driven by the degree of crack growth rate deceleration in Region B. Scatter in life for the cold worked coupons was a factor of 5.3, even though they all received the same degree of cold working—in theory.

### **3.4 Analytical Assessment of Residual Stresses**

#### **3.4.1 Evaluation of StressCheck<sup>®</sup> Incremental Plasticity Algorithm**

The  $p$ -version finite element software StressCheck<sup>®</sup> recently incorporated an incremental plasticity algorithm that allows us to compute plastic strains for plastic strains reversals (which can occur in a cold working processes for large values of cold working). Previous to software release 7.1, a very robust but limited deformation plasticity algorithm was the only method for simulating plastic strains in a cold working model. The deformation plasticity algorithm was very useful for computing plastic strains for models with monotonically increasing loads, and for small cold working levels (for which a linear superposition of stresses works well). However, if the load had a large reversal, for instance, when large cold working levels were applied, a ‘reverse plasticity’ warning would be given when the nonlinear solution process was finished. It was always unclear what effect ‘reverse plasticity’ had on the overall solution; after applying the new incremental plasticity algorithm to the same cold working model, the effect the reverse plasticity has on the residual stresses, especially near the hole, is now more clear.

A cold working verification document was attached to the July 2008 Bi-Monthly Status report, IncrementalPlasticityVerifications.pdf. Results have been commented on by ESRD, Inc, the developers of StressCheck<sup>®</sup>. In this study, the results from 3 papers in the open literature (primary authors: Brot, Kang, and Burlat) were compared with AP/ES cold working simulations with StressCheck<sup>®</sup>. The first paper, by Brot, (2007) was presented at ASIP Conference in 2007;

the second, by Kang, et al (2002) and the third, Burlat, et al, (2008) were published in engineering journals. Brot contracted with ESRD to perform the simulations with StressCheck<sup>®</sup>, so these results were useful as a benchmark for understanding the process of introducing cold working with the incremental plasticity algorithm. Kang, et al examined the cold working of a hole centered in a square plate, with a full three dimensional simulation of the cold working process. Burlat, et al, examined a similar plate that had a centered hole in a rectangular plate. Burlat also performed a full three dimensional simulation; both Burlat and Kang used ABAQUS, a commercial *h*-version finite element code. StressCheck<sup>®</sup>, a *p*-version code, while superior in many respects to ABAQUS, is inferior in one key respect—only two dimensional simulations of the cold working process are possible (there is a 3D capability to do three dimensional simulations, but the simulations are only quasi-3D, as so far the analysis capability is restricted to a constant radius mandrel). Reaming of the hole, an integral part of the cold working process, also cannot be readily modeled with StressCheck<sup>®</sup>.

The comparisons between the StressCheck<sup>®</sup> results and the results in the 3 papers chosen are quite favorable (which might be a coincidence—as each comparison takes couple of days to perform and document, time constraints permitted only 3 comparisons). We were able to repeat the Brot results with a great degree of fidelity; the comparisons with the Kang results were good; and the comparisons with the Burlat results were mixed, though easily explained. Burlat used a kinematic hardening rule in his plasticity simulations, while, at first, we were using an isotropic hardening rule in StressCheck<sup>®</sup> (mostly out of ignorance as to the differences between isotropic and kinematic hardening). Because the material is modeled as a bilinear elastic-plastic, StressCheck<sup>®</sup> allows the use of “pure isotropic hardening,” “pure kinematic hardening,” or a mix of the two. The differences in the computed residual stresses for these two extremes in the hardening rule are shown in Figure 37 and Figure 38 below.

It is clear that the StressCheck<sup>®</sup> “kinematic hardening” results are consistent to the Burlat results, both qualitatively and quantitatively, Figure 37 and Figure 38 below. However, is also clear that the StressCheck<sup>®</sup> “isotropic hardening” results are comparable to the Burlat results only in the intermediate region that is compressive and is between the near hole region and the tensile region 1 hole diameter or more away from the hole edge. This leaves open the question as to which hardening rule to use when confronted with predictions of a particular material’s fatigue behavior. There has been some work in the literature to address this issue by combining finite element calculations with experimental measurements—essentially you are judging the qualitatively behavior of the measured stress-strain curve for a material undergoing cyclic loading. Therefore, whether the material behaves as one undergoing isotropic hardening, or kinematic hardening, or a mix of the two, becomes part of the constitutive law that describes the mechanical behavior of that particular material. One such study, by Fersini and Pirondi (2005), concludes that a combined nonlinear hardening model works best for aluminum alloy 2024-T3, while an isotropic hardening rule seems to work best with aluminum alloy 7475-T7351. One such shortcoming of such an approach of course is the dearth of cyclic stress strain curves that are in the open literature; if you need this data, you can almost be certain you will have to generate this data yourself.

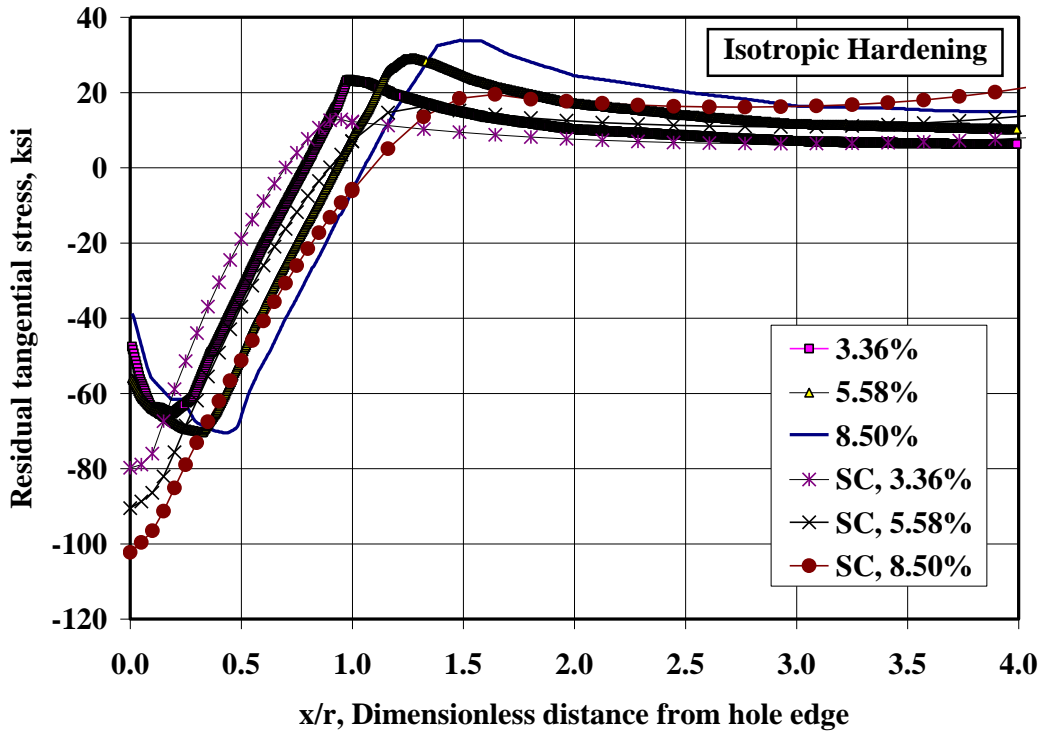


Figure 37. Comparison with Burlat Cold Working Simulations, Isotropic Hardening.

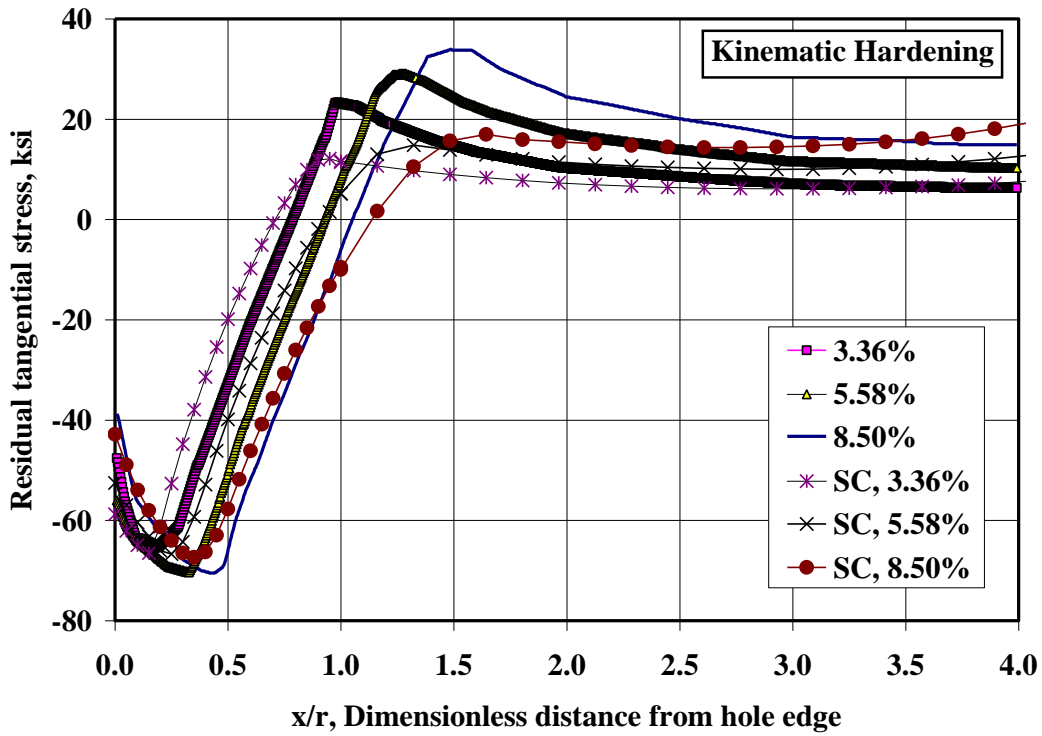


Figure 38. Comparison with Burlat Cold Working Simulations, Kinematic Hardening.

### 3.4.2 Verification of StressCheck<sup>®</sup> Against NRC Analysis

NRC has a long term project to predict and measure residual stresses caused by cold working processes. In the first few years of this project, they have concentrated on obtaining good quality finite element results that simulate the entire cold working process, from insertion and extraction of the mandrel, to the reaming process that is recommended by FTI, the manufacturers of the cold working machine NRC uses. These simulations are in full 3D, so that differences between residual stresses on the so-called entrance and exit sides or planes of the plate can be computed. Their finite element tool of choice is MSC/MARC 2005. There is a very detailed description of fairly substantial analyses of cold working in aluminum alloy AA2024-T3 extrusion that NRC presented at Aging Aircraft Conference in 2007 Shi, et al (2007). In this paper, the effects of cold working level, offset edge distance (edge margin), sleeve orientation, sleeve thickness, friction coefficients, plate thickness, and plane (that is, exit, entrance or middle) were examined.

With such a large parameter space, obviously a prohibitively large number of comparisons are interesting; however, we will present just a few representative comparisons for this report. Figure 39, Figure 40, and Figure 41 below illustrate the differences between residual stresses computed for one cold working level (4%) and four (4) edge margins,  $e/D=0.8$ ,  $e/D=1.2$ ,  $e/D=2.0$ , and  $e/D=5.0$ . In addition, these three figures illustrate the differences in residual stresses computed on three planes: entrance plane (that is, the side of the plate opposite of the side where the mandrel is inserted—this is also opposite of side where the extraction tool is located), the exit plane (opposite the entrance plane), and the middle plane (halfway between the entrance and exit planes). Unfortunately, the entrance plane is where cracks at the hole edge are most likely to nucleate, and the plane least amenable to inspection normally. Substantial differences are observed for both differences in edge margins and computation plane, though each residual stress curve seems to have qualitatively the same shape—small compressive stress at the hole edge, dropping down (becoming more negative) away from but still near the hole, a valley of compressive stress then the stress increasing approximately on a straight line, becoming positive (tensile), peaking in tension, then gradually decreasing as you travel in increasing distance from the hole edge. Increasing the edge margin generally does a couple of things: lowers the tension peak, moves the tension peak away from the hole, and increases the magnitude of the ‘compressive bucket’ that occurs near but not right at the hole edge.

In addition to illustrating the edge margin effect, comparisons of the 3 figures illustrate the effect of computation plane; that is, there are substantial differences in the residual stress magnitudes (quantitative) and trends (qualitative) as you move from the entrance to the exit planes. Since stress is a substantial driver in crack propagation, there probably will be substantial differences in crack growth curves for cracks growing on one of the 3 planes; deciding which plane to use will be part of the logic of the life prediction approach developed in Phase II.

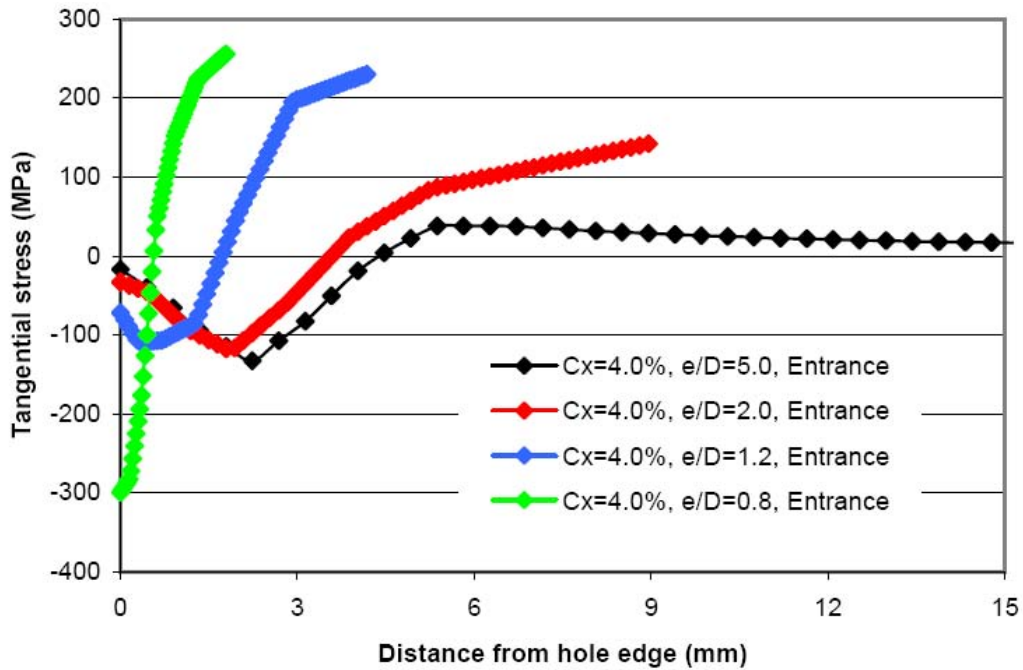


Figure 39. Effect of Edge Margin on Residual Stress on Entrance Plane.

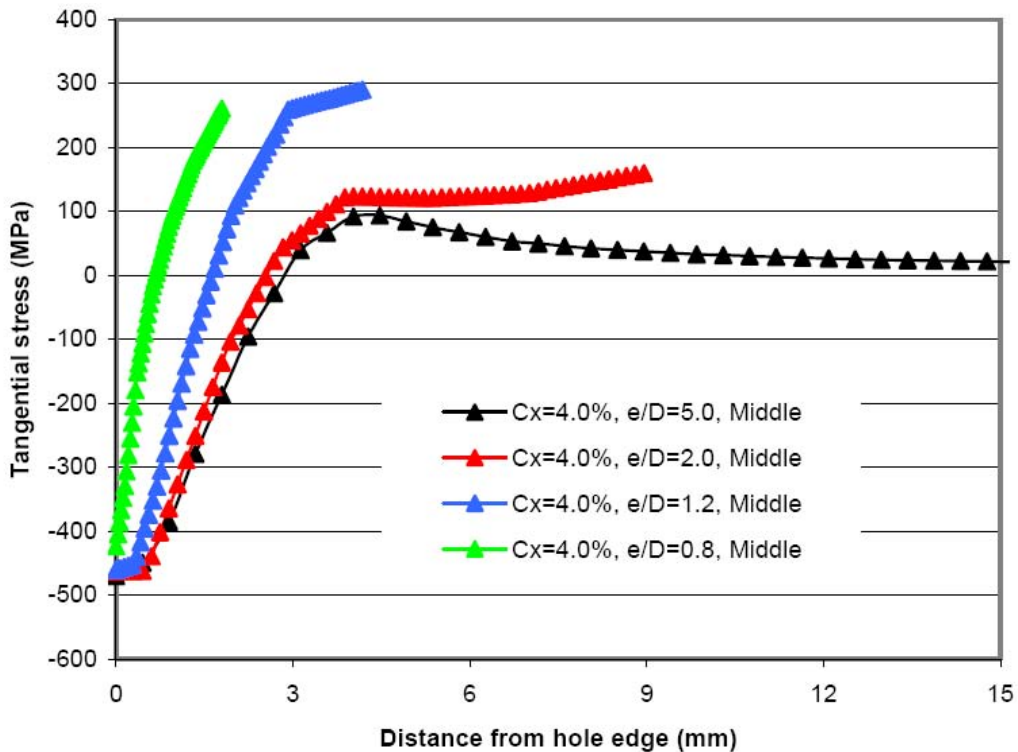


Figure 40. Effect of Edge Margin on Residual Stress on Middle Plane.

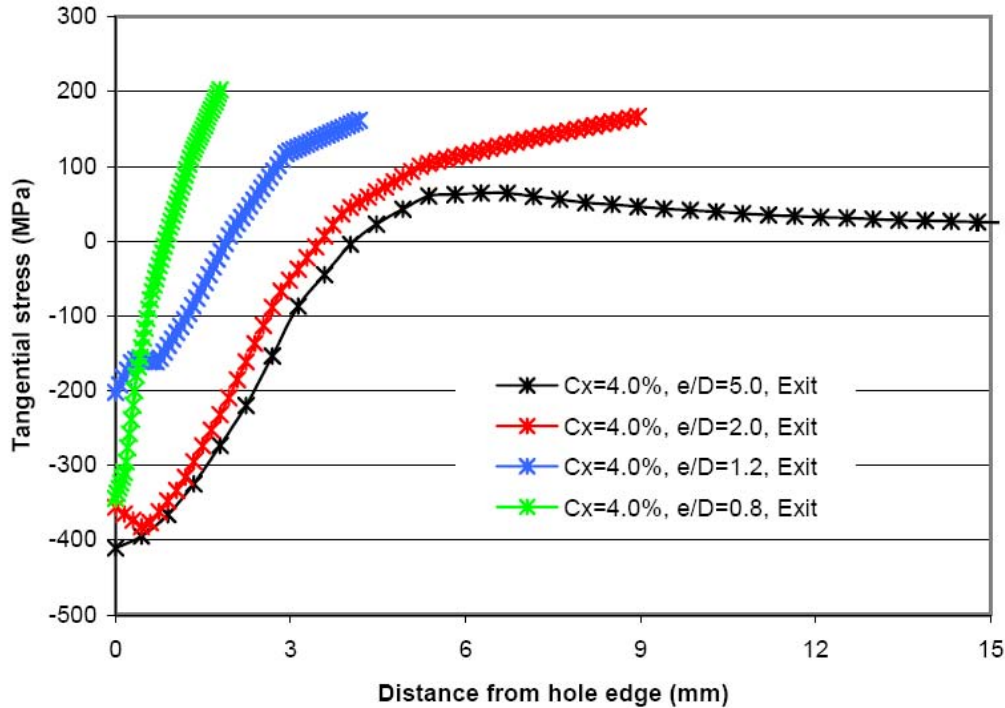


Figure 41. Effect of Edge Margin on Residual Stress on Exit Plane.

Because the material that NRC is testing this year is aluminum alloy AA7065-T651, a similar finite element study as their Aging Aircraft paper will be necessary to fully document differences in cold working the two aluminum alloys (as far as AP/ES knows, this study was not available for public consumption as of December 31, 2008).

### 3.4.3 AP/ES Modeling of NRC Aging Aircraft 2007 Paper Results

StressCheck<sup>®</sup> was used to simulate the results reported in the Shi, et al, (2007) paper. In this paper, whose results were summarized in a bi-monthly MSR, “CW Bi-Monthly Status Report # 2,” Shi, et al (2007) simulated the cold working of a rectangular plate with a single offset hole. Various levels of cold working, as well as various levels of offset were simulated in the Shi paper. Here, we present comparisons with only Shi’s 4% cold working case with the e/D (offset) of 2.0. Shi also presented results for 3 planes (as their simulations were completed in three dimensional models); “Entrance,” “Exit,” and “Middle” planes—these names are consistent with the corresponding identifiers in the FTI cold working process. However, since our present simulations are in 2D, the experience of other researchers, (see for example Burlat (2008)) suggests that the results from a 2D simulation are most consistent with the results from the middle plane of a 3D simulation; therefore, the middle plane results from the NRC simulations will be compared to the StressCheck<sup>®</sup> results.

APES originally encountered some difficulty obtaining StressCheck<sup>®</sup> results which were consistent with the NRC results; the reason was the inconsistencies in the elastic-plastic material constitutive relations used for the NRC and APES simulations. Typically, to simulate a nonlinear, elastic-plastic material, the FEA analyst will use one of at least 3 methods to describe the material constitutive relation: elastic-perfectly plastic, Ramberg-Osgood (sometimes called “power law”), or tabular format. The choice, while left up the analyst, is most often dictated by

the shape of the monotonic stress-strain curves, many of which are found in handbooks such as MIL-HDBK-5. The Shi paper described the material curve as aluminum 2024-T3 extrusion, with Young's modulus  $E = 10,800 \text{ ksi}$ ,  $\sigma_{yield} = 40 \text{ ksi}$ , and the statement that the "...stress strain curve from MIL-Handbook-5H was also used." APES at first tried to use the yield stress  $\sigma_{yield} = 40 \text{ ksi}$  given in the Shi paper, and using the Ramberg-Osgood power law coefficient from Figure 3.2.3.1.6(o) (page 107 in MIL-HDBK-5G),  $n = 37$ . The StressCheck<sup>®</sup> computed residual stresses using these coefficients ( $E = 10,800 \text{ ksi}$ ,  $\sigma_{yield} = 40 \text{ ksi}$ ,  $n = 37$ ) did not compare well to the NRC results, particularly close to the hole edge. A shift in the yield stress to  $\sigma_{yield} = 52 \text{ ksi}$  (a more likely value of the yield stress in Figure 3.2.3.1.6(o)) improved the comparison a little bit, but the computed residual stresses were still far enough away from the NRC results so as to invite further inquiry to NRC. As there are many stress strain curves in MIL-HDBK-5H, APES asked G. Shi at NRC precisely which curve was used in the NRC Aging Aircraft paper, and discovered that Shi used the curve Figure 3.2.3.1.6(x) (page 107, MIL-HDBK-5H), which is the 'full range' stress strain curve, from zero load until the coupons fractured. These "full range" stress strain curves differ from the curves that show the Ramberg-Osgood curve fits in at least two important respects: the strain range (x-axis) of the "full range" curves are an order of magnitude larger than the Ramberg-Osgood curve fits, and the "full range" curves rarely if ever show the power law coefficients which would be useful for inputs to the FEA. By using a Ramberg Osgood material curve, and by hand, adjusting the yield stress and power law coefficient, the "full range" curve can be fit reasonably well by using  $\sigma_{yield} = 49 \text{ ksi}$  and  $n = 12.2$ . The residual hoop stress for these three (3) attempts are shown in Figure 42 below. While the biggest variation in the hoop stress is due to variations in the yield stress, there was a large variation between the hoop stresses computed with  $\sigma_{yield} = 52 \text{ ksi}$ ,  $n = 37$  and  $\sigma_{yield} = 49 \text{ ksi}$ ,  $n = 12.2$  parameter sets. How do these compare to the Shi results reported in the NRC Aging Aircraft 2007 paper? The 'best' results are those with the  $\sigma_{yield} = 49 \text{ ksi}$ ,  $n = 12.2$  parameter set; the StressCheck<sup>®</sup> computed residual hoop stress is laid over the top of a picture of the middle plane results from the NRC paper, for 4% cold working and  $e/D=2.0$ , in Figure 43. As can be seen, the StressCheck<sup>®</sup> results compare very well with the middle plane results from the NRC 3D simulations.

These finite element simulations show the sensitivity of the stress field predictions to the material constitutive relation, and the importance of understanding the real behavior of the material. Comparisons of finite element (FE) results from two different FE software programs allowed us to discover differences in the two FE codes, and also highlighted the sensitivity of the stress fields associated with the cold work process to variation of basic material behaviors. The best methods for obtaining the material behaviors for cold working solutions will be an important aspect of the Phase II approach; the proposed methods will be consistent with APES's HOLSIP methods for fracture mechanics solutions.

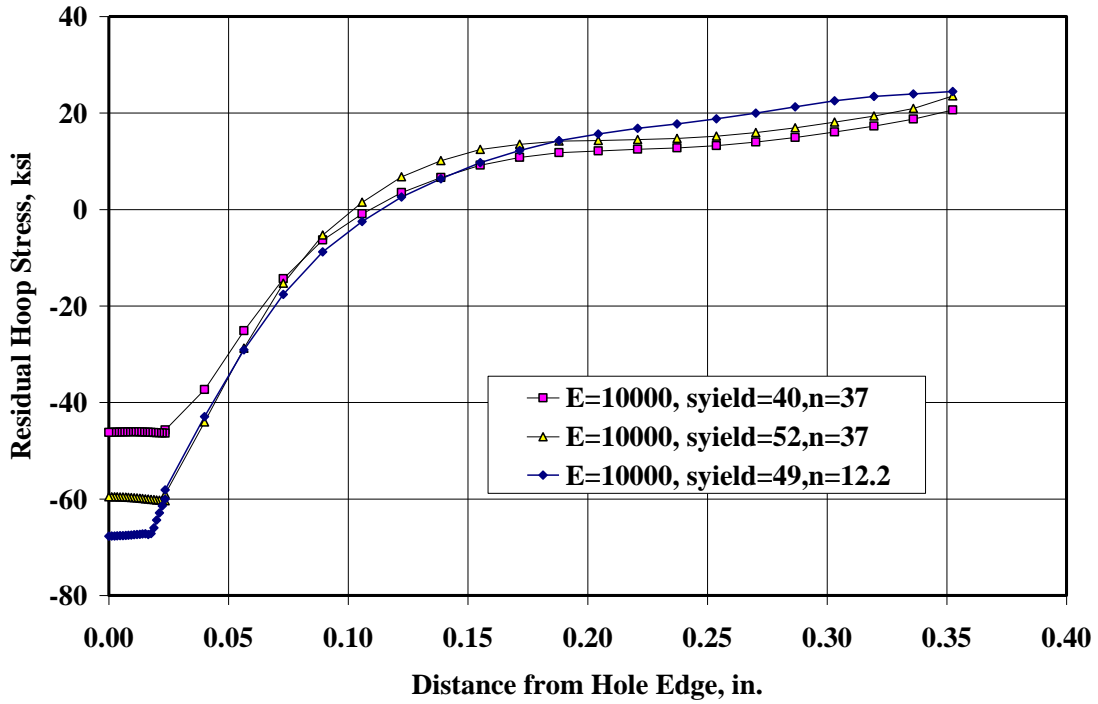


Figure 42. StressCheck® Simulations Demonstrate Effect of Varying Material Constitutive Relations (All Materials are Ramberg-Osgood Curve Fits).

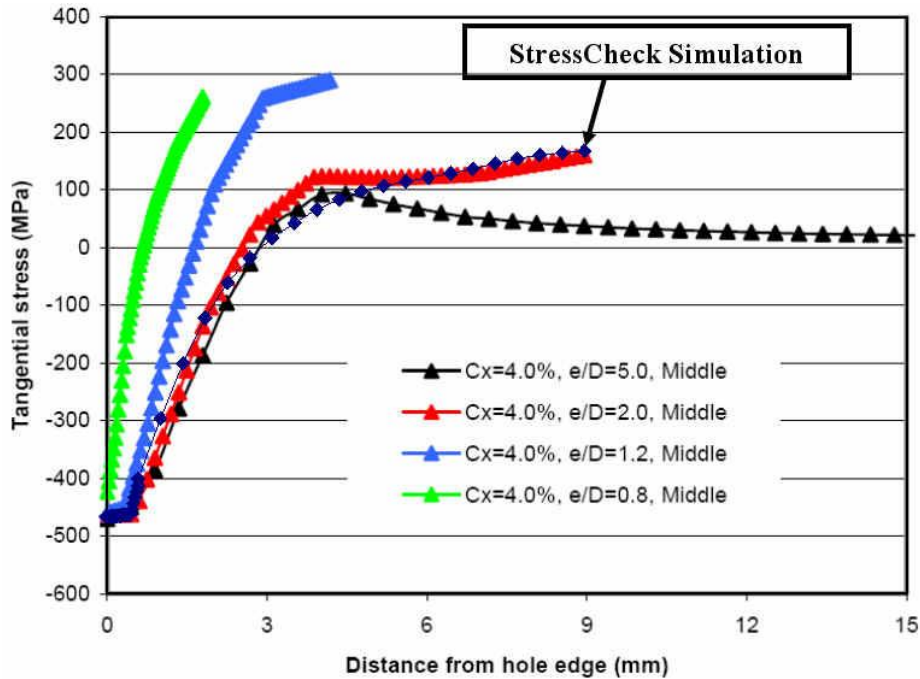


Figure 43. StressCheck® Simulation Compares Favorably to NRC's FEA Results.

### 3.4.4 Phase I Test Coupon Residual Stresses

Finite element analyses of the test coupon used for this program were completed during this Phase I project. The precise level of cold working on the coupons was not available, though each coupon should have received nominal 4% cold working; therefore, this value is used for all predictions documented in this section. The coupon material is 0.25 in. thick aluminum alloy 7075-T651 plate. The MIL-HDBK-5 Ramberg-Osgood material properties, Young's modulus 10,000 ksi,  $S_{70E} = 70 \text{ ksi}$ ,  $n = 32$  were used unless indicated otherwise. The  $p$ -version finite element software we use, StressCheck<sup>®</sup>, allows only a 2D simulation of the cold working process; therefore there is no 'exit side' and 'entrance side.' Typically, a 2D (plane strain) simulation of the cold working process has been shown to be near the middle plane values of a 3D simulation; a 2D (plane stress) simulation has been shown to be near the surface plane values of a 3D simulation, Kang, et al (2002). The cold working process has two steps, simulating the insertion of the mandrel (which expands the hole), and the extraction of the mandrel (which allows the hole to contract). The net result is zero radial stress on the hole surface, but nonzero hoop stress. Figure 44 presents four (4) results: "Expanded Hole" is the hoop stress after the mandrel has been inserted; "Cold worked hole" is the hoop stress after the mandrel is removed, "CW Hole+Tension" is the hoop stress after cold working and a 36 ksi stress is applied far field; "Open, NonCW Hole" is the hoop stress with a 36 ksi far field stress applied to an open, offset hole. Each is a stress distribution across the entire section at the centerline of the hole. A few things of note—obviously, with 36 ksi tension, the stress is very high at the hole edges for the open, non cold worked hole. The other interesting pattern is the behavior of the stress after the hole has been cold worked; namely, the stresses near the hole edges have similar behavior, both in magnitude and locations of local peaks. For instance, the "CW Hole+Tension" hoop stress is 33.8 ksi at one hole edge, and 36.7 ksi at the other hole edge. Each hoop stress dips down, then increases to a local peak (60.4 ksi near one side of the hole and 59.4 ksi near the other) at about the same distance from the hole edges, (0.1177 in. near one side and 0.1295 in. near the other).

The finite element analyses suggest two things: the failure flaw could nucleate on either side of the hole, and alternate failure locations could be realized at the peak tension locations away from the hole edge, approximate 0.10 in. to 0.15 in. from the hole edge (While at present the finite element techniques do not account for the differences between entry and exit side, the data suggests the entry side will be predominant as the prime failure location between the two hole sides).

A summary of our findings is found below.

#### FINDINGS:

- The new incremental plasticity algorithm in StressCheck<sup>®</sup> yielded computed residual stresses that were completely consistent the finite element computed residual stresses in the open literature.
- The key difference between computed residual stress levels for isotropic vs. kinematic hardening in the plastic material models is the stress field for 'high' (near yield) compressive stresses near the hole edge.
- The analyst must be very careful to describe the material constitutive model as faithfully as possible. Even when specifying the source of the material curve, the analyst must be

careful—for instance, very large differences in the computed residual stress fields were observed when comparing one material curve to another in MIL-HDBK-5 for the same material and heat treat (say compare results using the Ramberg Osgood curve to the “Full strain” curve in MIL-5).

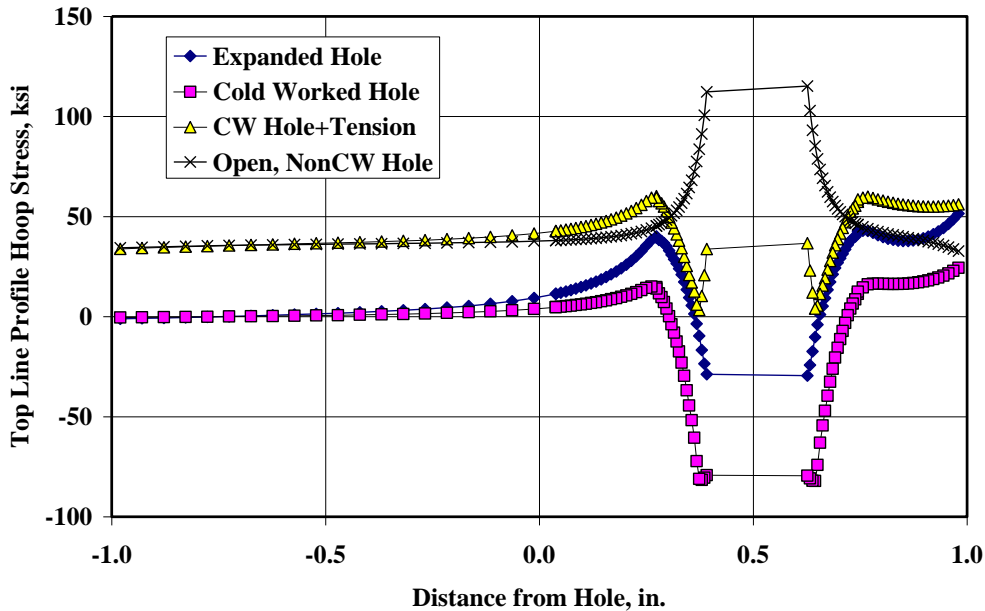


Figure 44. StressCheck® Computations of Cold Worked and Non Cold Worked Coupons.

### 3.5 Holistic Life Predictions of Cold Worked Specimens

#### 3.5.1 Analysis Method and Baseline Specimens

A simple Microsoft Excel macro was written to rapidly analyze crack propagation under a varying input stress field. AFGROW and other crack growth tools can be cumbersome when examining the rough order-of-magnitude (ROM) result sensitivities to various input variables, due to the way the tools enforce and restrict input values. The inputs to the Excel macro include (1) a starting crack length  $c$ , (2) discrete points on a  $da/dN$  (same as the  $dc/dN$  curve) vs.  $\Delta K$  crack growth rate curve for a single stress ratio  $R$ , (3) discrete points on a  $\beta$  vs.  $c$  curve, and (4) discrete points on a stress  $\sigma$  vs.  $c$  curve. Log-log interpolation was used between the points of the  $da/dN$  curve and linear interpolation was used between the points of the  $\beta$  vs.  $c$  curve and the  $\sigma$  vs.  $c$  curve. The macro propagated the starting crack using blocks of 100 cycles, Equation (1) below, and the crack growth rate curve.

$$\Delta K = \beta(\Delta\sigma)\sqrt{\pi c} \quad (1)$$

The  $\beta$  vs.  $c$  curve was extracted from AFGROW for a single edge corner crack model, using parameters (in inches)  $W = 0.3531 \text{ in.}$ ,  $t = 0.25 \text{ in.}$ , and  $c = a = 0.0004 \text{ in.}$ . This geometry

represents the ligament of the test coupon geometry, from the hole to the edge of the coupon. The ligament width is slightly smaller than nominal to account for the cold worked condition. The starting crack lengths were set smaller than the IDS of 0.0007 inches in order to provide an output curve that could be interpolated from  $c = 0.0004 \text{ in.}$  to  $c = 0.0007 \text{ in.}$ . The crack aspect ratio was allowed to develop naturally in AFGROW, and only the beta curve for the  $c$  dimension (the surface crack length) was extracted.

The assumed crack growth rate curve for aluminum 7075-T651 plate was assembled from various industry data sources and is shown in Figure 45. It is known to be based on somewhat limited data, and is also known to contain test artifacts due to the type of test used to collect the crack growth rates (compact tension). These artifacts produce a threshold behavior at low values of  $\Delta K$  (below  $\Delta K = 4$  or so), which is typically not observed in specimens cracking from holes. Region I crack growth data ( $5 < \Delta K < 20$ ) was projected to low  $\Delta K$  values (Figure 45) in order to remove this threshold and to allow crack growth predictions to occur from the crack-nucleating particle sizes found during fractographic analyses. These sizes were typically around 0.0007 inch, and this size is used as the starting crack length for the analyses.

For the baseline analyses, the  $\sigma$  vs.  $c$  curve used was the uncracked stress distribution across the cracking plane due to a constant 25.5 ksi far-field stress (the peak stress was 37 ksi; however, the r.m.s. (root-mean-square) stress was closer 68% of the peak—25.5 ksi). Average values of elastic and plastic material properties were used, as this correlated best to the non-cold worked test results. A constant stress ratio of  $R = 0.1$  was used, consistent with the bulk (or r.m.s.) of the cycles in the test spectrum. Figure 46 shows a plot of the un-cracked elastic stress distribution across the cracking plane, the stress distribution when a nonlinear plasticity analysis is used, and the average of these two curves  $\sigma_{Kt-FF}$  that was used for the  $\sigma$  vs.  $c$  curve (due to far-field loading) during the Excel macro analyses.

During development of the test matrix, 0.0007 inch was used as the assumed starting crack length for sensitivity studies involving the test spectrum. Non-cold worked tests were run and AFGROW was used to ensure that the predicted life from 0.0007 inch was approximately 25,000 cycles, a typical life for the non-cold worked tests. A majority of the cycles in the variable amplitude (VA) test spectrum are at a stress ratio of  $R = 0.1$  and a maximum stress of 25.5 ksi. Severe overloads in this test spectrum occur at a peak stress of 37 ksi. The marked bands on the fracture faces of the coupons can only be used to compute an average experimental  $da/dN$  between marks, therefore an equivalent constant amplitude (CA) spectrum is used to compare analysis and experiment. For the baseline non-cold worked tests, AFGROW results using a constant amplitude (CA) spectrum with a peak stress of 25.5 ksi and a stress ratio  $R = 0.1$  matched the AFGROW results with the variable amplitude spectrum very well (Figure 47). Figure 47 also shows the minimal difference between using the AFGROW model for a corner crack at a hole and using the Excel macro (which assumes a single edge corner crack model and imposes a stress distribution curve,  $\sigma_{Kt-FF}$ ).

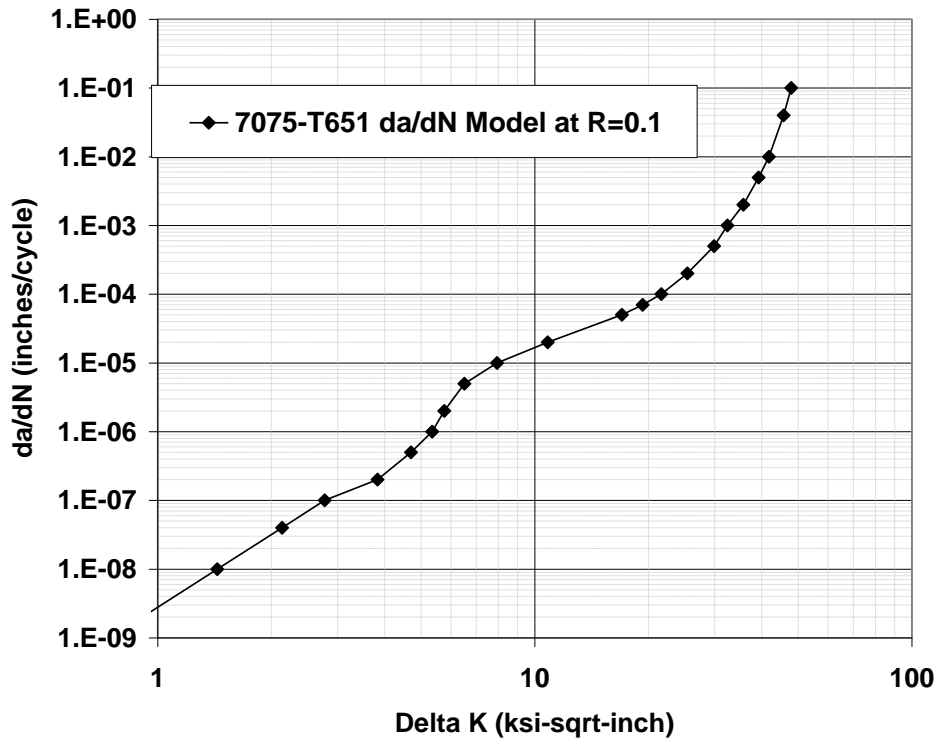


Figure 45. R=0.1 Crack growth rate assumptions for baseline analyses.

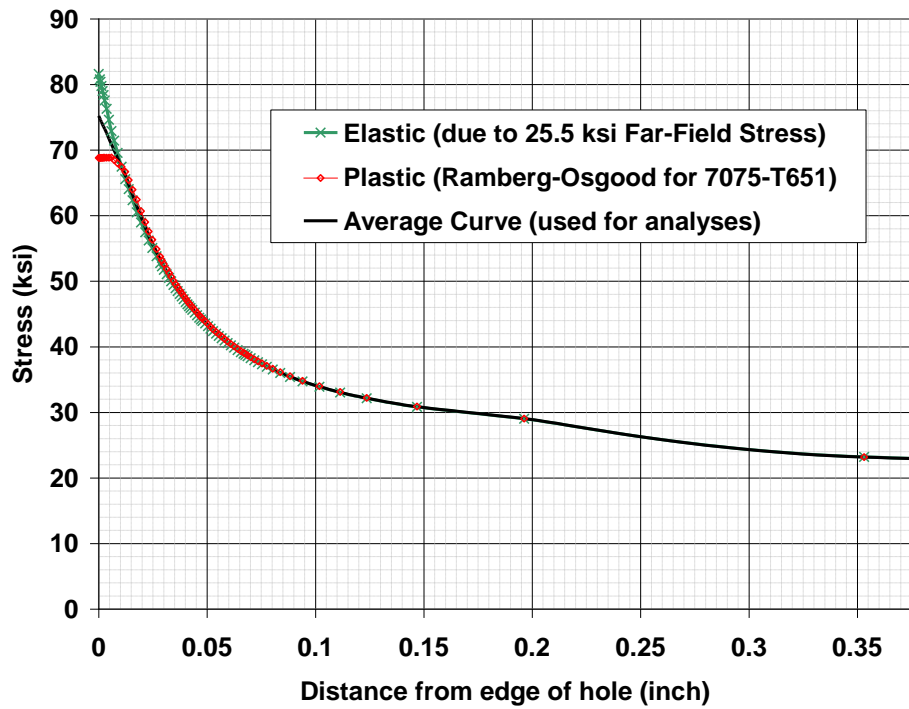


Figure 46. Uncracked average stress distribution curve  $\sigma_{K_I-FF}$  used for Excel macro predictions.

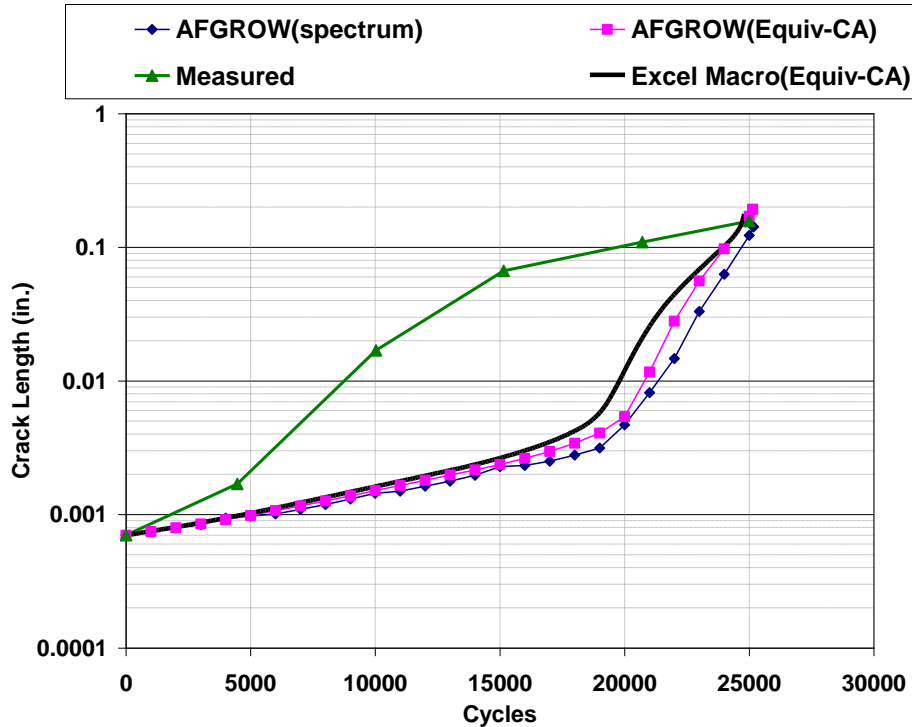


Figure 47. Comparison of variable amplitude prediction, constant amplitude prediction, Excel macro method, and crack length measured from one baseline non-CW experiment.

The experimentally measured crack length is also shown on Figure 47, and demonstrates a qualitatively and quantitatively different behavior compared to the analytically predicted crack lengths. It may be that the relatively high stress level of the test spectrum is causing plasticity and affecting the crack growth rates measured in the experiments. However, the minimal data pool of measured crack growth rates from the non-cold worked specimens is not sufficient for providing a thorough review and adjustment of the baseline crack growth rates.

### 3.5.2 Results for Cold Worked Coupons

In addition to the non-cold worked marker band measurements mentioned previously, crack growth rates were also obtained from the marked fracture faces of several cold worked specimens. A typical result was chosen (specimen CW 3D16) for analytical studies. Figure 48 shows a comparison of these experimental crack lengths against several methods for analyzing crack growth from a fastener hole. First, the traditional damage tolerance approach (a 0.05 in. initial flaw) is shown, then the current industry method, where the fatigue benefits of cold working a hole are accounted for by empirically assuming a 0.005 in. initial flaw instead of a 0.05 in. flaw. Clearly, this empirical technique is nearly two orders of magnitude too conservative in this case. Finally, a crack growth analysis was performed from a crack size typical of the fatigue-nucleating intrinsic discontinuity, 0.0007 in. Even this prediction is over one order of magnitude too conservative. In addition, none of these methods even qualitatively capture the shape of the CW 3D16 crack growth curve shown in Figure 48. We obviously must somehow take into account the apparently significant effects of the cold work residual stresses during life predictions.

The first effect of cold working on crack growth life is the most obvious: the residual hoop stresses reduce the local maximum stress experienced at any given crack length. This effect can be modeled by simply adding the stress profile function used in the baseline analysis  $\sigma_{Kt-FF}$  (Figure 46) to the compressive residual hoop stress function  $\sigma_{R/S-Hoop}$ .  $\sigma_{R/S-Hoop}$  can be computed in several ways: finite-element analysis (FEA), X-Ray diffraction measurements (XRD), strain gage measurements, back-calculation, or other methods not used in the program.

The second effect of cold working examined is the significant reduction in R-ratio that occurs when sustained (residual) hoop stresses  $\sigma_{R/S-Hoop}$  are superposed with cyclic stresses  $\sigma_{Kt-FF}$ . For example, consider a given crack length with a local maximum stress of 60 ksi and minimum stress of 6 ksi ( $R = -1.0$ ) due to cyclic stresses. If this crack length also has a residual hoop stress  $\sigma_{R/S-Hoop} = -40 \text{ ksi}$ , the resulting stress cycle has the same delta in stress values (the residual hoop stress are subtracted from both  $\sigma_{max}$  and  $\sigma_{min}$ ), but at greatly reduced R-ratio (20 ksi to -34 ksi,  $R = -1.7$ ). A general rule of thumb is that R-ratios smaller than -0.33 do not provide any additional crack growth rate increase for identical  $\sigma_{max}$  or  $K_{max}$  values. For the cold worked analyses considered here, because the compressive hoop residual stresses  $\sigma_{R/S-Hoop}$  are generally on the order of the local tensile stress concentration values  $\sigma_{Kt-FF}$ , we make the simplification that all crack propagation during cold worked analyses will use  $R = -1.0$  crack growth rate data (equivalent data to  $R = -0.3$ ) and that only the  $\sigma_{max}$  or  $K_{max}$  values are important.

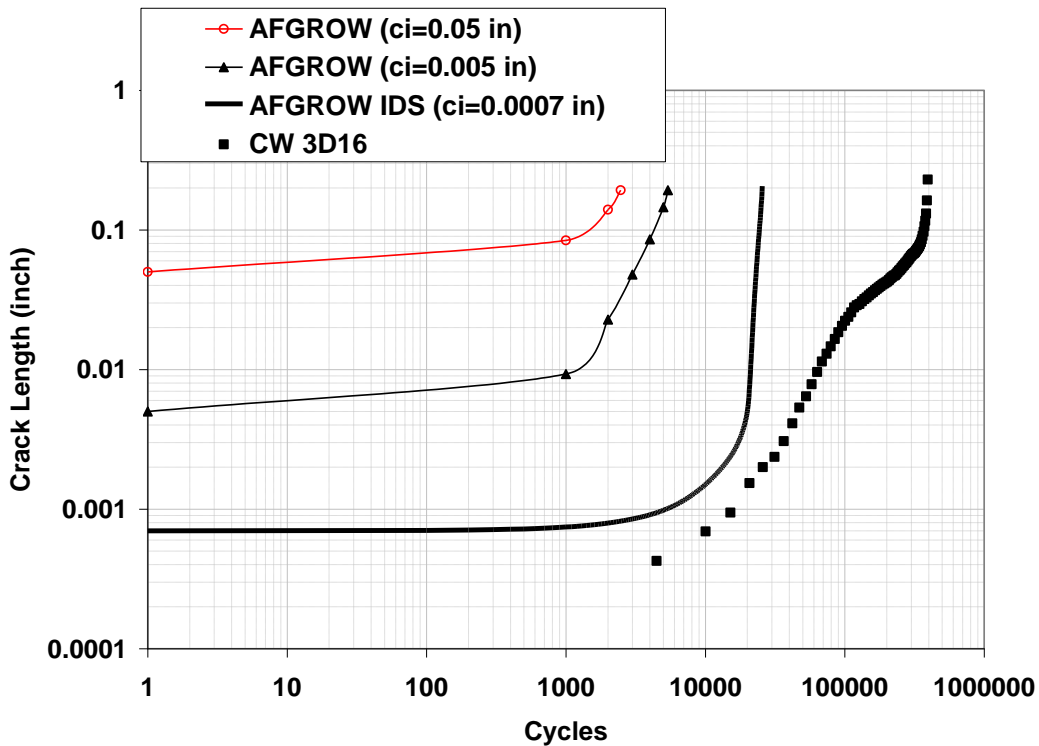


Figure 48. Comparison of industry predictive methods with cold worked test result.

The third effect of cold working to consider is the radial residual stresses  $\sigma_{R/S-Radial}$ . Radial stresses due to far-field tension are typically small and are neglected, but the cold working process produces significant compressive radial residual stresses. These, together with the tensile stresses due to far field loading and the compressive hoop residual stresses, form a biaxial stress state that increases the crack growth rate when compared to tensile stresses alone. Tada et al (2000) provides a method for computing the Mode I Stress Intensity Factor for a single through crack at a hole in an infinite plate under both a uniaxial and a biaxial stress condition. This method is used to compute a biaxial correction factor  $CF_{biaxial}$  (Equation 2), where  $K_{uniaxial}$  is the Mode I Stress Intensity Factor under  $(\sigma_{Kt-FF} + \sigma_{R/S-Hoop})$  and  $K_{biaxial}$  is the Mode I Stress Intensity Factor under  $(\sigma_{Kt-FF} + \sigma_{R/S-Hoop})$  on the major axis and  $\sigma_{R/S-Radial}$  on the minor axis.

$$CF_{biaxial} = \frac{K_{biaxial}}{K_{uniaxial}} \quad (2)$$

This correction factor is simply a multiplier on the Mode I Stress Intensity Factor (SIF),  $K_I$  and can be applied to any one of  $K_I$ ,  $\beta$ , or  $\sigma$  in Equation (1).

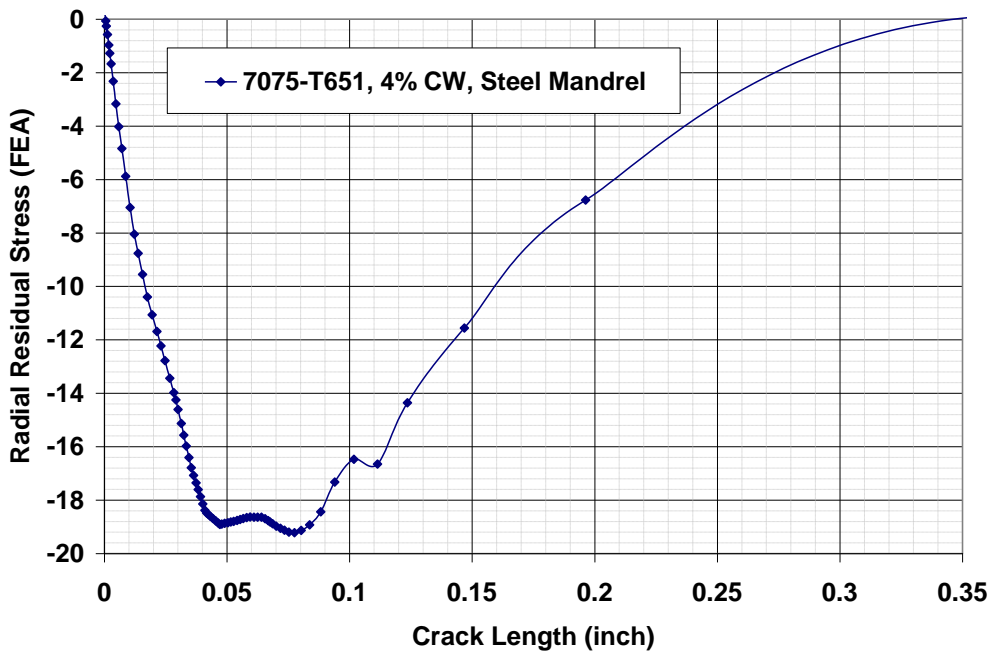


Figure 49. Radial residual stress profile assumed for all analyses.

First consider the back-calculation method for computing the residual stresses. To simplify matters, assume that the radial compressive stresses are a known and fixed quantity. These radial stresses were determined by StressCheck<sup>®</sup> FEA cold work analysis, using aluminum alloy 7075-

T651 material properties, a steel mandrel, 4% cold work level, and the geometry of the test coupon. Figure 49 shows the radial residual stresses computed with StressCheck<sup>®</sup>. Figure 50 shows the  $dc/dN$  data used in the cold work analyses. All crack propagation during the cold work analyses is assumed to be driven by  $K_{max}$  at a stress ratio  $R \leq -0.3$ . The curve of Figure 50 does not change for  $R$  ratios less than  $-0.3$ .

The marker bands from the cold worked specimen CW 3D16 provided a direct measurement of  $dc/dN$  between marks every 5,340 spectrum cycles, in general. An average crack length  $c$  was computed between every pair of adjacent marks. By assuming the  $R = -0.3$   $da/dN$  curve of Figure 50, an average  $K_{max}$  value was determined for each average crack length  $c$ . The AFGROW  $\beta$  value for the single edge corner crack was obtained and used to compute the effective  $\sigma_{max}$  from the  $K_{max}$ ,  $\beta$ , and average crack length  $c$  (Equation 1, using the maximum  $K_I$  and  $\sigma$  values instead of  $\Delta K$  and  $\Delta\sigma$  values).

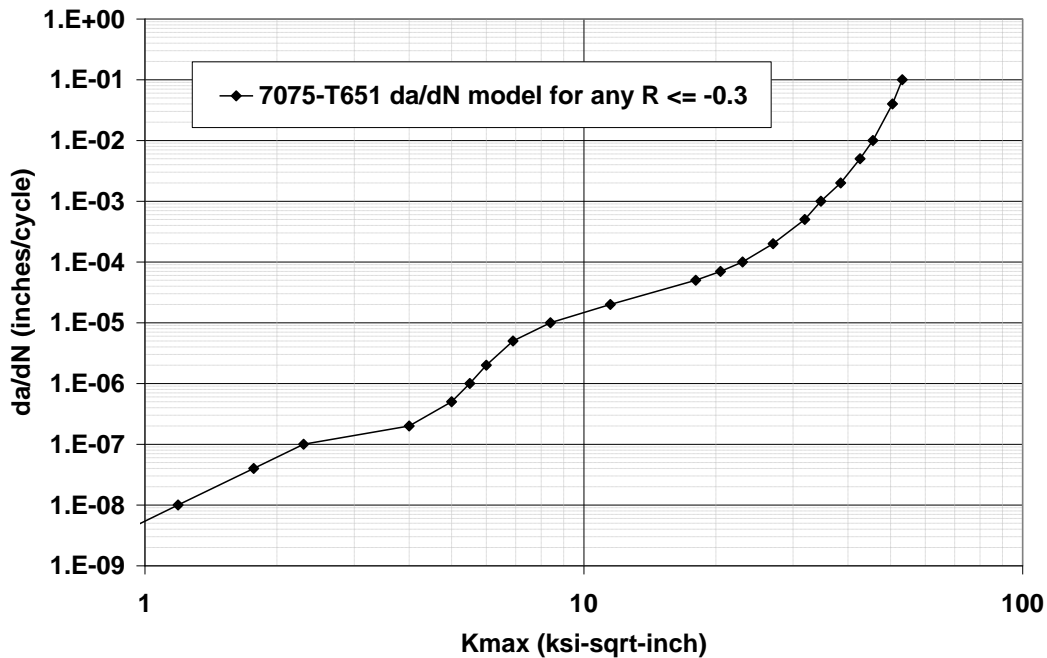


Figure 50. Crack growth rate curve used for cold work analyses. Residual hoop stresses cause a shift from positive to negative  $R$ -ratios.

This experimental, effective  $\sigma_{max}$  already contains the effect of the biaxial stress state, so we remove the biaxial correction factor  $CF_{biaxial}$  using an iterative process since we are interested in back-calculating the hoop residual stress  $\sigma_{R/S-Hoop}$ . An iterative process is used since  $CF_{biaxial}$  is a function of  $\sigma_{R/S-Hoop}$ . This leaves a  $\sigma_{max}$  that is **not** corrected for biaxial stress state; this uncorrected  $\sigma_{max}$  is then set equal to  $(\sigma_{KI-FF} + \sigma_{R/S-Hoop})$ . Since  $\sigma_{KI-FF}$  is known (the average curve of Figure 46), we obtain the back-calculated  $\sigma_{R/S-Hoop}$  stress distribution, Figure 51. Figure 51 also shows the  $\sigma_{R/S-Hoop}$  distributions calculated by several analytical methods, including

FEA for two different materials and XRD. Note that the XRD measurements could not be obtained close to the hole, so an assumed extrapolation to  $-30$  ksi is shown in a dashed line on Figure 51. This assumed scenario is labeled “XRD-1”.

Figure 52 shows  $c$  vs.  $N$  life predictions for the three scenarios of Figure 51, plotted against the experimental crack growth curve for cold worked specimen CW 3D16. Clearly, the finite-element analyses are not performing well for computing  $\sigma_{R/S-Hoop}$ , but the average XRD data and the assumed XRD-1 extrapolation perform remarkably well. The XRD-1 prediction not only comes close to matching the total coupon test life for CW 3D16, but also picks up the  $c$  vs.  $N$  curve shape, including the critical inflection point around the 100,000 cycle point. This inflection point is seen in nearly all of the individual CW experiments and is one of the results characteristic of the cold work process in these coupons.

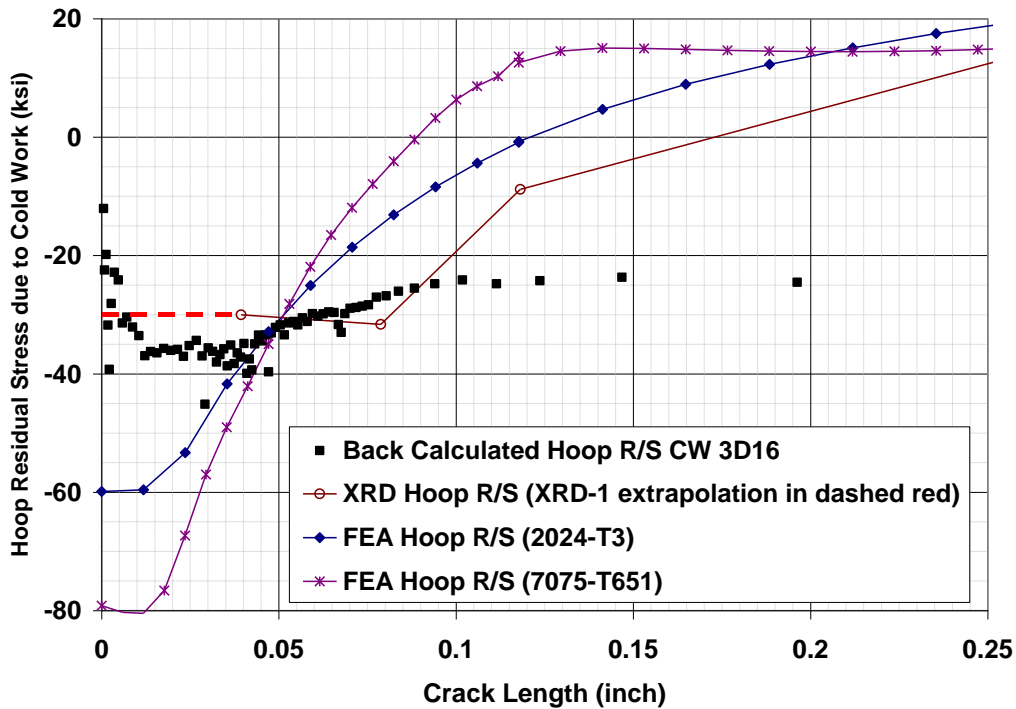


Figure 51. Back-calculated  $\sigma_{R/S-Hoop}$  compared to stress profiles from FEA and XRD.

As a check, a curve was also drawn through the back-calculated CW 3D16 data of Figure 51 and was used to perform a CW crack growth analysis from a 0.0004” initial flaw. As expected, that curve plots almost directly atop the CW 3D16 crack growth data points in Figure 52.

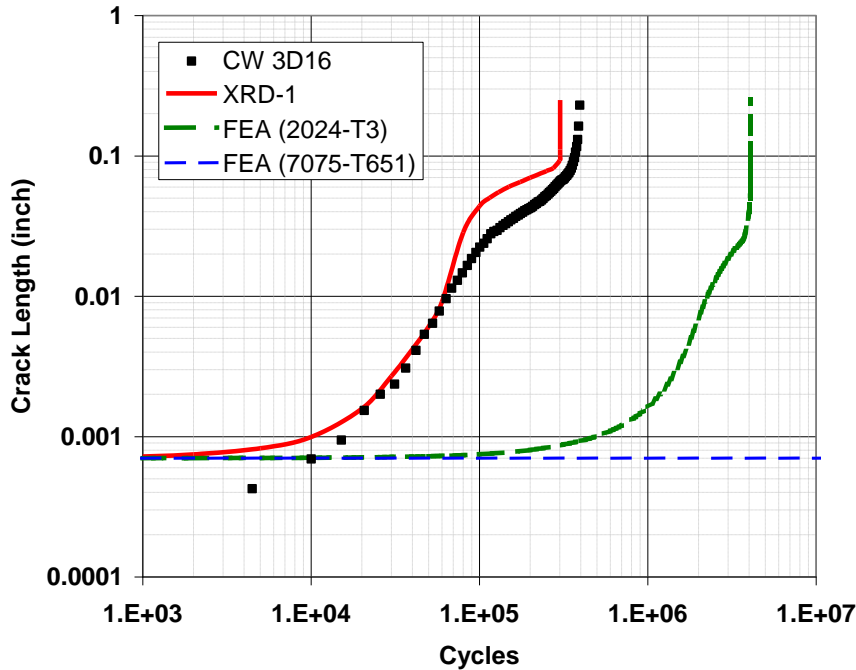


Figure 52. Life predictions for several  $\sigma_{R/S-Hoop}$  scenarios.

### 3.5.3 Sensitivity of Predictions to Model Components

In Figure 51, note the difference in  $\sigma_{R/S-Hoop}$  profiles between the back-calculated data and the XRD-1 curve. Intuitively, this difference may seem to be fairly significant, yet the XRD-1  $\sigma_{R/S-Hoop}$  profile results in a crack growth curve remarkably close to the CW 3D16 crack growth curve. This indicates that the  $\sigma_{R/S-Hoop}$  measurements may not require as much resolution and accuracy as anticipated. It is clear, however, that the FEA techniques for obtaining  $\sigma_{R/S-Hoop}$  are not performing well and require additional examination.

Scenario XRD-1 is based solely on a single line location on the coupon: the entrance side, on the “top” line (the crack nucleation point of all the cold worked specimens), four points in a line along the cracking plane (the “top” line is on the shortest ligament from the hole to the edge of the coupon). This data is an average of the XRD measurements from all CW coupons, along this line. Figure 53 displays more detailed XRD data: the maximum and minimums were determined across all cold worked coupons, for multiple locations around the hole and from both the mandrel entrance and exit side. Two heavy dashed lines show the overall maxima and minima boundaries, scenarios XRD-min and XRD-max. XRD-max was extrapolated horizontally to -16 ksi. A horizontal extrapolation of the XRD-min scenario would be too severe (this is known from FEA R/S studies) so a linear extrapolation was used to -40 ksi at the edge of the hole based on the bounds of the back-calculated  $\sigma_{R/S-Hoop}$  of Figure 51. Figure 54 shows the results of this sensitivity to the range of XRD hoop stress measurements. When adding the XRD-min minimum residual hoop stresses  $\sigma_{R/S-Hoop}$  to the  $\sigma_{Kt-FF}$  tensile stresses, the resultant stress state becomes

negative at a crack length of about 0.025 inch. Hence, the crack arrests in this scenario as seen in Figure 54.

Figure 55 and Figure 56 shows further crack growth progressive sensitivities to input variables, beginning with (1) the baseline stress due to far field loading  $\sigma_{Kt-FF}$ . Effects are progressively added: (2) the hoop residual stress  $\sigma_{R/S-Hoop}$ , (3) the stress ratio reduction from  $R=0.1$  to  $R<-0.3$ , (4) the biaxial correction factor  $CF_{biaxial}$ , and the plots are compared with (5) the experimental crack growth curve for CW 3D16. Figure 55 displays life predictions consistent with earlier predictions, where the initial flaw size is 0.0007 inch. Figure 56 shows the minimal sensitivity to the assumed initial flaw size: Figure 56 plots have the exact same assumptions as Figure 55 plots, with the exception that the initial flaw size is 0.0004 inch instead of 0.0007 inch.

From Figure 55 and Figure 56, the biaxial correction factor and the initial flaw size appear to be second order effects when compared to the residual hoop stresses  $\sigma_{R/S-Hoop}$  and the stress ratio shift.

Future studies aimed at identifying the important variables in a cold worked analysis should include comparisons of FEA and XRD radial stresses, sensitivities to radial stresses, more sensitivities to  $da/dN$  crack growth rates, comparisons to AFGROW analysis with residual stresses, examination of the scatter in cold worked test results, and investigations into the effects of plasticity on crack growth rates.

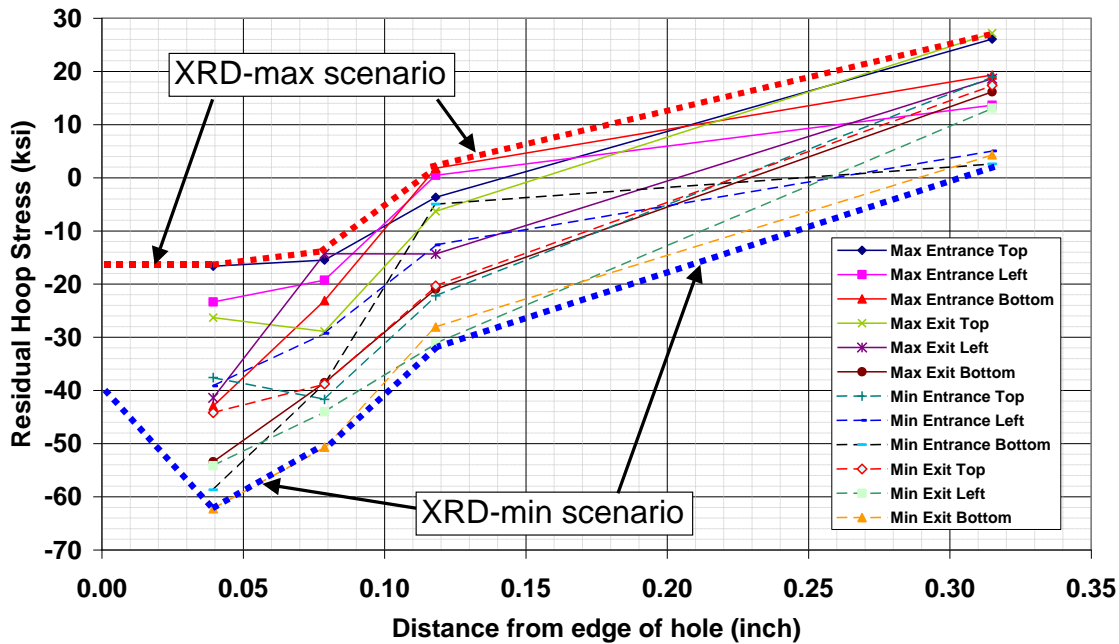


Figure 53. Bounding scenarios for XRD Residual Hoop Stress  $\sigma_{R/S-Hoop}$ . Maxima and minima are taken across all CW coupons, all three locations (top, left, bottom), and both the entrance and exit side of the specimen.

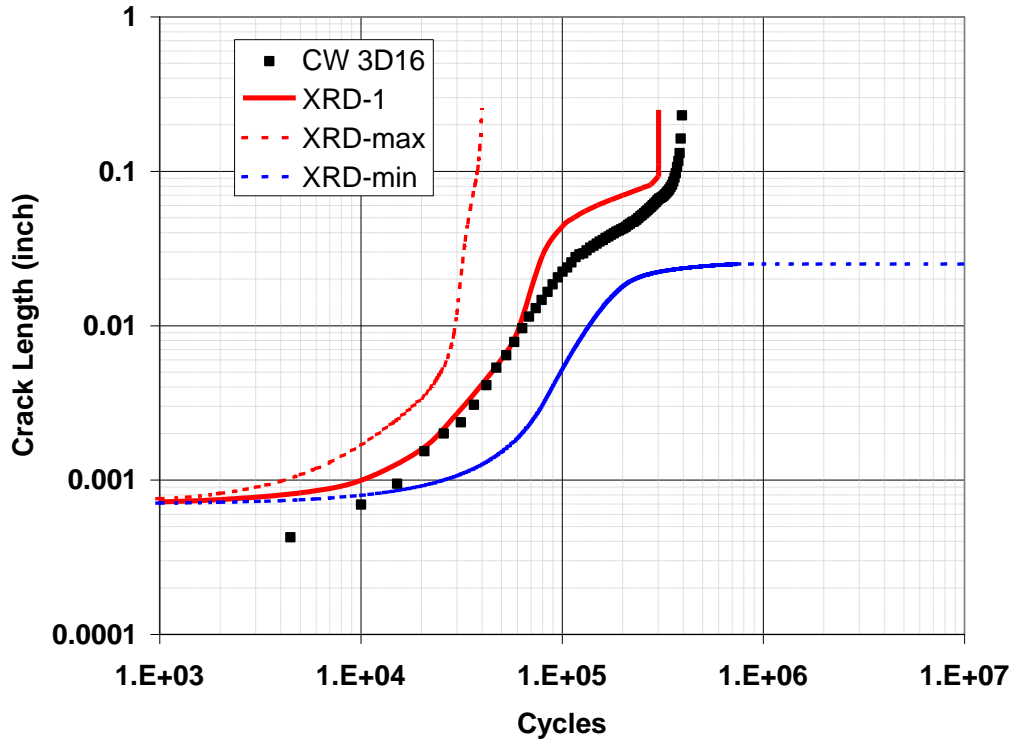


Figure 54. Life predictions using bounding scenarios XRD-min and XRD-max.

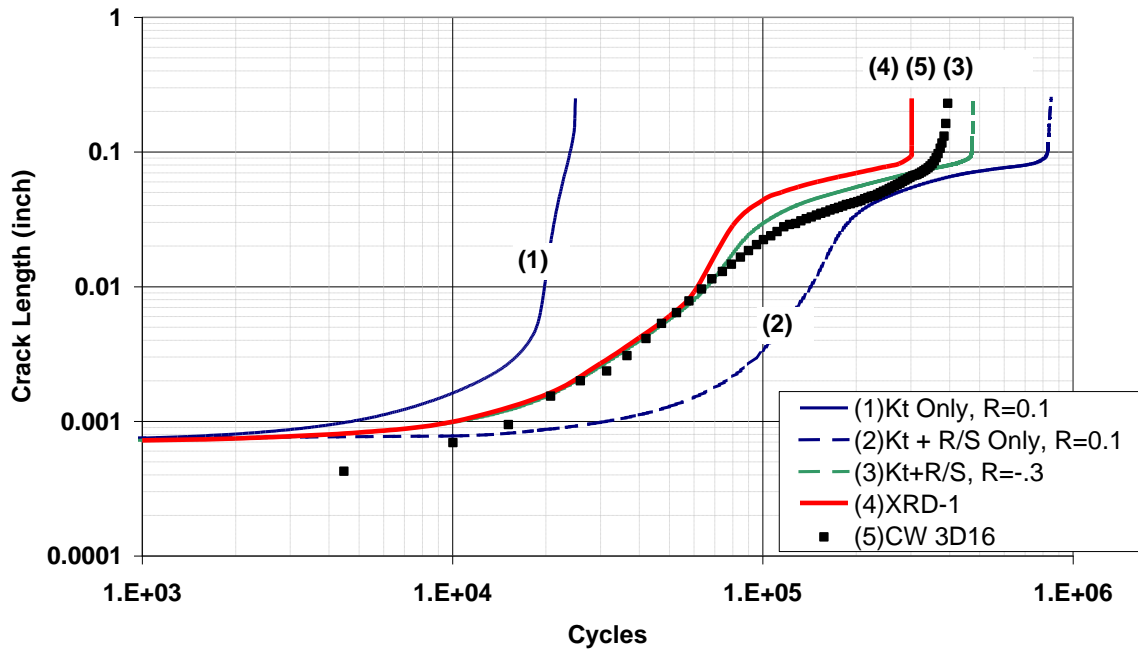


Figure 55. Progressive sensitivities with initial crack = 0.0007 inch.

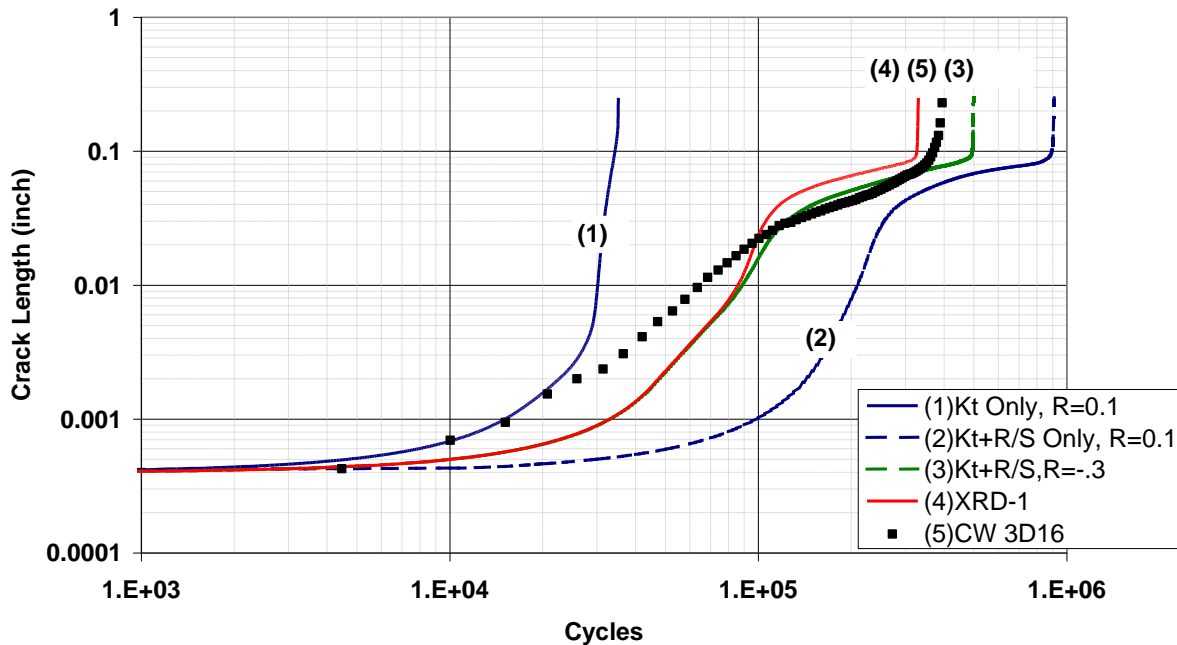


Figure 56. Progressive sensitivities with initial crack = 0.0004 inch.

A summary of our findings is found below.

**FINDINGS:**

- Non-cold worked (baseline) Coupons: It was difficult to correlate fatigue crack propagation predictions to the (experimental) crack propagation observations in the non-cold worked coupons. Normally, this is expected, as typically fatigue life data (in sources such as MIL-HDBK-5) show a wide variation in fatigue lives at the same stress levels, from 1 to 3 orders of magnitude depending on the stress level. Unexpected was the difficulty encountered predicting the qualitative shape of the  $a$  vs.  $N$  curves—the predicted  $a$  vs.  $N$  curve showed a long low slope as the crack begins to grow from the IDS and rapidly ramps up (increases in slope) as failure approaches. However, the observed  $a$  vs.  $N$  curve showed the opposite trend--a short high slope as the crack begins to grow from the IDS, then a long period of low slope crack growth, and finally a very short, high slope period as failure approaches. Reasons for this anomalous behavior are unclear; it is likely that the large stress levels (and hence, plasticity) play a significant role in the observed behavior.
- Cold worked Coupons: Many authors in the literature have attempted to develop models that can be used to predict the behavior of fatigue cracks near cold worked holes—however, as often is the case, methods that seem to work well in one study does not work well in another study (such as weight function method of Grandt (1975), which was shown to not work well in Toparli et al (1997)). It appears we still have a long way to go before we can develop robust, full validated life prediction methods that properly account for cold working.

- The APES models use the approach advocated by the Holistic Life Assessment Method; namely, by properly accounting for residual stress states, material properties, plasticity, biaxiality and mean stresses, a reasonably accurate life prediction model can be developed that captures the fatigue lives and the crack growth ‘paths’ (that is, the shape of the  $a$  vs.  $N$  curve) in cold worked coupons. We believe that capturing the correct cracking behavior (aspect ratios,  $a$  vs.  $N$  curve shapes) is critical to understanding the damage mechanisms.

### **3.6 Coordinate Phase II Demo Articles with A-10 and F-16 ASIP**

To ensure that the Phase II program is structured to best support the USAF customers, progress from Phase I was shared with the A-10 and F-16 ASIP offices and personnel at conferences such as ASIP 2008 and HOLSIP 2009; however, due to the lack of cold working test results until just near the end of the Phase I, we were not able to make significant progress in this task during Phase I. We will continue to seek the ASIP office inputs during Phase II. We consider this to be a crucial step in the success of the Phase II effort, as it will greatly increase the chance of useable technology exiting Phase II of the program and increases chances of securing “Phase III” funding, perhaps in the form of sustaining engineering contracts, from these outside agencies.

## 4 Commercialization Potential

APES continues to focus on the research and development of analytical processes that simulate fatigue from nucleation, through short crack growth, to structural failure of components. This advanced service life assessment capability places APES into the unique position to pursue comprehensive solutions to problems across many air vehicles platforms and multiple industries that need to assess and maintain the integrity of their structures. APES efforts have improved fatigue analytical models that account for surface integrity effects in the nucleation phase from constituent particles, fretting, effects of many types of corrosion, and the interaction of widespread or multiple site damage (WFD or MSD). APES successes have been leading the industry in life prediction approaches that are presently being pursued by others in the AFRL and other DoD organizations. APES models are readily integrated into or linked with the existing life prediction methodologies and codes, such as FASTRAN and AFGROW. The framework utilized by APES considers the infrastructure, structural integrity concepts, and philosophies of all aircraft users: Navy, US Air Force, and commercial/general aviation. This robust process enables our advances in life assessment methods to transition from the research stage through verification, and into application on air vehicles in three to four years. Our Commercialization and Business Plan support the development and transition to expedite the capture of benefits afforded by improved life assessment methods.

The approach of this Phase I was geared toward developing this process for a select type of damage progression, namely crack growth in residual stress fields and the influence that an evolving or relaxing stress state has on life prediction. With this effort came the concurrent development and validation of non-destructive inspection techniques that can be directly integrated into existing USAF maintenance programs using equipment already in the USAF inventory. The development of a successful assessment process facilitates the application of the solutions to many other applications such as aircraft, spacecraft, automobiles, ships, bridges, and mechanical equipment systems. The advantage that would be afforded to APES and other project participants, which includes the multiple aircraft customers and agencies, is that the Integration process is established along with the solution. The process thus enables rapid and cost effective incorporation into the particular customer's infrastructure and provides opportunities for APES to grow as a consulting engineering business, which is our forte. The successful completion of this SBIR, considering all three phases, thus results in documentation of the technical adequacy and feasibility, documentation of the business case that will provide an example of the return on the investment of application of the solutions to particular aircraft problems, and tailoring of the methodology for integrating into current, already established ASIP concepts, ensuring delivery into practice. The proposed plan focuses on capturing the validated technology and tailoring advances in technology to practical applications.

Success of this technology development and implementation will improve chances for exploiting additional opportunities in the complex problems being encountered during the life cycle of the aircraft structure. These business opportunities are not limited to U.S. markets alone, as the methods' implementation supports European customers' and our allies' fleet, especially the Canadian fleet.

A potential evolution in time for development and transition of these technologies to military and commercial customers is outlined in the commercialization results schedule (Table 6).

Table 6. Commercialization results schedule

| Commercialization Results \ Year  | 1 | 2 | 3 | 4 | 5 | 6 |
|---|---|---|---|---|---|---|
| 1. SBIR Phase I   | ■ | ■ |   |   |   |   |
| <b>2. Exit TRL 3</b>  |   | ⌘ |   |   |   |   |
| 3. SBIR Phase II: Focused demonstration using selected application on USAF asset: A-10 and F-16               |   | ■ | ■ | ■ |   |   |
| <b>4. Exit TRL 4</b>  |   |   |   | ⌘ |   |   |
| 5. Document & define a Phase III Program in cooperation with cold work supplier FTI.                          |   |   |   | ■ |   |   |
| 6. Application to Ogden ALC Aircraft Problem/<br><b>Enter TRL 5</b>   |   |   |   | ⌘ |   |   |
| 7 Submit for Approval to MCO (Military Certification Office) and to FAA (Federal Aviation Admin.).            |   |   |   | ■ |   |   |
| <b>8. Exit TRL 5/Enter TRL 6</b>  |   |   |   |   | ⌘ |   |
| 9 Repeat Process for other residual stress applications or surface treatments or additional customer vehicles |   |   |   |   | ■ | ■ |

## 5 Conclusions

This report is the final deliverable for the Phase I Small Business Innovation Research (SBIR) Topic, AF081-088, Verification of Cold Working and Interference Levels at Fastener Holes executed by Analytical Processes and Engineered Solutions (APES), Inc., the Texas Research Institute-Austin (TRI-Austin), National Research Council of Canada (NRC), Edison Welding Institute (EWI) and Direct Measurements, Incorporated (DMI).

The overall objective of Phase I was to perform the initial research to understand the residual stress behavior around cold-worked holes that are subsequently subjected to operation load cycles. The desired end state is to define the path for developing a comprehensive analytical simulation of the service life capability in multiple applications that compliment USAF fleet infrastructures. The research knowledge gained in Phase I formulated a sound approach for Phase II technology development and concurrent demonstration. The program that evolved factors in substantial USAF ‘buy-in,’ which should expedite the products into benefits for the air vehicles.

Specific goals accomplished in Phase I program were to:

4. Use multiple NDI methods (X-ray diffraction, Digital Image Correlation, Direct Measurement gauges, and Eddy Current techniques) to collect viable engineering data that provides data as to the “states of stress,” including residual stresses, in and around cold-worked holes. These data also included provisions for potential relaxation and/or redistribution of stresses. Each of the NDI methods used had particular merits, but none emerged as the “silver bullets,” the perfect NDI tool.
5. Regression of data collected and advanced fractographic examination of the failure process identified unique behaviors that post test analytical studies were able to replicate. Corroboration of the failure scenarios and analytical processes provides the framework for developing robust application models and methods.
6. Establish the process for expediting potential solutions for inclusion of the benefits of the subject SBIR into USAF aircraft by utilizing and tailoring ASIP formats and concepts.

All goals were successfully met.

The literature review focused on previous attempts to develop models and correlate coupon life predictions to fatigue experiment results (none of the literature we reviewed described fractography of cracks propagating through residual stress fields). Attempts in the literature to successfully predict the fatigue lives of cold worked structures have so far been inconsistent—methods such as weight functions which essentially use Green’s functions to ‘convert’ stresses to Mode I Stress Intensity Factors (SIFs) work well for one author but not for another. Weight functions have been shown to often be excellent predictors of SIFs, but it is apparent that 1) weight functions for the crack opening stress fields is not enough 2) analysts has so far missed key damage drivers (besides the crack opening stresses, that is) or 3) both. Direct application of residual stress, either as computed with a numerical method such as finite elements or “measured” by NDI tools, and classical LEFM are not adequate. The crack propagation predictions made by applying “conventional” damage tolerance methods does not reliably approximate the time or path of failure and is thus unacceptable to the long range objectives.

This Phase I effort included evaluation of the capabilities of several NDI techniques to measure and characterize residual stresses from the cold working process and after subsequent fatigue loading. Measurement techniques applied before, during, and after the fatigue experiments were used to capture crack propagation trends that were used to validate life prediction models. Residual stress measurements were made with four (4) techniques: x-ray diffraction (XRD), digital image correlation (DIC), eddy current and DMI optical strain gages. The four methods each have restricted applicability and limitations, but each provides a distinct opportunity. XRD was one of the most expensive of the 4 and thus number of data points is restricted by budget. The XRD data appeared reliable but the scope or depth of field of the measurement needs to be tempered with modeling parameters and the specific scope of measurement. XRD methods are suitable for pre-experimental applications, and some post laboratory measurement, but not feasible in the present state for in-service aircraft applications. The DIC, a considerably less expensive method than XRD, produced high-resolution residual strain values. The DIC was considered the most promising method for further laboratory experiments, and also as having great potential for in-service applications. The DMI gages offer valuable unique identity bar coding of each location, and could have an important tracking benefit as well as long term shifting of stress criticality. While the technology has considerable technical merits, the available products are not substantiated and have significant restrictions for our solutions. The Eddy Current methods appear to have the best potential as a cost effective solution in the field, but further development is needed.

Fifteen (15) coupons were tested in Phase I—five (5) non-cold worked and ten (10) cold worked. Each coupon was fatigue tested with a variable amplitude spectrum designed to produce excellent crack propagation marks on aluminum 7075-T651, the alloy tested in this program. Each of the ten (10) cold worked coupons had the same nominal offset,  $e/D \sim 1.5$  and the same nominal cold working level,  $CX \sim 4\%$  (residual stress measurements by XRD and DIC revealed substantial differences in stress fields presumably the same CX level). Cold working improved the lives of the specimens on average 1500% over non-cold worked specimen lives.

Analytical model development was challenging; there seem to be little guidance from the literature review, as techniques that appeared to work for one set of experiments did not work for others. Previous methods used only the residual stresses that were perpendicular to the crack plane; these stresses would tend to open or close a crack. However, most methods tended to over-predict the experimental lives by 2 to 10 times, indicating key damage drivers were probably being ignored in their analyses. Examination of the fracture surfaces from our experimental program revealed that the crack propagation featured three (3) distinct regions—a short but steep region of crack growth, followed by a long but shallow region of crack growth (which consisted of majority of the entire crack propagation life), and finally, a short and steep region of rapid crack growth until the coupon failed. This behavior was in stark contrast to the ‘predicted’ behavior using only the residual stresses—typically, there were only two distinct regions—a long shallow region followed by the short, steep region to coupon failure. Clearly, a key mechanism of crack growth was being missed. Our analyses points to a few possible candidates: 1) plasticity is affecting the crack growth more than just by residual stress, and/or 2) other mechanisms such as biaxiality of the stress field are significantly affecting crack propagation., and/or 3) relaxation or redistribution of residual stresses states. Excellent post-diction were achieved through a combination of modeling methods establishing confidence in our selected path forward. Phase I provided a series of controlled experiments using advanced experimental methods and interesting results from innovative post-diction techniques. The end

result is a well-defined Phase II approach for research activities that is designed to address unresolved issues that will enable engineering solutions to be formulated for the problem.

## **6 Unresolved Issues and Recommendations**

The unresolved issues in this project are dominated by questions about the accuracy and utility of residual stress measurements and the validation of the proposed predictive models.

### **6.1 Residual Stress Measurements**

Each residual stress (RS) measurement technique has a unique set of capabilities and limitations. Eddy current (ET or EC) measurements tend to have the lowest implementation cost and would have the quickest transition to industry, but potentially is the least accurate of any of the techniques considered. Direct Measurement, Inc. (DMI) gages have intermediate cost, accuracy, and readiness. Digital Image Correlation (DIC) and X-ray diffraction (XRD) are the most expensive and potentially the furthest away from widespread field use, but show the most promise of obtaining accurate, useful, measurements.

#### **6.1.1 X-ray diffraction (XRD)**

X-ray diffraction is one of the most expensive techniques for measuring residual stresses, while also being potentially the most accurate. Because of those two qualities, XRD appears to be useful primarily to validate the measurements of other, less costly techniques such as the DMI gages. XRD is known for being able to measure stresses over a small area, smaller than a grain size—this sensitivity could cause the XRD to provide spurious residual stress measurements, which can result in erroneous conclusions about the residual stresses. These issues will have to be addressed in Phase II.

#### **6.1.2 DMI**

There appeared to be several challenges associated with the effective use of the DMI gages. The gages were easily damaged in the cold working process—in addition to damaged gages that caused the gage readers to perhaps produce erroneous results, at least one gage pulled off completely and had to be reattached, causing a complete loss of information about the initial residual stress state of the coupon. In addition, reading the gages, while the gages were mounted on vertical coupons, was somewhat problematic—the test lab technician struggled to keep the reader flush against the coupon (whereupon the reader will not record a strain reading), the technician struggled to hold the reader up to the gage long enough to get a reading, alignment usually required the technician to watch the screen on the Tablet PC and the reader simultaneously and is difficult when the two are not side by side, and a mouse was installed on the system, as the stylus supplied with the SR-2 system proved difficult to operate.

The OEM of the gages, Direct Measurements, Inc. has presented evidence in other published studies that the gages appear to be able to detect the presence of cracks as they propagate. While we did not witness such obvious behavior in this program, we have not ruled out the possibility that we will see crack propagation in these gages in future tests.

#### **6.1.3 DIC**

Will the DIC work better than the DMI gages, in the lab or even operationally? Will the DIC paint interfere with the ability to do surface eddy current measurements? These questions still need to be answered.

#### **6.1.4 Eddy current (ET or EC)**

ET was used early in the project and determined to be not as effective as we anticipated—the ET could not effectively distinguish between cold worked and non-cold worked materials. A small modeling study was commissioned to investigate modeling and measurement issues, and came to the conclusion that the ET could detect deformations caused by the cold working process—it was not known if the ET measurements will be sensitive enough to detect small relaxations in the residual stress, or if there the probes or operators could be trained to detect the residual stresses of cold working at all.

### **6.2 Modeling**

#### **6.2.1 Crack Retardation**

Retardation parameters and models have a sizeable influence on the predicted crack growth life; there are a number of retardation models commonly used in the aircraft industry, including Willenborg and Wheeler models. In Phase I, we used only the Willenborg model, as a transitional customer for this program, the A-10 ASIP manager, uses this model. However, we observed substantial sensitivities to small changes in the retardation parameter; therefore a small series of tests on non-cold worked coupons will be necessary to characterize the retardation parameter for 7075-T651.

#### **6.2.2 Three-dimensional Effects of Cold working**

It has been observed by several researchers that the residual stress field that remains after the cold working process has been completed varies significantly from the entrance to the exit sides of the plate being cold worked. A visual inspection of their results reveals what appear to be fairly substantial differences; however, life prediction analyses to quantify the differences in structural lives were not completed in Phase I and will have to be explored in the future.

#### **6.2.3 Residual Stress Relaxation**

It has been known for several years that residual stresses induced by cold working can change with time, environment, or applications of stress cycles. We did not observe residual stress relaxation in Phase I; however, we tested at only one (high) stress level and one cold working level, and therefore this still may be an issue at other cold working levels, stress levels, or environment changes.

#### **6.2.4 Material Behavior**

##### **6.2.4.1 Monotonic and Cyclic Stress Strain Relationships**

Monotonic stress strain curves for many materials such as 2024, 7050, and 7075 are available in standard handbooks such as MIL-HDBK-5. However, even handbooks as comprehensive as MIL-HDBK-5 cannot have every possible material curve for every material. In addition, there are very few cyclic stress strain curves in MIL-HDBK-5 or elsewhere in the open literature; cyclic stress strain curves have often been shown to be able to capture the behavior of a material during fatigue loading, particularly for large (that is, plastic) strains. Therefore, it will be necessary to either locate an untapped source for the cyclic material curves of 7075-T651, or to measure these curves ourselves in Phase II.

#### **6.2.4.2 Initial Discontinuity State (IDS) Material Model Creation**

We have an extensive material database for aluminum alloys 2024-T351 and 7050-T451. This database consists not only of the crack growth rates for the materials, but also the IDS distributions that characterize the materials. This procedure was developed jointly by APES and NRCC, and uses microscopy of fracture surfaces to measure “failure flaws” and pair those with crack growth rate curves that capture the observed fatigue lives. However, we do not have a comparable database for aluminum alloy 7075-T651, which we use in Phase II.

#### **6.2.4.3 Isotropic and Kinematic Hardening**

There are large differences in computed residual stress fields due to variations in hardening rules for modeling plasticity in the material. We did not know a priori if 7075 is isotropic hardening, kinematic hardening, or a blend of the two; therefore a small test program that will reveal the character of the hysteresis loops in the cyclic stress strain curve will be necessary to adequately characterize this behavior.

## 7 References

- Brooks, C.L., Prost-Domasky, S. and Honeycutt, K (1998) “Determining the Initial Quality State for Materials,” Presented at the 1998 USAF Aircraft Structural Integrity Program Conference, San Antonio, Texas, December 1998.
- Brooks Craig L., Mills, Thomas B., Prost-Domasky, Scott A., Honeycutt, Kyle, and Young, Nichole (2003) “Advancements in Holistic Life Prediction Methodology Exfoliation Effects on Upper Wing Structure Subject to Static and Fatigue Loads, “ Final Report submitted to S&K Technologies.
- Brooks, C.L., Prost-Domasky, S.A., Honeycutt, K.T., Mills, T.B., and Young, N. (2006) Fretting Fatigue Model. AFRL-VA-WP-TR-2006-3080, Final Report for 01 May 2003 – 30 April 2006, SBIR Phase II Report, May 2006. 150 pages.
- Brot, Abraham and Matias, Carmel (2007) “The Effects of Residual Tensile Stresses Induced by Cold-working a Fastener Hole,” Proceedings, USAF Aircraft Structural Integrity Program (ASIP) Conference.
- Burlat, M., Julien, D., Lévesque, M., Bui-Quoc, T. and Bernard, M. (2008), “Effect of Local Cold Working on the Fatigue Life of 7475-T7351 Aluminium Alloy Hole Specimens,” Engineering Fracture Mechanics, Volume 75, Issue 8, pp. 2042-2061.
- Carlson, S. S. (2008), “Experimentally Derived Beta Corrections to Accurately Model the Fatigue Crack Growth Behavior at Cold Expanded Holes in 2024-T351 Aluminum Alloys”, Thesis, University of Utah.
- Cathey, W.H. and Grandt, A.F., Jr. (1980), “Fracture Mechanics Consideration of Residual Stresses Introduced by Coldworking Fastener Holes,” Journal of Engineering Materials and Technology, pp. 85-91.
- Direct Measurements, Inc. (2008), “DMI Residual Strain Measurements of Cold Work Expansion in Fastener Holes in 7075-T6 Aluminum Plate,” 2008, available for download at: <http://directmeasurements.com/coldexpansion.html>
- Engineering Software Research and Development, Inc., (ESRD, Inc.) (2008), *StressCheck*<sup>®</sup> *Master Guide*, Version 8.0, 2008, St. Louis, Missouri.
- Fersini D. and A.Pironi, A. (2005), “Numerical Simulation of the Residual Stress Intensity Factor K<sub>res</sub> in Cracked Specimens,” Proceedings, 22nd DANUBIA-ADRIA Symposium on Experimental Methods in Solid Mechanics, Monticelli Terme / Parma - Italy
- Grandt, A.F., Jr. (1975), “Stress Intensity Factors for Some Through-cracked Fastener Holes,” International Journal of Fracture, Volume 11, No. 2, pp. 283-294.
- Kang, Jidong, Johnson, W. Steven and Clark, David A. (2002), “Three-Dimensional Finite Element Analysis of the Cold Expansion of Fastener Holes in Two Aluminum Alloys,” Journal of Engineering Materials and Technology, Volume 124, Issue 2, pp. 140-145.
- Mills, T., Honeycutt, K., Brooks, C., Sharp, P.K., Loader, C., and Crawford, B. (2004a), “Development and Demonstration of an Holistic Structural Integrity Process using the Initial Discontinuity State Concept for 7050-T7451 Aluminum,” Proceedings, Aircraft Structural Integrity Program Conference, Memphis TN.

- Mills, T.B., Honeycutt, K.T., and Brooks, C.L., (2004b), "Demonstration of a Holistic Structural Integrity Process Using Corrosion/Fatigue Interactions from Laboratory Experiments and Field Experience," Proceedings, 6th International Aircraft Corrosion Workshop, Solomon's MD.
- Moreira, P. M. G. P., De Matos, P. F. P., Pinho, S. T., Pastrama, S. D., Camanho, P. P., and De Castro, P. M. S. T. (2004), "The Residual Stress Intensity Factors for Cold-worked Cracked Holes: a Technical Note," *Fatigue & Fracture of Engineering Materials and Structures*, Volume 27 Issue 9, pp. 879-886.
- Pavier, M. J., Poussard, C. G. C. and Smith, D.J. (1999), "Effect of Residual Stress Around Cold Worked holes on Fracture under Superimposed Mechanical Load," *Engineering Fracture Mechanics*, Volume 63, pp. 751-773.
- Petroski, H.J. and Aschenbach, J.D. (1978), "Computation of the Weight Function from a Stress Intensity Factor," *Engineering Fracture Mechanics*, Vol. 10, pp. 257-266.
- Pilarczyk, R. T. (2008), "Experimentally Derived Beta Corrections to Predict Fatigue Crack Growth at Cold Expanded Holes in 7075-T651 Aluminum Alloy", Thesis, University of Utah.
- Prost-Domasky, Scott A., Brooks, Craig L., and Honeycutt, Kyle T. (2003) "The Application of  $p$ -version Finite Element Methods to Fracture-dominated Problems Encountered in Engineering Practice," *Computer & Mathematics with Applications*, Vol. 46, No. 1, pp. 125-139.
- Rice, J.R. (1972), "Some Remarks on Elastic Crack-Tip Stress Field," *International Journal of Solids in Structures*, Vol. 8, pp. 751-758.
- Saunders, Terry J. and Grandt., Alten F., Jr. (2000), "The Effect of Edge Distance on Coldworking Fastener Holes," Proceedings of the Fourth Joint DoD/FAA/NASA Conference on Aging Aircraft, St. Louis, Missouri, 20 pages.
- Shi, G., Yanishevsky, M., and Li, G. (2007), "A Parametric Study on Modeling of Residual Stress Profiles Induced by the Hole Cold Expansion Process," Proceedings, Aging Aircraft Conference 2007; Palm Springs, California, April 16-19.
- Tada, Hiroshi, Paris, Paul C., and Irwin, George R (2000), *The Stress Analysis of Cracks Handbook*. Third Edition, ASME Press.
- Toparli, M., Ozel, A. and Aksoy, T. (1975), "Effect of the Residual Stresses on the Fatigue Crack Growth Behavior at Fastener Holes," *Materials Science and Engineering*, Volume A225, pp. 196-203.
- Van Dijk, G.M. and de Jonge, J.B. (1975), "Introduction to a Fighter Aircraft Loading Standard for Fatigue Evaluation (FALSTAFF)," National Aerospace Laboratory, the Netherlands (NLR), Report # NLR MP 75017U, 1975.
- Wanhill, R.J.H. (2009), "Invited Contribution. Thirty Years from the Paper 'Gust Spectrum Fatigue Crack Propagation in Candidate Skin Materials,' *Fatigue of Engineering Materials and Structures*, Vol. 1, pp. 5-19," *Fatigue and Fracture of Engineering Materials and Structures*, Vol. 32, pp. 2-4.

## APPENDIX

### *X-Ray Diffraction (XRD) Measurements*

Table A-1 X-Ray Diffraction (XRD) Measurements.

|               |             |                    |                 | <b>Radial</b> | <b>Hoop</b>   |             | <b>Radial</b> | <b>Hoop</b>   |
|---------------|-------------|--------------------|-----------------|---------------|---------------|-------------|---------------|---------------|
|               |             |                    | <b>Distance</b> | <b>Stress</b> | <b>Stress</b> |             | <b>Stress</b> | <b>Stress</b> |
| <b>Coupon</b> | <b>Side</b> | <b>Orientation</b> | <b>in.</b>      | <b>ksi</b>    | <b>ksi</b>    | <b>Side</b> | <b>ksi</b>    | <b>ksi</b>    |
| 3D16          | Entrance    | TOP                | 0.0394          | -31           | -16.65        | Exit        | -25.94        | -42.83        |
| 3D16          | Entrance    | TOP                | 0.0787          | -38.06        | -15.47        | Exit        | -32.88        | -32.49        |
| 3D16          | Entrance    | TOP                | 0.1181          | -32.38        | -3.79         | Exit        | -40.22        | -6.32         |
| 3D16          | Entrance    | TOP                | 0.3150          | -3.36         | 26.06         | Exit        | -0.36         | 27.19         |
| 3D16          | Entrance    | LEFT               | 0.0394          | -42.85        | -23.36        | Exit        | -25.75        | -41.4         |
| 3D16          | Entrance    | LEFT               | 0.0787          | -43.41        | -21.15        | Exit        | -36.53        | -42.46        |
| 3D16          | Entrance    | LEFT               | 0.1181          | -37.97        | -1.84         | Exit        | -36.27        | -22.91        |
| 3D16          | Entrance    | LEFT               | 0.3150          | -1.76         | 5.02          | Exit        | -2.83         | 16.9          |
| 3D16          | Entrance    | BOTTOM             | 0.0394          | -38.38        | -42.94        | Exit        | -40.31        | -53.41        |
| 3D16          | Entrance    | BOTTOM             | 0.0787          | -41.3         | -24.16        | Exit        | -46.97        | -50.66        |
| 3D16          | Entrance    | BOTTOM             | 0.1181          | -39.34        | -4.61         | Exit        | -45.97        | -28.09        |
| 3D16          | Entrance    | BOTTOM             | 0.3150          | -4.83         | 2.58          | Exit        | -4.49         | 12.62         |
| 3D22          | Entrance    | TOP                | 0.0394          | -30.7         | -31.27        | Exit        | -16.5         | -26.32        |
| 3D22          | Entrance    | TOP                | 0.0787          | -41.57        | -41.69        | Exit        | -38.36        | -37.3         |
| 3D22          | Entrance    | TOP                | 0.1181          | -33.46        | -22.21        | Exit        | -41.08        | -19.69        |
| 3D22          | Entrance    | TOP                | 0.3150          | -1.91         | 18.97         | Exit        | 0.53          | 17.37         |
| 3D22          | Entrance    | LEFT               | 0.0394          | -38.78        | -28.18        | Exit        | -26.01        | -47           |
| 3D22          | Entrance    | LEFT               | 0.0787          | -43.97        | -19.25        | Exit        | -37.24        | -34.14        |
| 3D22          | Entrance    | LEFT               | 0.1181          | -31.47        | -1.18         | Exit        | -38.77        | -14.34        |
| 3D22          | Entrance    | LEFT               | 0.3150          | -3.32         | 11.76         | Exit        | -1.32         | 13.07         |
| 3D22          | Entrance    | BOTTOM             | 0.0394          | -41           | -46.71        | Exit        | -42.32        | -59.45        |
| 3D22          | Entrance    | BOTTOM             | 0.0787          | -45.2         | -26.77        | Exit        | -50.09        | -38.55        |
| 3D22          | Entrance    | BOTTOM             | 0.1181          | -30.58        | 1.78          | Exit        | -42.92        | -20.94        |
| 3D22          | Entrance    | BOTTOM             | 0.3150          | -4.92         | 19.33         | Exit        | -9.37         | 4.32          |
| 3D30          | Entrance    | TOP                | 0.0394          | -20.37        | -32.18        | Exit        | 2.73          | -31.26        |

|      |          |        |        |        |        |      |        |        |
|------|----------|--------|--------|--------|--------|------|--------|--------|
| 3D30 | Entrance | TOP    | 0.0787 | -37.55 | -29.05 | Exit | -28.7  | -31.42 |
| 3D30 | Entrance | TOP    | 0.1181 | -36.02 | -7.42  | Exit | -34.57 | -20.33 |
| 3D30 | Entrance | TOP    | 0.3150 | -2.54  | 19.19  | Exit | -1.13  | 22.26  |
| 3D30 | Entrance | LEFT   | 0.0394 | -36.89 | -34.03 | Exit | -26.3  | -42.93 |
| 3D30 | Entrance | LEFT   | 0.0787 | -44.01 | -22.93 | Exit | -34.94 | -14.3  |
| 3D30 | Entrance | LEFT   | 0.1181 | -31.27 | 0.47   | Exit | -37.45 | -31.19 |
| 3D30 | Entrance | LEFT   | 0.3150 | -6.17  | 13.61  | Exit | -4.01  | 13.79  |
| 3D30 | Entrance | BOTTOM | 0.0394 | -41.82 | -58.69 | Exit | -37.47 | -61.39 |
| 3D30 | Entrance | BOTTOM | 0.0787 | -43.65 | -38.6  | Exit | -51.31 | -41.85 |
| 3D30 | Entrance | BOTTOM | 0.1181 | -31.95 | 1.19   | Exit | -46.89 | -21.94 |
| 3D30 | Entrance | BOTTOM | 0.3150 | -4.41  | 6.76   | Exit | -4.24  | 16.16  |
| 5B32 | Entrance | TOP    | 0.0394 | -17.71 | -32.4  | Exit | -19.03 | -36.26 |
| 5B32 | Entrance | TOP    | 0.0787 | -40.72 | -37.2  | Exit | -35.7  | -38.79 |
| 5B32 | Entrance | TOP    | 0.1181 | -33.25 | -7.07  | Exit | -37.27 | -17.52 |
| 5B32 | Entrance | TOP    | 0.3150 | 2.4    | 25.09  | Exit | -3.51  | 25.83  |
| 5B32 | Entrance | LEFT   | 0.0394 | -30.47 | -27.81 | Exit | -24.53 | -46.17 |
| 5B32 | Entrance | LEFT   | 0.0787 | -43.58 | -24.15 | Exit | -37.73 | -44.01 |
| 5B32 | Entrance | LEFT   | 0.1181 | -34.96 | -6.94  | Exit | -41.06 | -29.19 |
| 5B32 | Entrance | LEFT   | 0.3150 | 1.72   | 13.2   | Exit | -6.11  | 13.21  |
| 5B32 | Entrance | BOTTOM | 0.0394 | -48.24 | -47.44 | Exit | -36.8  | -62.26 |
| 5B32 | Entrance | BOTTOM | 0.0787 | -46.95 | -23.1  | Exit | -51.38 | -42.21 |
| 5B32 | Entrance | BOTTOM | 0.1181 | -40.29 | -4.97  | Exit | -33.69 | -21.23 |
| 5B32 | Entrance | BOTTOM | 0.3150 | -5.92  | 6.84   | Exit | -5.95  | 14.5   |
| 5B35 | Entrance | TOP    | 0.0394 | -35.74 | -37.59 | Exit | -22.51 | -44.19 |
| 5B35 | Entrance | TOP    | 0.0787 | -43.13 | -34.71 | Exit | -31.78 | -28.92 |
| 5B35 | Entrance | TOP    | 0.1181 | -27.8  | -3.68  | Exit | -28.68 | -10.39 |
| 5B35 | Entrance | TOP    | 0.3150 | 0.11   | 24.86  | Exit | -1.84  | 21.62  |
| 5B35 | Entrance | LEFT   | 0.0394 | -38.46 | -39.17 | Exit | -28.83 | -54.17 |
| 5B35 | Entrance | LEFT   | 0.0787 | -46.28 | -29.26 | Exit | -34.54 | -40.83 |
| 5B35 | Entrance | LEFT   | 0.1181 | -39.33 | -12.64 | Exit | -34.97 | -21.88 |
| 5B35 | Entrance | LEFT   | 0.3150 | 1.66   | 11.35  | Exit | -3.02  | 18.62  |

|      |          |        |        |        |        |      |        |        |
|------|----------|--------|--------|--------|--------|------|--------|--------|
| 5B35 | Entrance | BOTTOM | 0.0394 | -29.68 | -49.98 | Exit | -37.56 | -59.52 |
| 5B35 | Entrance | BOTTOM | 0.0787 | -48.75 | -34.23 | Exit | -43.5  | -42.99 |
| 5B35 | Entrance | BOTTOM | 0.1181 | -41.52 | 1.57   | Exit | -39.43 | -27.78 |
| 5B35 | Entrance | BOTTOM | 0.3150 | -2.21  | 7.71   | Exit | -8.11  | 16.03  |

**Digital Image Correlation (DIC) Measurements**

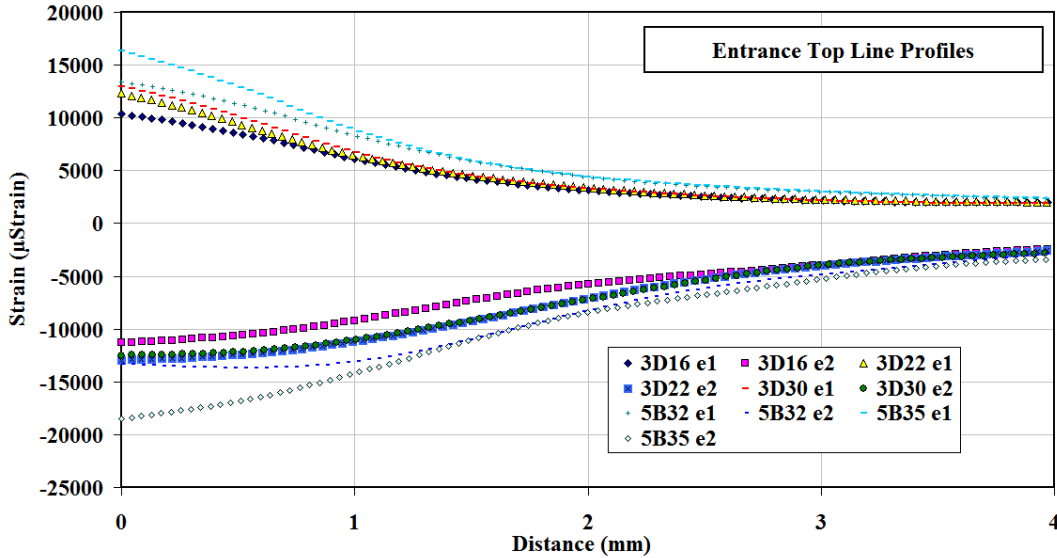


Figure A-1 Digital Image Correlation Strains  $e_1$  and  $e_2$ . Entrance Side, Top Line Profiles.

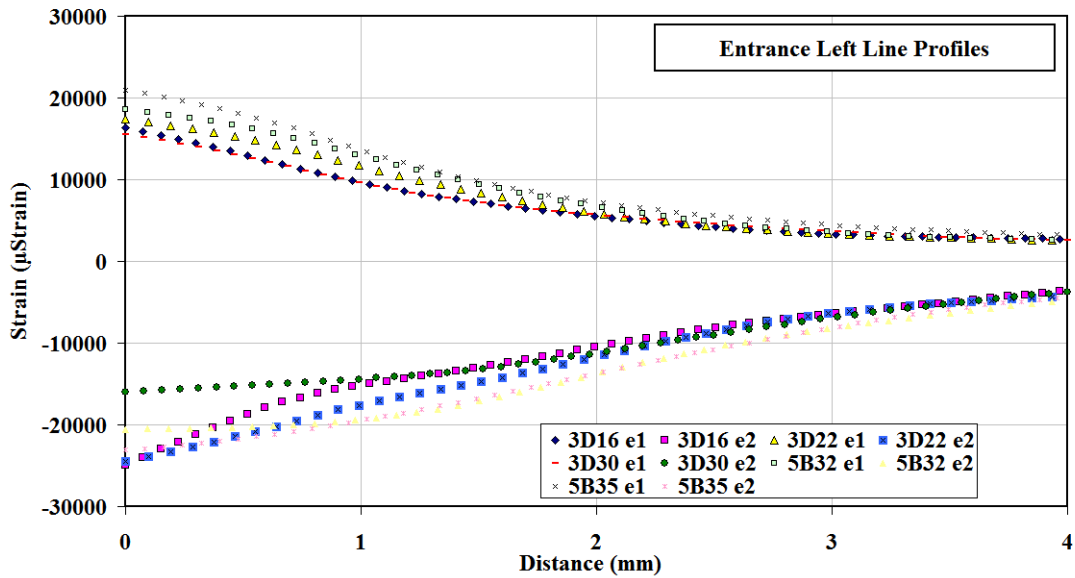


Figure A-2. Digital Image Correlation Strains  $e_1$  and  $e_2$ . Entrance Side, Left Line Profiles.

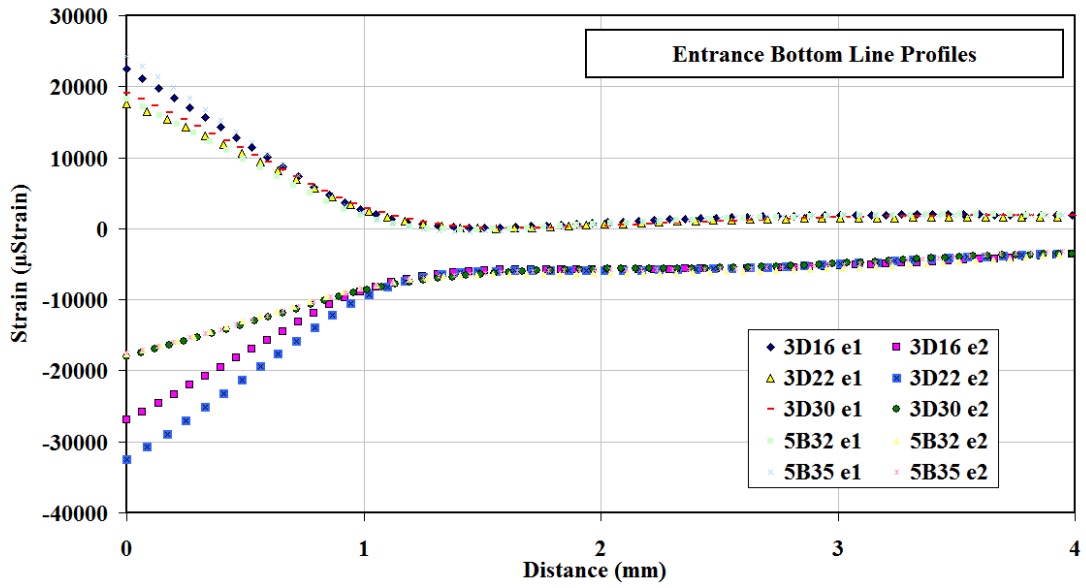


Figure A-3. Digital Image Correlation Strains  $e_1$  and  $e_2$ . Entrance Side, Bottom Line Profiles.

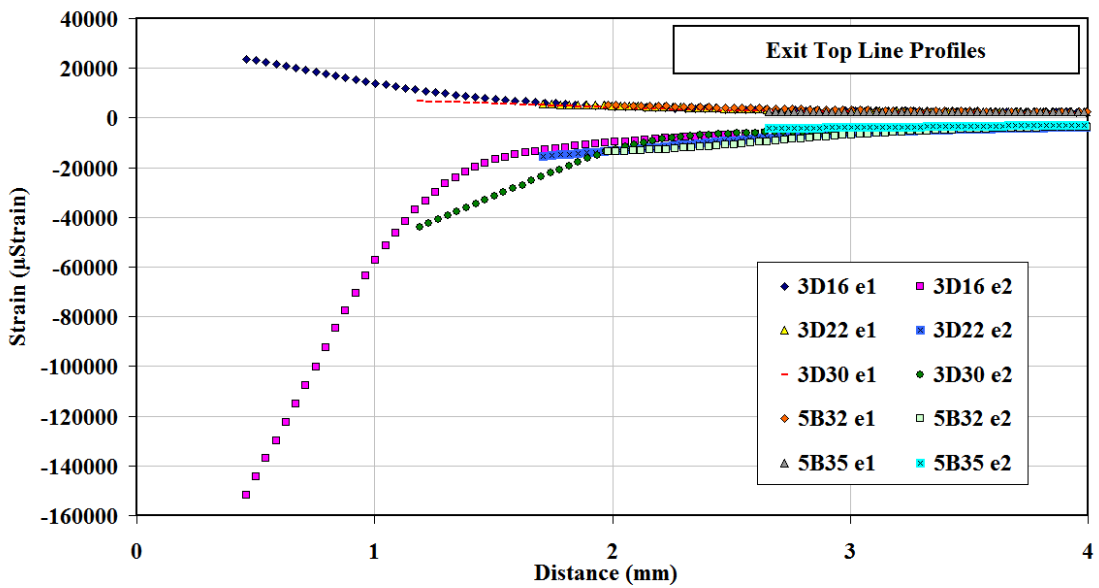


Figure A-4. Digital Image Correlation Strains  $e_1$  and  $e_2$ . Exit Side, Top Line Profiles.

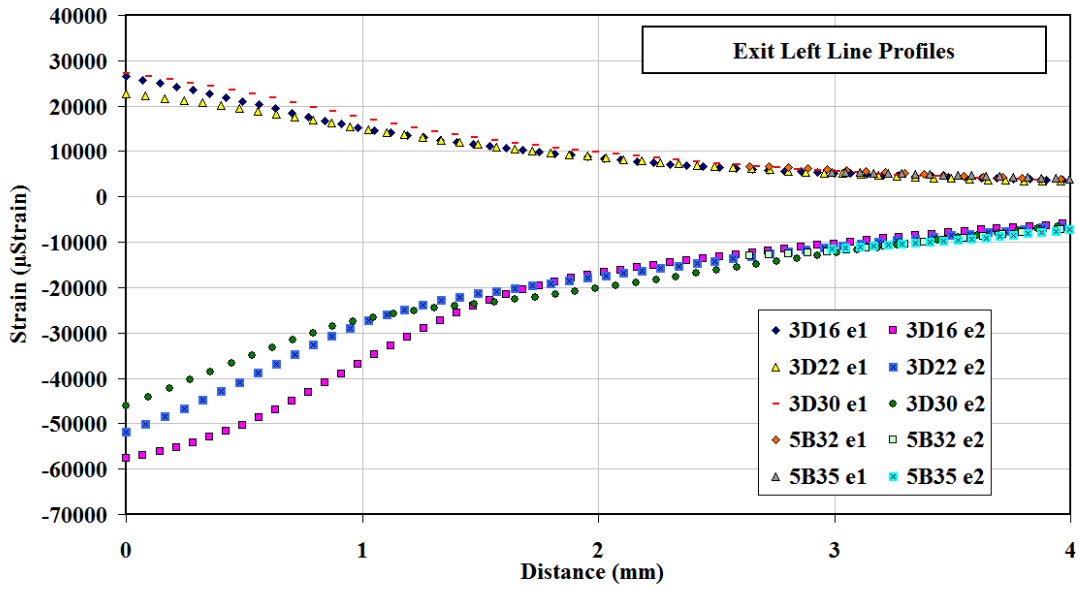


Figure A-5. Digital Image Correlation Strains  $e_1$  and  $e_2$ . Exit Side, Left Line Profiles.

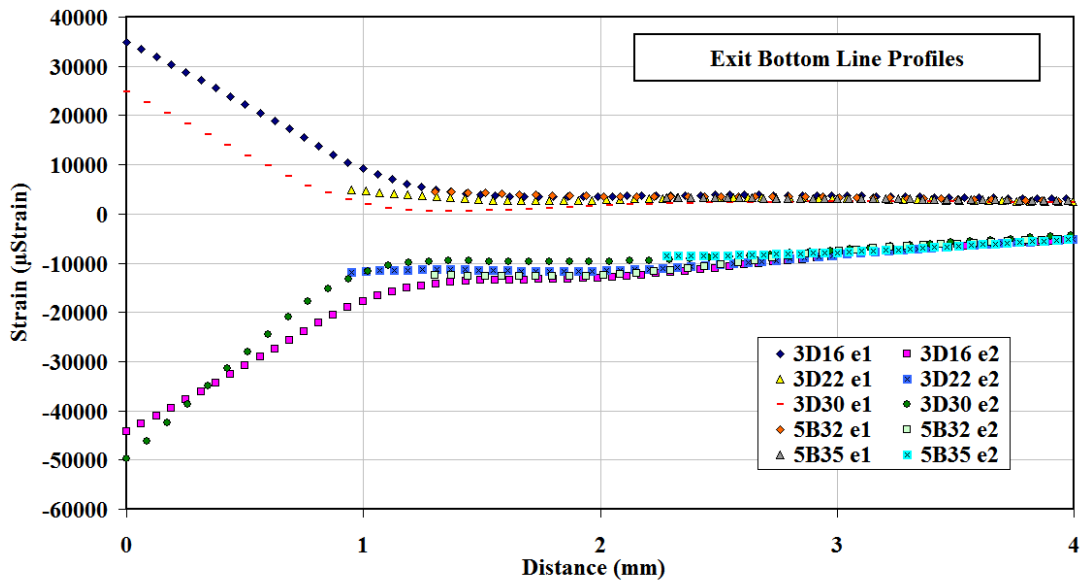


Figure A-6. Digital Image Correlation Strains  $e_1$  and  $e_2$ . Exit Side, Bottom Line Profiles.